2006:62

DOCTORAL THESIS

Development of a Novel Experimental Technique for Studying Zeolites – combining Zeolite Coated ATR Elements and FTIR Spectroscopy

Mattias Grahn

Luleå University of Technology
Department of Chemical Engineering and Geosciences
Division of Chemical Technology

2006:62 | ISSN: 1402-1544 | ISRN: LTU-DT -- 06/62 -- SE

Development of a Novel Experimental Technique for Studying Zeolites – combining Zeolite Coated ATR Elements and FTIR Spectroscopy

Mattias Grahn

November 2006

Luleå University of Technology

Department of Chemical Engineering and Geosciences

Division of Chemical Technology

Abstract

Thin zeolite films have great potential in several novel application areas such as structured catalysts, membranes and sensors. To fully exploit the advantages of these films it is of great importance to determine the adsorption properties of the films. A powerful technique for studies of phenomena at surfaces or in thin films is FTIR/ATR-spectroscopy (Fourier Transform Infra Red / Attenuated Total Reflection).

In this work, MFI zeolite films were prepared on ATR elements using two methods. One method produced 200 nm thick films with small crystals (<200nm). The other method was used for preparing b-oriented ZSM-5 films. These films were discontinuous and ca 420 nm thick and consisted of well intergrown, and substantially larger crystals, ca 1.1 μm in diameter.

Silicalite-1 coated elements were evaluated as gas sensors and the sensitivity for a hydrocarbon was compared with a standard 10 cm gas cell. The sensitivity was approximately 85 times higher for the coated elements at low hydrocarbon concentration. The response time was investigated by exposing the coated element to a step increase of an analyte and recording the response as a function of time. The response was relatively fast, equilibrium was achieved after approximately 250 s, but already after a few seconds, a strong signal could be detected.

The coated elements were also used for determining single gas adsorption isotherms. The studied systems were n-hexane/silicalite-1, p-xylene/silicalite-1 and p-xylene/ZSM-5. The observed isotherms for temperatures between 323 and 423 K were typical for microporous materials with a fast increase of the amount adsorbed at low partial pressures. p-Xylene isotherms of type I were observed as opposed to the type IV isotherms reported in literature for powders. This difference was assigned to strain in the films and/or to reduced flexibility of the MFI framework when attached to a support. Further, some capillary condensation occurred at higher pressures in the films consisting of smaller crystals, which was assigned to condensation in open grain boundaries. Henry's constants and heats of adsorption determined from low-pressure data agreed well with previous reports. Measurements with polarized radiation revealed that p-xylene molecules are mainly oriented with their long axis in the b-direction of the crystals and it was also observed that some kind of rearrangement of n-

hexane occurs with increasing loading, both of these findings were in agreement with previously reported results.

Keywords: MFI, zeolite, adsorption, sensor, FTIR, ATR

Acknowledgements

First of all, I would like to thank my supervisor, Professor Jonas Hedlund for your guidance during this work and for your constant enthusiasm. Further, I would like to thank Associate Professor Allan Holmgren who has been my assistant supervisor, for his support and helpful discussions regarding spectroscopy. The former head of the division, Prof. Johan Sterte is acknowledged for giving me the opportunity to work within this research group.

I thank Margareta L. Larsson for teaching me how to run the spectrometer and getting me started with this work. I am also grateful to Zheng Wang for a fruitful collaboration within this project. Further I would like to thank all the friends and colleagues at the Department of Chemical Engineering and Geosciences with special thanks to Fredrik Jareman and Jonas Lindmark for helping me with miscellaneous computer problems.

Special thanks to Antonina Lobanova for performing such an excellent Masters thesis. It was great fun advising you.

The Swedish Research Council (VR) is gratefully acknowledged for its financial support.

I would like to give my warmest thanks to my parents and my brother for your support and encouragement. Finally, I wish to thank my girlfriend Johanna for always supporting me and for having such patience with me and our children. I love all very dearly!

Mattias Grahn,
Luleå, November 2006.

List of Papers

This thesis is based on the work contained in the following papers, referred to in the text by roman numbers.

I **Zeolite coated ATR crystals for new applications in FTIR-ATR spectroscopy**
Zheng Wang, Margareta L. Larsson, Mattias Grahn, Allan Holmgren and Jonas Hedlund
Chemical Communications 24 (2004) 2888

II **Zeolite coated ATR crystal probes**
Zheng Wang, Mattias Grahn, Margareta L. Larsson, Allan Holmgren, Johan Sterte and Jonas Hedlund
Sensors and Actuators B: Chemical 115 (2006) 685

III **Silicalite-1 coated ATR elements as sensitive chemical sensor probes**
Mattias Grahn, Zheng Wang, Margareta L. Larsson, Allan Holmgren, Jonas Hedlund and Johan Sterte
Microporous and Mesoporous Materials 81 (2005) 357

IV **Adsorption of n-hexane and p-xylene in thin silicalite-1 films studied by FTIR/ATR spectroscopy**
Mattias Grahn, Allan Holmgren and Jonas Hedlund
Submitted

V **Orientation of p-xylene in zeolite ZSM-5 films studied by FTIR/ATR spectroscopy**
Mattias Grahn, Antonina Lobanova, Allan Holmgren and Jonas Hedlund
Manuscript

VI **A Novel Experimental Technique for Estimation of Molecular Orientation in Zeolite**
Mattias Grahn, Antonina Lobanova, Allan Holmgren and Jonas Hedlund
Accepted for presentation and full length paper submitted for publication in the proceedings of the 15th International Zeolite Conference, Beijing, China

Contents

Introduction

Background

Zeolite is a class of materials possessing some very interesting properties. These materials are inorganic with large surface area and a well-defined system of micropores. Consequently, much research effort has been directed to closely examine the properties of zeolites.

For the last decade or so, several techniques for preparing thin structured films of zeolites on various types of supports have emerged. These films have a great potential for utilization in new sophisticated applications such as membranes for separations or catalysis, and in sensors. Zeolite membranes can separate molecules in a mixture based on size, shape, or adsorption strength. Thin film catalysts may show different properties as compared to traditional catalysts based on powders.[1] Further, the often strong adsorption of molecules in zeolites[2] makes them interesting in sensor applications where a thin film coating assures shorter response times compared to large crystals.[3] However, the small sample quantities that the film constitutes make them difficult to analyze with several traditional techniques. Due to this lack of suitable analysis methods, there has been a constant demand for developing novel characterization methods in order to better understand the properties of the films. Moreover, as a consequence of this lack of suitable methods, it has often been assumed that the properties of the film are the same as for large crystals.

A characterization technique that has been successfully utilized for studying other types of films is Fourier Transform Infrared (FTIR) spectroscopy in combination with the Attenuated Total Reflection (ATR) sampling method. When combined with zeolite films, this technique could become a powerful tool for studying the properties of zeolite films, and zeolite coated ATR elements might also serve as a very sensitive and selective chemical sensor probe.

Scope of the present work

The scope of the present work was to prepare MFI films on ATR elements and to test these coated elements as chemical sensor probes. This study was limited to comprise a few hydrocarbons.
Further, the adsorption properties of some important hydrocarbons in MFI films were investigated using the FTIR/ATR technique. Adsorption isotherms, Henry's constants, adsorption enthalpies and adsorbate orientation were determined and compared to data reported for powder.

Literature Survey

Molecular Sieves and Zeolites

Molecular sieves is a group of porous materials that can separate components in a mixture based on molecular size or shape. Small molecules are able to enter the pore structure whereas molecules larger than the pore openings cannot enter the pore system.

A subgroup of molecular sieves is the zeolites. A zeolite is a type of mineral with properties of great interest for the chemical industry.[4] The first report of a zeolite mineral appeared in the middle of the 18th century and was written by the Swedish mineralogist A. Cronstedt. This type of mineral loose water rapidly upon heating, thus seeming to boil, and the name zeolite stems from the greek words zeo (to boil) and lithos (stone). Zeolites are crystalline, hydrated aluminosilicates consisting of a three-dimensional network of $[SiO_4]^{4-}$ and $[AlO_4]^{5-}$ tetrahedra.[4] The tetrahedra are linked together by sharing oxygen atoms. More than 160 different zeolite frameworks, both natural and synthetic, have been identified up to today.[5]

A general formula for representing zeolite structures can be written as:[6]

$$M_{x/n}[(AlO_2^-)_x(SiO_2)_y]\cdot wH_2O$$

where M is the cation of valence n and w is the number of water molecules. The charge balancing cation is usually a metal cation, ammonium- or alkylammonium cation. The charge balancing cations are rather mobile and thus exchangeable, which results in an ion-exchange capacity for the zeolite. This ion-exchange capacity has led to an extensive use of zeolite as water softener in detergents. The y/x ratio is the important silicon to aluminum ratio, which is always ≥ 1. Some of the physical and chemical properties of the zeolite are determined from the aluminum content in the zeolite; for instance, more aluminum in the framework results in a more hydrophilic zeolite. If the charge balancing cation is substituted for a proton, the acid form of the zeolite is obtained. Zeolites are commonly used as acid catalysts in various chemical processes.[7]

In this work, the zeolite ZSM-5 and the molecular sieve silicalite-1 was used. Silicalite-1 is strictly speaking not a zeolite since it contains no (or very little) aluminum, it is rather a pure silica analogue of the zeolite ZSM-5, and both have an MFI-type framework. The absence of aluminum in the framework of silicalite-1 makes it less hydrophilic than its zeolite analogue. Further, silicalite-1 has very low ion exchange capacity since there is no charge balancing cations in the pure silica framework.

An important feature of the zeolites is their well-defined pore systems, see Figure 1. The structure of the pore system is determined by the crystal structure of the zeolite and that can be one-, two or three-dimensional. Further, the pores may have tubular shape or contain periodic cavities, and they may be straight or zig-zag. The pore diameters in known zeolites are between 3 and 13 Å,[8] the small diameters results in high specific surface area, values of several hundreds m^2/g are common. The large surface area also gives zeolites a high adsorption capacity, which makes them interesting as selective adsorbents.[2]

According to IUPAC,[9] pores can be classified based on their size, as micropores, mesopores or macropores:

Micropores	d < 2 nm
Mesopores	2 < d <50 nm
Macropores	d > 50 nm

The classification is arbitrary and based on nitrogen adsorption measurements on different porous materials.[10]

Two types of pores are present in ZSM-5; straight pores with pore openings of 0.53 x 0.56 nm running in the b-direction and intersecting sinusoidal pores extending in the a-direction with pore openings of 0.51 x 0.55 nm, see Figure 1.

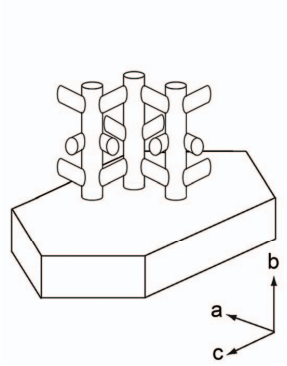

Figure 1. Schematic figure of MFI-crystal with channel system and crystallographic axes.

Zeolites are prepared by hydrothermal treatment of a well defined synthesis mixture consisting of a silica-, alumina- and alkali source.[7] In addition a structure directing agent, or template, is usually added to the synthesis mixture to obtain the desired zeolite structure. In the synthesis of MFI, quaternary ammonium cations are often used as template molecules, one example of such a molecule is the tetrapropylammonium $[TPA]^+$ ion.[7] Subsequent to synthesis, the TPA has to be removed from the zeolite channels and/or intersections to open up the pore system, this is usually achieved by calcination at high temperatures.

Zeolite films

Zeolite films are of great interest due to their large potential in a variety of applications, such as:[11]

- Membranes
- Sensors
- Catalysts

Zeolite membranes for separation is perhaps the application where most research has been focused because of their potential for carrying out difficult separations e.g. separation of close-boiling components. The separation may be governed by sieving,[12, 13] by different diffusivities[14] or by preferential adsorption.[13, 14] Further, in membrane applications, a thin, defect free film would be desirable. The thinner the film the smaller the mass transport resistance, and a defect free film is desireble to achieve as high selectivity as possible.[15, 16] The purpose of using zeolites in sensors is usually to improve sensitivity and selectivity by preferential adsorption, in addition, thin films assure a fast response time of the sensor.[3] In thin film catalysts, the product composition might be tailored by making use of different diffusion rates for different molecules in the zeolite, and by changing the film thickness it would be possible to alter the product composition.[1]

In general, when thin zeolite films are desirable, the films are usually prepared on some kind of support for mechanical stability and several methods for preparing supported zeolite films have been developed, for example:

- In-situ crystallization (direct synthesis)
- Seeding methods
- Dry gel conversion (vapour phase transport)

In this work the two first methods were used for preparing films. In the in-situ method, the support is immersed and hydrothermally treated in a synthesis solution to grow a film.[17-19] Seeding methods were developed in parallel by the groups of Tsapatsis[20] and Sterte and Hedlund.[21] The seeding methods consists of two main steps, firstly, small zeolite seed crystals are deposited on the support

and secondly, the seed crystals are intergrown to a dense film by hydrothermal treatment in an appropriate synthesis solution. Different methods for attaching the seeds to the substrate have been reported. For example, in the method developed by Sterte and Hedlund, which was also used in the present work, the substrate is treated with a cationic polymer solution to render the surface positively charged. The negatively charged seed crystals are subsequently attached electrostatically to the surface to form a closely packed layer of seeds on the surface.

Defects in zeolite films

In most applications it is desirable to keep the amount of defects in the film to a minimum to obtain a high selectivity. Defects are usually classified into *pinholes*, *cracks* and *open grain boundaries*. Pinholes are believed to be a result of incomplete seeding or insufficient film thickness.
Cracks is the defect type that has been studied mostly and they are believed to form during calcination of the film. Geus and van Bekkum[22] suggested that a mismatch in the thermal expansion between the MFI film and support caused crack formation. They measured the unit cell parameters during calcination and found shrinkage in the a-direction whilst an expansion in the b-direction was observed. The effect of orientation on crack formation was studied by den Exter et al.,[23] they attributed cracks observed in the (a, b) oriented film to stress in the films induced by shrinkage in the a-direction and expansion in the b-direction upon calcination.

Grain boundaries between adjacent crystals are an inherent feature of polycrystalline films and Dong et al.[24] reported that the grain boundaries may open during calcination of zeolite membranes.

The presence of open grain boundaries and cracks in zeolite film may cause capillary condensation of e.g. hydrocarbons in the defects reducing the selectivity, and in adsorption measurements capillary condensation may lead to difficulties in determining the saturation capacity of the adsorbent.[25]
On the other hand, condensation in defects may in some applications be exploited like in porosimetry measurements[26] of membranes. Porosimetry is a

method for assessing membrane quality and can also be used for estimating defect distributions in membranes.[27]

Strain in zeolite films

Several groups have reported that the unit cell parameters differs between zeolite powder and supported zeolite films.[24, 28, 29] This has further been attributed to strain in the crystals in the film.[29] Dong et al.[24] investigated the microstructure evolution of MFI films during template removal by calcination. They employed high-temperature X-ray powder diffraction (HT-XRPD) and the results were compared to powder samples formed in the liquid bulk during crystallization. In that study, randomly oriented films were grown on yttria-doped zirconia and α-alumina supports. It was found that the unit cell volume in the zeolite films were larger than the unit cell of the zeolite powder after calcination, indicating that the crystals in the film are subjected to strain.

Jeong et al.[29] studied strain in preferentially c-oriented MFI membranes during calcination utilizing X-ray diffraction with a synchrotron X-ray source. Again it was found that the unit cell parameters for the MFI film differed as compared to MFI powder. After calcination, the crystals in the film were compressed along the a/b-axis and elongated along the c-axis.

In a recent study, Lassinantti-Gualtieri et al.[30] investigated crack formation during calcination in preferentially a-oriented MFI membranes employing high-temperature synchrotron X-ray powder diffraction. In that study, the unit cell parameters were monitored during the calcination procedure and in concert with previous findings, the unit cell parameters were found to differ between the zeolite film and zeolite powder. After calcination the crystals in the film were subjected to tensile strain in the b-direction whereas the crystals were subjected to compressive strain in the c-direction. Strain in zeolite films may not only be involved in crack formation, but has also been postulated to affect the performance of zeolite membranes.[29]

Adsorption

The phenomenon of adsorption plays an important role in heterogeneous catalysis as well as in separation applications. Two main types of adsorption processes exists; *chemical* adsorption, also denoted *chemisorption*, and *physical* adsorption.

Chemisorption involves the creation of bonds between the adsorbent and the adsorbate and resembles chemical reactions. Most of the reactions being catalyzed by a solid are believed to involve an intermediate step with chemisorption of at least one of the reactants.

Physical adsorption is caused by intermolecular forces, both van der Waal, and electrostatic forces comprising polarization, dipole and quadrupole interactions.[2] Physical adsorption resembles condensation of vapors rather than actual chemical reactions, as in chemisorption. Physical adsorption is the main phenomenon employed in adsorptive separation processes.[2] Further, physical adsorption is used for determining specific surface area as well as pore sizes and pore size distributions of adsorbents.[31]

Physical adsorption from gas phase is always an exothermic process, and the heat of adsorption is a direct measure of the bond strength between the surface and the adsorbate. In general, the heat of adsorption in chemisorption is significantly larger than in physical adsorption. However, for physical adsorption in zeolites the heat of adsorption is often of the same magnitude as in chemisorption.[25] Usually, physical adsorption is a very rapid process since it does not require activation energy, although in microporous materials, like zeolites, the uptake may be determined by the rate of diffusion of the adsorbate within the pore system of the adsorbent.[2]

Physical adsorption is an equilibrium process, which is fully reversible and equilibrium is quickly achieved, unless the process is restricted by slow diffusion of the adsorbate.[2]

Moreover, physical adsorption is typically nonspecific in contrast to chemisorption, which is highly specific,[31] taking place only on certain specific

sites on the surface. As a consequence, chemisorption is restricted to forming a monolayer, whereas in physical adsorption, both monolayers and multilayers may form. At low partial pressures monolayer adsorption is dominating whilst at higher partial pressures multilayers may form.[31] In zeolites, multilayer adsorption may be prevented for sterical reasons, if the dimension of the adsorbate and the pore diameter are of the same size.

Adsorption isotherms

Adsorption isotherms are usually classified according to Brunauer,[2] see Figure 2. Microporous materials usually show type I isotherms. The type I isotherm is also referred to as a Langmuir type of isotherm, typically there is a steep increase in surface coverage with increasing pressure at low partial pressures. At higher partial pressures the isotherms starts to level off towards a distinct saturation limit, corresponding to a completely filled pore system. Type II isotherms represent multilayer adsorption on non-porous solids. Type IV isotherms are typical for porous materials containing mesopores with capillary condensation occurring in the mesopores. Types III and V are rare and occurs in systems where the forces of adsorption are relatively weak.

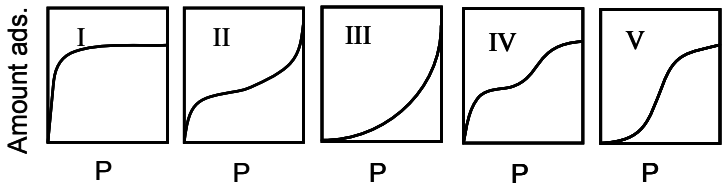

Figure 2. Brunauer's five types of adsorption isotherms, with the amount adsorbed as a function of the partial pressure (P) of the adsorbate in gas phase.

At low partial pressures of the adsorbate, there will be a low surface coverage, and the adsorbed molecules may be regarded as isolated from their neighbours. Assuming a homogenous surface, the relationship between the partial pressure and the amount adsorbed on the surface will be linear.[2] This relationship is often referred to as Henry's law because of the similarity to the limiting behaviour of gases dissolved in liquids.

For Henry's constant expressed in pressure, Henry's law is written as:

$$q = K_H P \quad (1)$$

In this relationship, q (mmol/g) is the adsorbate loading, K_H is Henry's constant (mmol/g Pa) and P (Pa) is the partial pressure of the adsorbate in gas phase. At higher partial pressures, the surface will begin to reach monolayer coverage, or alternatively, in zeolites the micropores will be completely filled. Further, as the loading increases molecules can no longer be regarded as isolated from their neighbours, and hence molecules adsorbed at adjoining sites will interact with each other. These factors will influence the amount adsorbed so that the linear relationship between the partial pressure and the surface coverage according to equation (1) is no longer valid. To model this behavior a number of adsorption models have been proposed, the perhaps most frequently used model is the so-called Langmuir model or the Langmuir isotherm.[2]

When deriving the Langmuir isotherm some assumptions are made:[31]

- Molecules are adsorbed at a fixed number of localized sites.
- Each site can hold one adsorbate molecule.
- The heat of adsorption is independent of surface coverage.

The Langmuir model has proved to adequately describe numerous adsorption systems including adsorption on zeolites[25, 32, 33] and can be expressed as:[10]

$$\Theta = \frac{q}{q_s} = \frac{bP}{1 + bP} \quad (2)$$

In this equation, Θ is the fractional loading, q_s is the saturation loading and b is the adsorption equilibrium constant. At high partial pressures, $q \rightarrow q_s$ and $\Theta \rightarrow 1$, whereas at low partial pressures, $bP << 1$ and:

$$\lim_{P \rightarrow 0} \left(\frac{q}{P} \right) = bq_s = K_H \quad (3)$$

Thus, at low partial pressures Henry's law is valid, and Henry's constant can be determined directly as the slope of the isotherm at low partial pressures. Henry's constant is like all equilibrium constants dependent on the temperature and by observing the temperature dependence, the isosteric heat of adsorption can be determined using the van't Hoff equation[2]:

$$-\left(\frac{\partial \ln K_H}{\partial T}\right)_q = \frac{-\Delta H_{ads}}{RT^2} \qquad (4)$$

In this equation, T is the temperature in Kelvin, ΔH_{ads} is the heat of adsorption and R is the gas constant. By further using $d(1/T)dT = -1/T^2$, equation (4) can be rearranged to:

$$\left(\frac{\partial \ln K_H}{\partial (1/T)}\right)_q = \frac{-\Delta H_{ads}}{R} \qquad (5)$$

Plotting $-\ln K_H$ versus 1/T should yield a straight line with slope $\Delta H_{ads}/R$ from which ΔH_{ads} can be determined.

Adsorption in zeolites

Adsorption in zeolites is of great importance due to the widespread use of zeolites in industry, and for their potential in novel catalytic and separation processes as well as sensitive and selective chemical sensors. Several methods such as gravimetry,[33, 34] calorimetry,[35] NMR spectroscopy,[36-38] XRD,[39-41] FT-Raman spectroscopy,[42-44] ellipsometry,[45] and Monte Carlo simulations[46-49] have been employed for studies of adsorption in zeolites.

Since the scope of the present work is to show that the ATR technique can be used for measuring the adsorption of molecules in MFI films and to test MFI coated ATR elements as chemical sensors, a short introduction to these areas will be given in the next sections.

Adsorption of n-Alkanes and Aromatics in MFI

Two adsorption systems that have been extensively studied are n-hexane/MFI and p-xylene/MFI.[50, 51] In the next two sections, a brief introduction will be given to the adsorption behaviour of n-alkanes and aromatics in MFI, with a focus on n-hexane and p-xylene.

n-Alkanes

Linear alkanes show an interesting adsorption behaviour in MFI.[33, 48, 49] For the shorter linear alkanes (ethane-pentane), simple Langmuir adsorption isotherms have been reported.[25, 32] For linear alkanes longer than pentane, inflections in the isotherms have been observed at a loading of about four molecules per unit cell.[33, 49, 52] Smit and Maesen[48] performed Monte Carlo simulations on n-hexane and n-heptane adsorbed in silicalite-1. They attributed the anomalous adsorption behaviour to a redistribution of the adsorbate molecules with increasing loading. At low partial pressures, the molecules are distributed uniformly in the pore system. At higher partial pressures, the molecules are increasingly adsorbed in the sinusoidal channels, leaving the intersections free. This allows the straight channels to be completely filled, hence maximizing the interaction with the MFI framework. At saturation, half of the molecules (4 molecules/unit cell) resides in the sinusoidal channels and the other half occupy the straight channels.[48, 49] The saturation loading of n-hexane in MFI is hence 8 molecules per unit cell or ~1.4 mmol/g. Further, for n-hexane, the redistribution occurs at about half the saturation loading.[48, 49] Mentzen[39] studied the n-hexane/MFI system with powder XRD and found a similar redistribution. However, as regarding the temperature dependence of the inflection, the results from experiments and simulations diverge. Experimental isotherms[52] suggest that the inflections in the isotherms becomes less pronounced at high temperatures whereas according to Monte Carlo simulations[49] the inflection becomes more pronounced at higher temperatures. In contrast to the results reported by Mentzen,[39] Vlugt et al.[49] and Smit and Maesen,[48] Morell et al.[37] employed powder- and single crystal XRD and could not observe a redistribution of n-hexane at room temperature. However, when the temperature was lowered to 180 K, the molecules were clearly localized in the straight- and sinusoidal channels, leaving the intersections free.

Hence, there seems to be an ordering of n-hexane in MFI at higher pressures, although the ordering may be difficult to detect at room temperature.

The composition of the zeolite may also influence the adsorption properties. Arik et al.[50] investigated the influence of the aluminium content on the adsorption properties of n-alkanes in ZSM-5. For n-hexane, both Henry's constant and the adsorption enthalpy decreased with decreasing aluminium content. As the Si/Al ratio varied from 12 to 400, Henry's constants decreased almost by a factor 5, at the same time the adsorption enthalpy decreased from -75.7 to -66 kJ/mol.

Aromatics

Adsorption isotherms of aromatics (benzene, toluene, ethylbenzene and p-xylene) in MFI show complex adsorption behaviour.[51, 53] At room temperature, all substances show isotherms with one or several steps or kinks. For instance, at room temperature, p-xylene which has been fairly well studied,[25, 34-36, 38, 41, 51, 54-58] show a type IV isotherm with a step at half the saturation loading.[34, 56-58] As the temperature is increased, the isotherm change shape from a type IV to a type I isotherm with a simultaneous reduction in the saturation loading. At room temperature, the saturation loading of p-xylene in MFI is 1.4 mmol/g, or eight molecules per unit cell, whilst at 373 K, the saturation capacity is 0.7 mmol/g.[58] Further, the appearance of the step in the isotherm is influenced by both the composition of the zeolite and type of charge balancing cation.[53, 59, 60] Takaishi et al.[60] and Song and Rees[53] both report that as the Si/Al ratio decreases, the step becomes less pronounced. Takaishi et al.[60] also compared two different cations, viz. H and Na, and found that the step in the isotherm occurs at higher pressures for the Na-form compared to the H-form. Mentzen and Gelin[59] observed that whereas a step appeared in the p-xylene isotherm for HZSM-5, no step appeared in CsZSM-5. In addition, the saturation capacity was lower for CsZSM-5.

The p-xylene/MFI system has also been studied using XRD,[40, 41, 61] NMR,[36, 38] FTIR microscopy[62] and Monte Carlo simulations.[54, 63] These investigations showed that at low loadings (up to 0.7mmol/g) the p-xylene is adsorbed in the

intersections with the long axis oriented mainly in the crystallographic b-direction, whereas at high loadings (above 0.7 mmol/g), the p-xylene adsorbs in the sinusoidal channels as well.

The tight fit between the p-xylene molecule (kinetic diameter: 5.85 Å) and the MFI channels, also induces changes in the MFI framework upon adsorption of p-xylene.[40, 41, 43, 61] Unloaded MFI at room temperature exhibits monoclinic symmetry.[64] As p-xylene starts to adsorb, an orthorhombic phase appears and up to a loading of two molecules per unit cell, the two phases coexists. At loadings between two and four molecules per unit cell, the monoclinic phase disappears. At loadings higher than four molecules per unit cell, when p-xylene starts to adsorb in the sinusoidal channels, a second orthorhombic phase appears. The adsorption of p-xylene also affects the shape of the channels and these become more elliptical upon adsorption of p-xylene.[41]

Zeolite films in Chemical Sensors

A chemical sensor is a device providing insight in the chemical composition of a system in real time.[65] Chemical sensors can further be classified based on detection principle as mass-, thermal-, electrochemical and optical sensors.

Three important concepts for chemical sensors are sensitivity, selectivity and response time.[65, 66] The sensitivity relates to how high or low concentration of the analytes the sensor can detect. Selectivity concerns the ability of the sensor to discriminate between different chemical compounds, and the response time is related to how fast a step change in concentration of an analyte is detected.

A common feature of all zeolite based sensors is that the temperature plays an important role since it may affect sensitivity, selectivity and response time. Since physical adsorption is governed by low temperatures, the sensitivity generally increases with decreasing temperatures. In contrast, the response time is governed by high temperatures as it depends on the diffusion rate, so there has to be a compromise between sensitivity and response time in zeolite based sensors.

Due to their adsorption properties, zeolite films have been utilized in sensor applications. Some examples are quartz crystal micro balances (QCM)[3] and surface acoustic wave (SAW)[67] devices, both of which are mass sensors. Klap et al.[68] reports the use of zeolite films in combination with pyroelectric devices, classified as a thermal sensor. Vilaseca et al.[69] coated a semiconductor with zeolite films to increase the selectivity of what is classified as an electrochemical sensor. Some examples of optical sensors utilizing zeolite films have been reported by Bjorklund et al.[45] who employed ellipsometry to detect the analytes, and Zhang et al.[66] who reported the use of a sensor working by adsorption induced reflectivity changes. The sensor detects changes in the reflectivity of a zeolite film on an optical fibre as analytes are adsorbed in the film.

In the present work, zeolite films were utilized in a novel optical sensor exploiting Internal Reflection Spectroscopy (IRS) in the infrared region.

Infrared spectroscopy

The detection technique used for the adsorption measurements is denoted FTIR/ATR -spectroscopy and will be introduced in this and the following sections.

FTIR spectroscopy is a technique where electromagnetic radiation in the infrared region interacts with a sample.[70] Radiation may be absorbed by the sample if the frequency of the radiation matches that of a molecular vibration. Only vibrations where the dipole moment changes during the vibration can absorb infrared radiation. As a consequence, infrared spectroscopy provides information about vibrations occurring within molecules (and about rotations of gas molecules). The vibrations may be e.g. stretching- or bending vibrations. For stretching vibrations, there is a change in the length of the bond, the change may be symmetric or asymmetric, whereas bending vibrations involve a change in the bond angles. The bonds vibrate at specific frequencies depending on the

masses of the atoms connected by the bond and the strength of the bond. The frequency is for convenience usually expressed in wavenumbers (cm^{-1}).

The relationship between radiation absorbed by the sample, and the sample concentration is given by an expression referred to as Lambert- Beer's law:

$$A = \log \frac{I_0}{I} = \varepsilon bc \qquad (6)$$

In this equation, A is the absorbance, I_0 is the intensity of the incident radiation and I is the intensity of the radiation leaving the sample. Further, ε is the absorptivity, a sample specific constant, b is the sample thickness and c is the sample concentration. The *spectrum* of a sample is the absorbance presented as a function of the wavenumber.

To expand the application areas of Infrared spectroscopy, several different experimental techniques have been developed, such as transmission, diffuse reflectance, photoacustic and internal reflection spectroscopy.

The ATR technique

Internal reflection spectroscopy is a technique where the IR beam is totally reflected at the interface between two media having different refractive indices, a waveguide (ATR element) and a sample.[71, 72] The electric field of the radiation can then interact with a sample placed in contact with the waveguide. Upon interaction with the sample, some of the energy will be absorbed by the sample leading to an attenuation of the energy, hence the technique is often referred to as the Attenuated Total Reflectance (ATR) technique. The technique was originally developed for a single reflection, however it was soon discovered that the sensitivity of the method could be increased by increasing the number of reflections inside the waveguide, see Figure 3.

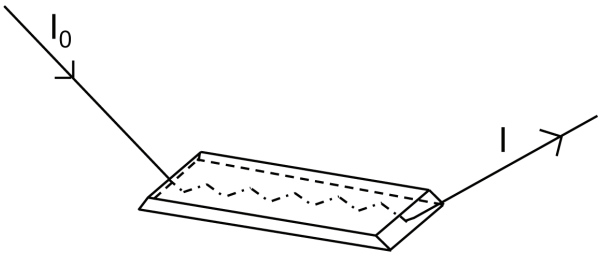

Figure 3. Schematic figure illustrating the ATR technique with the internal reflection of the IR beam in a trapezoidal ATR element.

A necessary condition for total internal reflection is that the angle of incidence is larger than the critical angle, $\theta_{crit} = \sin^{-1} n_{21}$, where $n_{21}=n_2/n_1$ is the ratio of the rarer medium's (sample) refractive index and the denser medium's (waveguide) refractive index. At each reflection, a standing wave is created perpendicular to the surface, and the electric field of this standing wave propagates a small distance out from the surface, with the amplitude of the electric field declining exponentially with distance from the surface, see Figure 4.

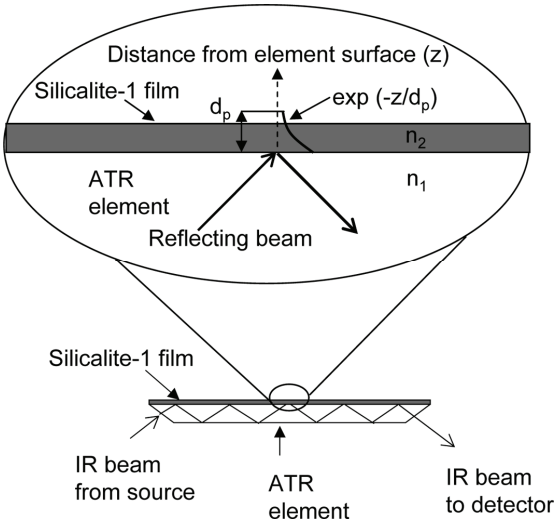

Figure 4. Principle of attenuated total reflection showing an element coated with a silicalite-1 film and the evanescent wave probing the film and the vicinity of the film.

The penetration depth, d_p, of the electric field has been introduced as a measure of how far out the electric field reaches:[71]

$$d_p = \frac{\lambda / n_1}{2\pi\left(\sin^2\theta - n_{21}^2\right)^{0.5}} \qquad (7)$$

In this equation, λ is the wavelength of the IR-radiation and θ is the angle of incidence.

The wavelength dependence of the penetration depth implies that ATR spectra and transmission spectra are not identical. In ATR spectroscopy, radiation with long wavelength will penetrate further into the sample than radiation with short wavelength, causing the bands at longer wavelengths to be more intense than the ones at shorter wavelength.

The penetration depth is usually a couple of hundred nanometers to a few micrometers, making ATR spectroscopy a very surface sensitive technique. For this reason, the ATR technique has become an important tool for studying surfaces and thin films, for instance adsorption of ions and flotation agents on mineral surfaces,[73, 74] diffusion in polymers,[75] structure of membranes,[76] hybrid clay-dye monolayers,[77] and catalytic reactions.[78]

Experimental

Film synthesis

ATR elements

Trapezoidal ATR elements of ZnS, Ge, ZnSe and ZrO_2 (50x20x2 mm) and Si (50x20x1 mm) having 45º cut edges were used. Some of the material properties for the elements are listed in Table 1.

Table 1. Some properties of the ATR elements.

Material	Refractive index at 2000 cm^{-1} (n)[79]	Spectral range (cm^{-1}) ATR[80]
ZnSe	2.43	20000-700
ZnS	2.25	14300-1000
ZrO_2	2.4*	25000-1800
Si	3.42	9400-1500
Ge	4.01	5000-880

* From ref. 80 determined at 1000 cm^{-1}

During film synthesis, zeolite film may be deposited on the cut edges of the element. In the first part of the work (**Paper I-III**), the cut edges of the element were protected by coating the surfaces with an epoxy polymer to prevent zeolite growth on these surfaces. In the second part (**Paper IV-VI**), no protective

coating was applied, instead the film was removed after synthesis by rubbing the edges with cotton soaked in a 0.4 % HF solution.

In order to obtain a surface suitable for seeding, the elements were cleaned prior to film synthesis. In the first part of this work (**Paper I-III**), the following cleaning procedures were used. The ZnS, ZnSe and ZrO_2 elements were immersed in acetone and treated in an ultrasonic bath for ten minutes and subsequently rinsed with distilled water. An alternative procedure[81] was used for the Si elements, which were first treated as described above. That treatment was followed by five minutes of boiling in a solution having the volume composition $5H_2O$: $1H_2O_2$: $1NH_3$, and then boiled another five minutes in a solution having a volume composition of $6H_2O$: $1H_2O_2$: 1HCl. Finally, the elements were rinsed in distilled water. The Ge element was treated in a third manner.[82] The element was first treated in the same way as the ZnS elements, in addition, the element was immersed in a 38 wt% HF solution for 5-10 s and then washed with distilled water. The element was subsequently immersed in a 27 wt% H_2O_2 solution for 10-15 s and then rinsed in distilled water. These two procedures were repeated four times to remove several atom layers of Ge. Finally, the element was oxidized by immersing the element in a 27 wt% H_2O_2 solution for 10-15 seconds. In the second part of this work (**Paper IV-VI**), the elements were cleaned using a three-step procedure. The elements were treated in acetone, ethanol and distilled water in an ultrasonic bath for ten minutes in each solution.

Preparation of films by seeded growth [I-IV]

To render the surface of the elements positively charged, the elements were treated in a 0.4 wt-% solution of a cationic polymer for five minutes. To remove excess polymer, the elements were rinsed with a 0.1 M ammonia solution. Subsequently, the charged reversed elements were immersed in a sol containing 60 nm silicalite-1 seeds. Finally, the seeds were grown into a continuous, polycrystalline silicalite-1 film by hydrothermal treatment at 100ºC for 24 h using a synthesis solution with molar composition 3TPAOH: $25SiO_2$: $1450H_2O$: 100EtOH. Following film growth, the elements were rinsed with a 0.1 M ammonia solution and then dried in an oven at 50ºC. Template molecules and protective polymers were finally removed by calcination at 500ºC.

Preparation of films using an in-situ method [V,VI]

Films were grown on the elements by hydrothermal treatment at 150°C for 5.5 h in a synthesis solution having the molar composition 3 TPAOH: 25 SiO_2: 1600 H_2O: 100EtOH: 0.25 Al_2O_3: 1 Na_2O. To remove any residue from the synthesis, the films were subsequently rinsed in a 0.1 M ammonia solution over night and then dried in an oven at 50°. Finally, the films were calcined in order to remove the template molecules.

Instrumentation

FTIR Adsorption measurements

Adsorption measurements were carried out using two different Infrared spectrometers. In the first part of this work (**Paper I-III**), a Bruker IFS 113V spectrometer equipped with a mercury cadmium telluride (MCT) detector was used. In the second part (**Paper I-III**), a Bruker IFS 66 v/S spectrometer equipped with a liquid nitrogen cooled MCT detector was used. In the work were polarized radiation was employed (**Paper V and VI**), a ZnSe wire grid polarizer was used for obtaining polarized radiation. The cells were mounted at a vertical ATR accessory supplied by Spectratech. Two different types of cells were used, in the early work (**Paper I and II**) a simple non-heatable stainless steel flow cell was used, see Figure 5. The cell was sealed with a viton o-ring and the gas was supplied via tubing through the lid of the spectrometer.

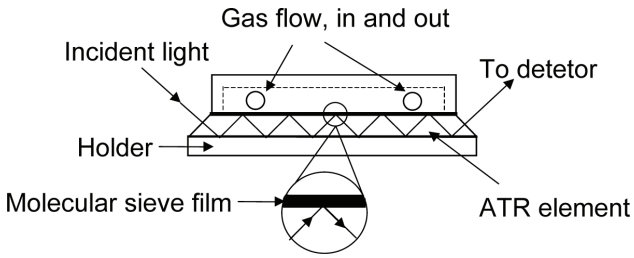

Figure 5. Schematic figure of the non-heatable flow cell.

In most of the work (**Paper II-VI**), a heatable flow cell was used allowing in-situ drying of the film as well as measurements at elevated temperatures. The

cell was manufactured from stainless steel and sealed with graphite gaskets, see Figure 6. Stainless steel tubing through the wall of the sample compartment was used for supplying gas to the cell. Heating cartridges were used for heating the cell and the temperature was measured and controlled via a thermocouple connected to a programmable temperature controller. To pre-heat the feed to the cell, the tubing going to the cell was lined with a heating band covered with insulation. The temperature of the feed was controlled separately, using a thermocouple linked to a PID temperature controller.

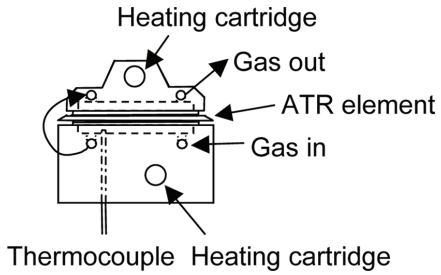

Figure 6. Schematic figure of the heatable flow cell

The composition of the feed to the cells was controlled using a gas delivery system, see Figure 7. The system consists of three mass flow controllers (MFC's) having different flow ranges and two saturators connected in series to ensure saturation of the gas stream. The first saturator was held at room temperature whereas the latter saturator was fitted with a cooling jacket connected to a circuit of thermostated cooling water. Usually, one of the mass flow controllers was used for controlling the flow of the carrier gas to the saturators, whereas one of the others was used for diluting the flow from the saturators to the desired partial pressure of the hydrocarbon.

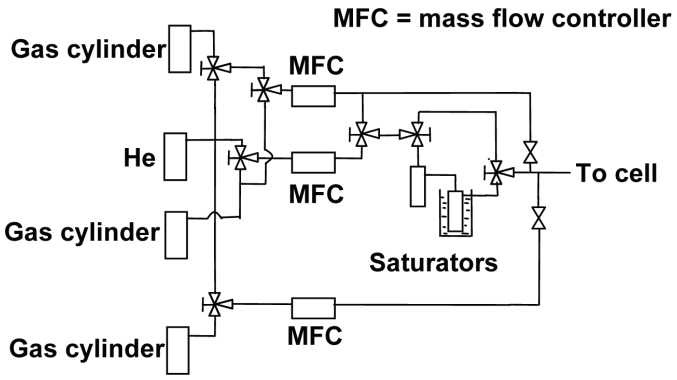

Figure 7. Schematic figure of the gas delivery system

A typical adsorption measurement was performed as follows. The film was first dried, then when the non-heatable cell was used, the films were dried by placing the ATR element in a beaker flushed with dry argon and the beaker was heated to 250ºC for at least 12 h. The element was then mounted in the cell under a flow of dry argon or nitrogen. When the heatable cell was used, the film was dried in-situ at a temperature of at least 260ºC under a feed of pure helium for 12 h. After drying, the cell was mounted in the spectrometer and a background spectrum was recorded by averaging at least 128 scans with a feed of pure helium to the cell. After recording the background, the feed was changed to helium containing a hydrocarbon and when equilibrium was reached, a spectrum was recorded by averaging at least 64 scans.

Additional Characterization

A Scanning Electron Microscope (SEM, Philips XL 30), was used for determining film thickness and investigating the surface morphology of the films. The microscope was equipped with a LaB_6 emission source. X-ray diffraction data was recorded on a Siemens D5000 powder X-ray diffractometer (XRD) and with a Philips XPERT powder diffractometer. The data was used for phase analysis of films and for determining preferential orientation of the crystals in the films. Pole figures were recorded using the latter instrument by scanning ψ and φ from 0° to 82.5° and from 0° to 360°.

Models

Concentration of adsorbed species

In the ATR technique, the Lambert-Beer equation given in equation (6) cannot be applied directly. Instead, Tompkins[83] developed a method applicable in ATR spectroscopy, the method has later been refined by Ohta and Iwamoto[84] and Sperline et al.[85] The absorption per reflection is given by:

$$A/N = \frac{n_{21}E_0^2\varepsilon}{\cos\theta}\int_0^\infty C(z)e^{-2z/d_p}\,dz \qquad (8)$$

In this equation, A is the integrated absorbance, N is the number of reflections, E_0 is the electric field amplitude at the surface of the element, ε is the integrated molar absorptivity determined in CCl_4 and C(z) is the concentration of the adsorbed species as a function of distance, z, from the surface of the element. In this work a step-type concentration profile was used where C(z)=constant for $0<z<d_a$ where d_a is the film thickness and C(z)=0 for $d_a<z<\infty$ i.e. the contribution from the gas phase was assumed negligible. Integration of equation (8) after insertion of the concentration profile yields:

$$A/N = k\frac{n_{21}E_0^2 d_p C}{2\cos\theta}\varepsilon\left(1-e^{-2d_a/d_p}\right) \qquad (9)$$

The correction factor, k, accounts for uncertainties in the effective film thickness, inhomogenitites in the film and grain boundaries etc, and for discrepancies in the molar absorptivities between the ones determined in CCl_4 as solvent and the real ones in MFI.

Further, the "effective thickness", d_e, defined as the distance required for obtaining the same absorbance in a transmission experiment as in an ATR experiment, is given by:

$$d_e = \frac{n_{21}E_0^2 d_p}{2\cos\theta} \qquad (10)$$

The value of d_e is dependent on the polarization of the radiation and can be estimated as:[72]

$$d_e = \frac{I_{0II}}{I_{0II} + I_{0\perp}} d_{e\,II} + \frac{I_{0\perp}}{I_{0II} + I_{0\perp}} d_{e\perp} \qquad (11)$$

I_{0II} and $I_{0\perp}$ represent the intensity of the radiation without sample for parallel- and perpendicular polarized radiation, respectively, see Figure 8. Furthermore, d_{eII} is the effective thickness for radiation with parallel polarization, given by:

$$d_{eII} = \frac{2n_{21} d_p \cos\theta \left(2\sin^2\theta - n_{21}^2\right)}{\left(1 - n_{21}^2\right)\left[\left(1 + n_{21}^2\right)\sin^2\theta - n_{21}^2\right]} \qquad (12)$$

Further, $d_{e\perp}$ is the effective thickness for radiation with perpendicular polarization given by:

$$d_{e\perp} = \frac{2n_{21} d_p \cos\theta}{1 - n_{21}^2} \qquad (13)$$

The refractive index of the ZnS element was set to 2.25[79] and the refractive index for the empty silicalite-1 films and for silicalite-1 films saturated with p-xylene were taken from the work by Nair and Tsapatsis.[86] To account for changes in the refractive index with adsorbate loading, linear models were applied (**Paper IV**). The adsorbate concentration was finally calculated using equations 9 to 13.

Determination of molecular orientation

An advantage with the ATR technique is that it is possible to determine average molecular orientation by using polarized radiation.[87, 88] The orientation of the molecules is determined by transforming the transition moment from the molecular coordinate system into the laboratory frame, and calculating the projection of the moment onto the electric field of the radiation at the surface of

the waveguide. The amplitudes of the electric field for a three layer system[88] (waveguide, film and gas), in y-, x- and z- direction are given by:

$$E_y = \frac{2\cos\theta}{\left(1-n_{31}^2\right)^{0.5}} \tag{14}$$

$$E_x = \frac{2(\cos\theta)\left(\sin^2\theta - n_{31}^2\right)^{0.5}}{\left(1-n_{31}^2\right)^{0.5}\left[\left(1+n_{31}^2\right)\sin^2\theta - n_{31}^2\right]^{0.5}} \tag{15}$$

$$E_z = \frac{2n_{32}^2\sin\theta\cos\theta}{\left(1-n_{31}^2\right)^{0.5}\left[\left(1+n_{31}^2\right)\sin^2\theta - n_{31}^2\right]^{0.5}} \tag{16}$$

In the equations above, n_{31} and n_{32} are the ratios of the refractive indices between the gas (n_3) and the element (n_1) and between the gas and the film (n_2), respectively. In this work the refractive index of the gas was set to 1.[89]

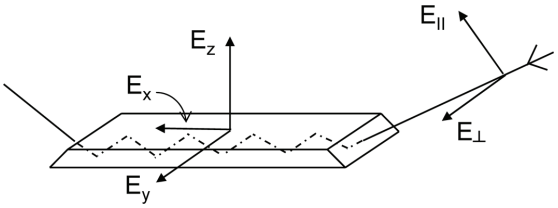

Figure 8. ATR setup with electric field components indicated. E_{II} and $E_\perp$ show the directions of parallel (p)- and perpendicular (s) polarized radiation, respectively. E_x, E_y and E_z are the electric field components in x, y and z directions, respectively.

By recording spectra with radiation that is polarized parallel to the plane of incidence (p-polarized) as well as radiation polarized perpendicular to the plane of incidence (s-polarized), the Dichroic ratio, D, for an absorbance band can be determined:

$$D = \frac{A_s}{A_p} \tag{17}$$

In this equation, A_s and A_p are the absorbances recorded with s- and p-polarized radiation, respectively. Assuming a unixaial distribution of the molecules, i.e. the only preferred tilt angle is between the surface normal and the main axis of the molecule, the dichroic ratio can be written as:

$$D = \frac{A_s}{A_p} = \frac{A_y}{A_x + A_z} = \frac{E_y^2\left(\sin^2\gamma\left(2-3\sin^2\Theta\right)+2\sin^2\Theta\right)}{\left(E_x^2+E_z^2\right)2\sin^2\Theta+\left(2-3\sin^2\Theta\right)\left(E_x^2\sin^2\gamma+2E_z^2\cos^2\gamma\right)} \quad (18)$$

In equation 18, γ is the preferred tilt angle of the main molecular axis from the laboratory z-axis (surface normal) and Θ is the angle between the direction of the transition moment and the main axis of the molecule. When Θ=0, i.e. the direction of the transition moment coincides with the direction of the main axis of the molecules, the expression for the dichroic ratio can be simplified to:

$$D = \frac{E_y^2\sin^2\gamma}{E_x^2\sin^2\gamma+2E_z^2\cos^2\gamma} \quad (19)$$

From equation 19, the tilt angle for p-xylene was determined (**Paper V** and **VI**). For an isotropic orientation distribution of the molecules, the dichroic ratio is given by:

$$D = \frac{E_y^2}{E_x^2+E_z^2} \quad (20)$$

By comparing the experimental dichroic ratio with the value for isotropic distribution, it is possible to get a rough estimate of the molecular orientation.

Results and discussion

Film synthesis and general characterization

Continuous silicalite-1 and ZSM-5 films were successfully grown on zinc sulphide (ZnS), silicon (Si), zirconia (ZrO_2) and germanium (Ge) using the seeding method. Only a few cracks in the film could be observed by SEM after calcination. Figure 9 show typical SEM images of films grown by seeded growth on a Si substrate.

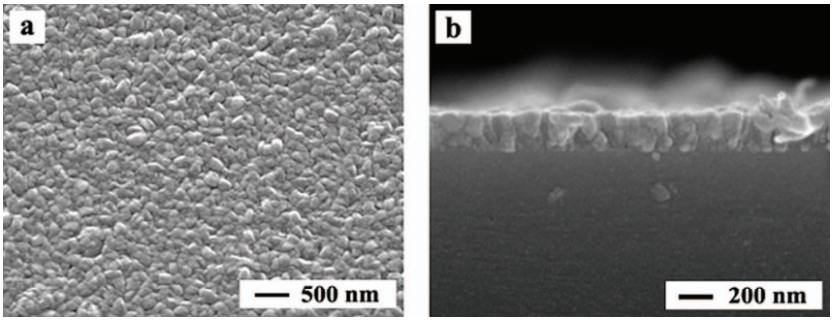

Figure 9. SEM top (a) and side (b) view images of a silicalite-1 film prepared by seeded growth on a Si substrate.

The top view image (a) shows that the top surface of the film consists of small crystals with an average crystal size of less than 200 nm. Moreover, the surface is rough and a careful examination reveals some voids between the crystals. Figure (b) shows that the film thickness is about 200 nm and that even smaller

crystals than at the top of the film is embedded in the interior of the film. This is expected, since the film is grown from seeds with a size of 60 nm.

Figure 10 shows SEM images of a ZSM-5 film grown on a ZnS substrate with the in-situ method. The images show that the film consists of well intergrown crystals with a thickness of about 420 nm, although a few pinholes were observed. Some parts of the substrate were not coated at all.

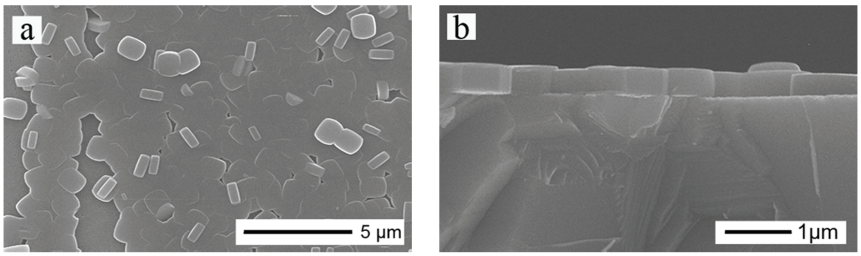

Figure 10. SEM top (a) and side (b) view images of a ZSM-5 film prepared grown in-situ on a ZnS substrate.

The images indicate that the film mostly consists of b-oriented crystals with an average crystal size of about 1µm, together with some a-oriented crystals. In addition there are a few crystals deposited on top of the film.

XRD patterns were collected for films prepared by seeded growth (**Paper II**) and for crystals formed in the bulk solution during synthesis (**Paper II**), as well as for the films prepared with the in-situ method (**Paper V**). The XRD pattern of purified crystals formed in the bulk was typical for randomly oriented MFI crystals, whereas the XRD pattern of the films showed that the films consisted of weakly a-oriented MFI crystals, in accordance with previous findings.[90]

Figure 11 shows an XRD pattern of a film prepared on a ZnS element with the in-situ method. The reflections labelled with * originates from ZnS whilst the reflection labelled with + emanates from the aluminium holder. The XRD pattern shows that the film consists of b-oriented MFI crystals.

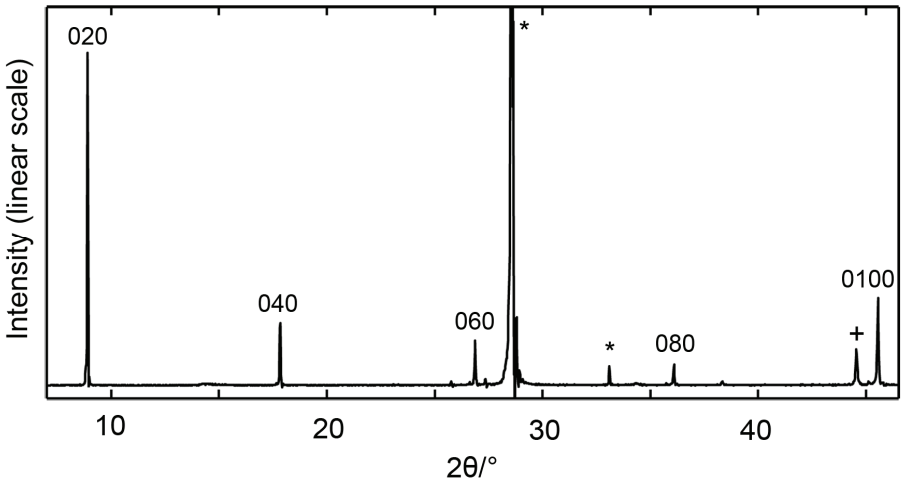

Figure 11. XRD pattern of the coated substrate using the in-situ method. The indexed reflections emanate from the ZSM-5 film and the reflections labeled with * stem from the ZnS substrate. The ZnS reflection at about 28.5° is about 14 times stronger than the (020) reflection. The reflection labeled with + originate from the aluminum holder.

The preferred orientation of the crystals in the film was further studied by pole figure analysis of the (020) reflection, see Figure 12. The recorded intensity is represented by ten iso-intensity lines, the first iso-intensity line corresponds to 17 % of the maximum intensity, and for each additional line the intensity increases with 8 %. Further, the guide circles are separated by 5° in ψ. The data shows that the b-axis of most crystals deviates less than 15° from the surface normal. The data also shows that the crystals are more tilted in the direction φ=90° and 270°, this was unexpected and will be investigated in more detail.

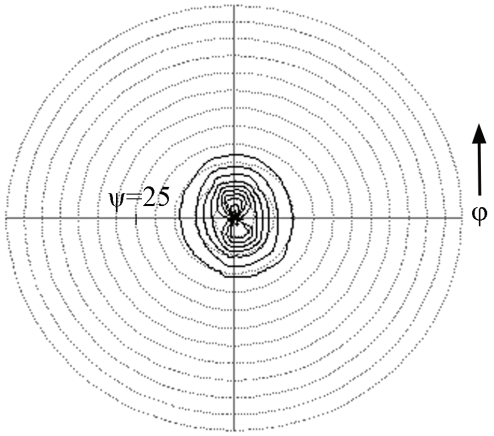

Figure 12. The (020) pole figure of a b-oriented film on a Zns ATR element.

Of the elements tested, the only material that did not perform well was ZnSe. Films grown on ZnSe were damaged during calcination and peeled off. This was probably due to oxidation of the element surface to ZnO during calcination, as ZnO reflections were observed in an XRD pattern recorded after calcination.

FTIR/ATR measurements

The films were further characterized using FTIR/ATR – spectroscopy (**Paper I**). A spectrum of a silicalite-1 film grown on a Si ATR element by seeded growth is presented in Figure 3 in **Paper I**. Absorption bands are observed in the region 2000-1600 cm^{-1}, assigned to overtones of vibrations in the silicalite-1 lattice. Moreover, a band is observed at 3743 cm^{-1}, which is a typical band for terminal SiOH - groups in silicalite-1.

Spectra of films grown on germanium showed an interference pattern. This may be due to the formation of a germanium oxide layer on top of the element and/or due to the formation of small pockets of air between the film and the element.

Sensitivity of ATR elements coated with MFI films as compared to uncoated elements [I-III]

To evaluate the ability of the FTIR/ATR technique to detect hydrocarbons adsorbed in MFI films, experiments were performed with, among others, n-hexane, p-xylene and ethyl benzene (**Paper I-III**). The absorbance from the coated element was compared with the absorbance obtained with an uncoated element. Figure 13 (a) shows the C-H stretching region of spectra recorded without (1) and with (2) a silicalite-1 film. The experiment was carried out at room temperature with a gas mixture containing 1.2 Pa of n-hexane in helium.

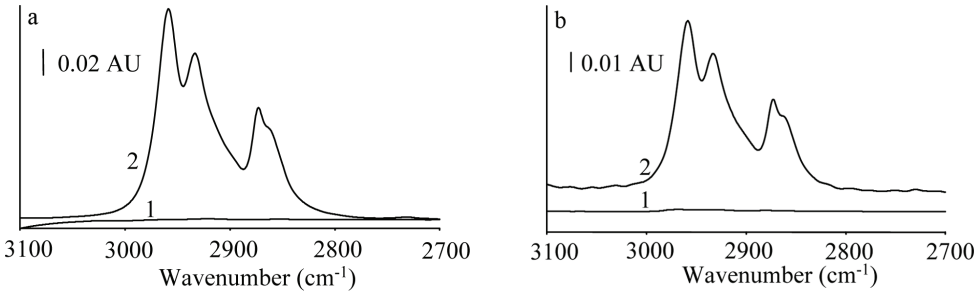

Figure 13. Figure (a) shows IR spectra of n-hexane recorded using an uncoated ZnS element (1) and a silicalite-1 coated element (2). Figure (b) shows IR spectra of n-hexane recorded using (1) a 10 cm gas cell, and (2) a Si element coated on one side with a silicalite-1 film. Both experiments were performed at room temperature with a n-hexane pressure of 1.2 Pa in helium balance to atmospheric pressure.

The uncoated element (1) showed only weak absorption bands, slightly above noise level, whereas distinct bands were obtained using the coated element (2). The peak height of the 2960 cm^{-1} absorption band was approximately 180 times higher for the coated element. The results for p-xylene and ethyl benzene also showed that the signals from the coated elements are much stronger than from uncoated elements. Further, in experiments carried out with the uncoated element at 373 K, where adsorption should be very low, no signal could be detected, not even at the highest n-hexane pressures used in this study. This indicates that the signal observed for the uncoated element at room temperature (Figure 13 (a) spectrum 1) originates from n-hexane adsorbed on the element surface, and that contribution from gas phase can be neglected.

Sensitivity of MFI coated ATR elements compared to a gas cell [III]

Gases that are infrared active can be analyzed in a transmission gas cell. Hence, for comparison experiments were carried out to compare the sensitivity of MFI coated ATR elements as compared with a 10 cm gas cell for detecting hydrocarbons, here exemplified by n-hexane in helium (**Paper III**). The experiments were performed at room temperature using a Si element coated with a silicalite-1 film on one side. The cells were fed with a gas mixture of n-hexane in helium with a n-hexane pressure of 1.2 Pa. Spectrum 1 and 2 in Figure 13 (b) were recorded with a 10 cm gas cell and a sislicalite-1 coated ATR element, respectively. By analyzing the 2967 cm^{-1} band, it was found that the coated element showed approximately 85 times higher absorbance.

A path length of 10 cm can not be considered a particularly long distance, since cells with path lengths of up to 40 m can be purchased and an increased path length in the gas cell would yield a higher absorbance. On the other hand, several methods could be used for increasing the absorbance in ATR spectroscopy. Coating both sides of the ATR element would yield a stronger absorbance, another method would be to decrease the angle of incidence since this would result in more reflections inside the waveguide. Further, increasing the film thickness would result in stronger absorbance since then more of the analyte would be available for detection by the evanescent field (this option would only be possible up to a certain limit depending on the penetration depth). Finally, an interesting way to increase the sensitivity would be to coat longer and thinner waveguides, such as optical fibers, facilitating more reflections, and hence a higher sensitivity.

Response time [III]

As was stated in the literature survey, the response time is an important feature of any sensor and a short response time is often desired. For this reason the response time of MFI coated ATR elements was tested (**Paper III**). In the experiment, a ZnS element coated on both sides with a film prepared by seeded growth was used. The number of scans was reduced to 10 for the shorter data acquisition time needed in this experiment. The film was subjected to a step

increase of n-hexane from 0 to 220 Pa, corresponding to a change in relative pressure from 0 to 0.01 at 300 K. By following the progression of the 2960 cm^{-1} band the response time was indicated. Equilibrium was reached after approximately 250 s, but already at the first point, averaged between approximately t=5 s to t=15 s, the absorbance was 79% of the value at equilibrium, indicating a relatively fast response of the sensor. Further, it is most likely that the response time will be even shorter for thinner films, higher temperatures and molecules with higher diffusivity in the adsorbent.

High sensitivity towards hydrocarbons, a fast response time in combination with the versatility of FTIR spectroscopy, makes zeolite coated ATR elements a very interesting technique for studying adsorption, diffusion and reactions in the films. The sensor seems promising for detection of low concentrations of hydrocarbons in gas phase.

Adsorption of n-hexane and p-xylene in MFI films

To evaluate zeolite coated ATR elements as a tool for studying adsorption in zeolite films in more detail, various experiments were performed by altering hydrocarbon partial pressure in the feed, and the temperature.

Spectra of adsorbed species [IV]

An example of a spectrum of n-hexane adsorbed in a silicalite-1 film prepared by seeded growth (**Paper IV**) is shown in Figure 14. The spectrum was recorded at 10 Pa and 323 K.

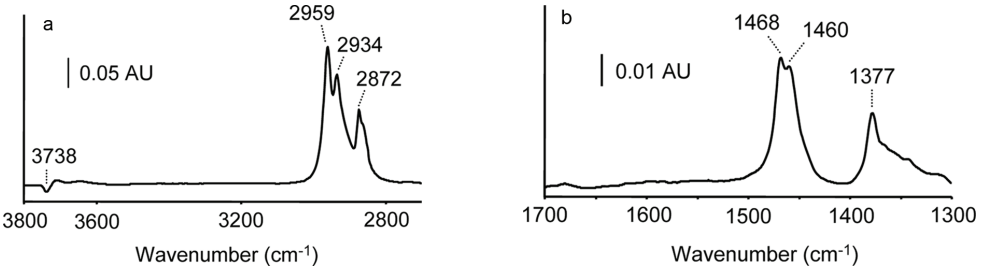

Figure 14. Infrared spectrum of n-hexane (10 Pa and 323 K) adsorbed in a silicalite-1 film. In a) the CH and OH stretching region is shown, whilst in b) the CH deformation spectral region is shown.

The absorption bands indicated in the region 3000-2700 cm^{-1} are assigned to CH_3- and CH_2 stretching vibrations,[70] whereas the bands indicated between 1500-1300 are assigned to CH_3- and CH_2 deformation vibrations. The negative band observed at 3738 cm^{-1} accompanied by the appearance of a new band at slightly lower wavenumbers, is assigned to silanol groups[91] perturbed by adsorbed n-hexane.

Figure 15 shows a spectrum of p-xylene adsorbed in a silicalite-1 film prepared by seeded growth (**Paper IV**). The spectrum was recorded at 323 K and a p-xylene pressure of 108 Pa.

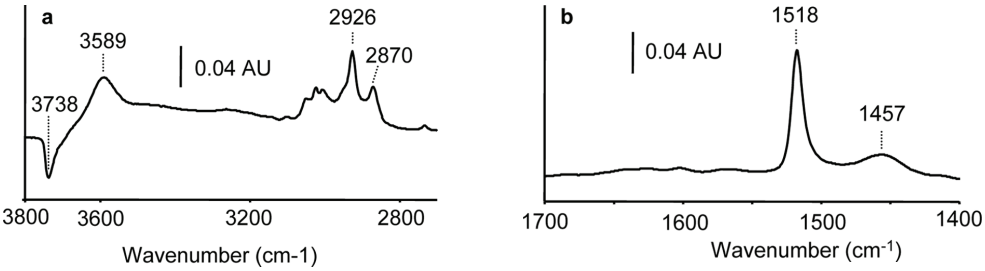

Figure 15. Infrared spectrum of p-xylene (108 Pa and 323 K) adsorbed in a silicalite-1 film. In a) the spectral regions of the CH- and OH stretching vibrations are shown, whereas b) shows the aromatic ring stretching- and CH asymmetric deformation vibration spectral regions.

Prominent bands originating from p-xylene appears in the regions 3200-2800 cm^{-1} and 1600-1400 cm^{-1} and again a negative band is observed at 3738 cm^{-1} together with the emergence of a new band at 3589 cm^{-1}. This shifted band is again assigned to silanol groups perturbed by, in this case, adsorbed p-xylene. The bands at 2926 and 2870 cm^{-1} are assigned to C-H stretching vibration and

C-H deformation overtone, respectively.[62, 92] The bands observed at lower wavenumbers, at 1518 and 1457 cm^{-1} are assigned to a stretching vibration of the aromatic ring and a C-H deformation vibration, respectively.[62, 92]

Spectra of adsorbed species generally showed strong absorption bands, and spectra for both n-hexane and p-xylene were very similar to previous reports.[91,93]

Adsorption isotherms [IV,V]

Bjorklund et al.,[45] determined adsorption isotherms for various substances in silicalite-1 films at room temperature by ellipsometry. They found that the saturation capacity of n-hexane in MFI was in good agreement with values reported for powder. By assuming that this was true also for our films, the correction factor k_{hexane} could be determined to 0.76, which is a reasonable value considering that the molar absorptivity was determined in CCl_4 and that the model used assumes a perfect film without any defects. The correction factor for p-xylene, k_{xylene}, was determined to 0.8, which also, considering the assumptions made, must be regarded as reasonable close to the ideal value of 1.

Adsorption isotherms of n-hexane in silicalite-1 films prepared by seeded growth were determined at five temperatures between 323 and 423 K (**Paper IV**), see Figure 16.

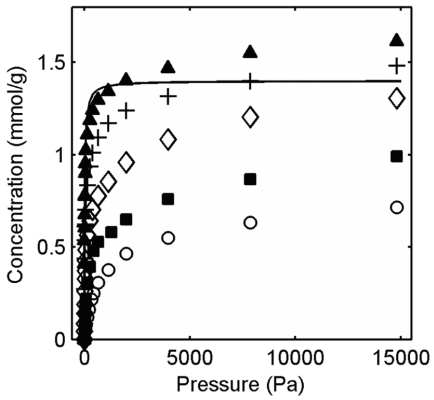

Figure 16. Adsorption isotherms for n-hexane in a silicalite-1 film determined experimentally at 323 (▲), 343 (+), 368 (◊), 393 (■), 423 K (○) in the present work. For comparison, calculated data[47] (Monte-Carlo simulations, 323 K) representing perfect, infinitely large, silicalite-1 crystals (solid line) is included.

The figure shows experimental isotherms from films together with an simulated isotherm reported by Schenk et al.[47] for a perfect zeolite structure without defects. The experimental isotherms are typical for microporous materials with a very fast increase in the amount adsorbed at low partial pressures. At low pressures the isotherms are also very similar to the simulated isotherm. However, at higher pressures, capillary condensation in grain boundaries seems to occur, as indicated by the rise in the isotherms at relative high pressures. This is reasonable since the film is comprised of small (<200 nm) crystals as was observed by SEM, and consequently, the concentration of grain boundaries is high. Similar experimental isotherms, also showing capillary condensation at higher pressures, have been reported for powder samples consisting of small crystals.[25, 94]

Henry's constants were determined from the slope of the isotherms at low pressures and the results are presented in Table 2 together with literature data.

Table 2. Henry's constants for n-hexane obtained in the present work and literature data.

	Henry's constant (mmol/(g*Pa))			
Temp. (K)	This work	Fox et al.[95]	Sun et al.[33]	Clark et al.[96]
323	0.21	0.41	0.023	0.98
343	0.076	0.088	0.005	0.22
368	0.018	0.016	$9.3*10^{-4}$	0.044
393	0.0040	0.004	$2.2*10^{-4}$	0.011
423	$8.6*10^{-4}$	$8.1*10^{-4}$	$4.7*10^{-5}$	0.0024

The reference data was obtained by Monte Carlo simulations,[95] gravimetry[33] and adsorption branch porosimetry.[96] The Henry's constants determined in this work agrees well with previously reported data. Further, the literature data scatter considerably, this may be related to the variety of techniques used as well as zeolite synthesis conditions. It should be noticed at this point, that the Henry's constants determined in this work would be within the range of values reported in the literature even with the correction factor, k_{hexane}, set to 1.

The adsorption enthalpy was determined to -63 kJ/mol, which agrees reasonably well with previously reported data of about -70 kJ/mol.[33, 52, 96]

Adsorption isotherms of p-xylene in MFI at various temperatures (**Paper IV** and **V**) are presented in Figure 17. The isotherms for p-xylene in a 200 nm thick silicalite-1 film with crystal size less than 200 nm (film grown from seeds) (a) and in a 420 nm thick ZSM-5 film with crystal size of about 1μm (in-situ growth) (b).

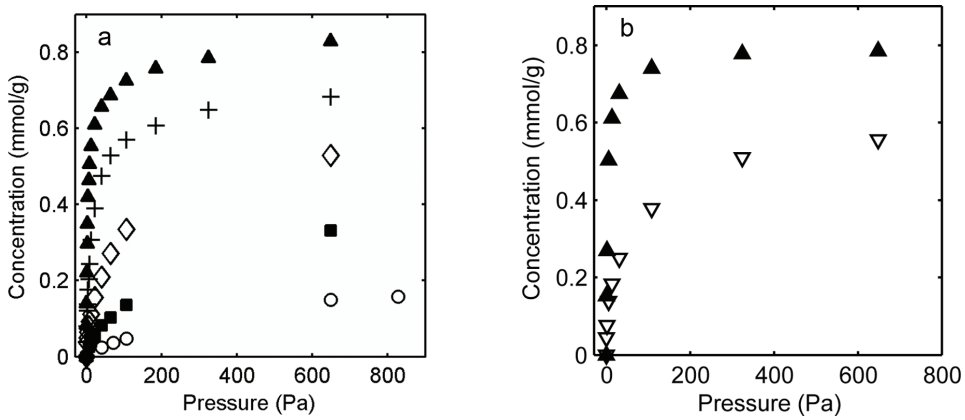

Figure 17. Adsorption isotherms for p-xylene in a silicalite-1 film (a) and in a b-oriented ZSM-5 film (b) determined at 323 (▲), 343 (+), 368 (◊), 373 (▽), 393 (■) and 423 K (○).

Again the isotherms are typical for microporous materials with a fast increase in loading at low pressures corresponding to adsorption in the micropores. At low pressures the isotherms are in excellent agreement with isotherms determined on powder. Furthermore, it can be seen that the isotherms resemble type I isotherms even at the lowest temperature (323 K) in this study. This finding was unexpected since, as was pointed out in the literature study, isotherms of p-xylene adsorbed in MFI powder and unsupported films show type IV isotherms with a distinct step at half the saturation loading at temperatures below ca. 353 K. Further, the maximum loading obtained in this work (~0.8 mmol/g) was reasonably close to the loading reported for the first step in the isotherms determined from powder (~0.7 mmol/g).[58] The type IV isotherms observed for p-xylene adsorption in MFI powder at low temperatures have been attributed to adsorption on two different sites.[40, 41, 61] At low pressures, p-xylene adsorbs in the intersections oriented mainly in the b-direction corresponding to the first step in the isotherm.[41] As the partial pressure is increased, p-xylene starts to adsorb in the sinusoidal channels, corresponding to the second step in the isotherm.[41, 58] The absence of a distinct step in the p-xylene isotherms determined in this work at low temperatures might stem from strain in the zeolite crystals in the film, or that the zeolite framework becomes less flexible when the crystals are bonded to a surface. Strain in supported MFI films have been reported by several groups.[24, 28-30] It was found that the strain slightly alters the dimension of the unit cell of the crystals in the film as compared to the unit cell in powder. Further, it was found that for membranes prepared with the same

seeding method as used in this work, the crystals experiences tensile strain in the b-direction, whereas compressive strain was observed in the a- and c directions.[30] Since there is a close-fit between p-xylene and the MFI channels, it is plausible that even a slight difference in the unit cell dimensions may have great effect on the adsorption properties. It is also conceivable that strain or a less flexible framework prevents the MFI framework from changing symmetry during adsorption of p-xylene, thus hinder adsorption in the sinusoidal channels. Furthermore, Monte Carlo simulations performed on another tight-fit system viz. benzene/MFI, have indeed shown that the outcome of the simulations were very sensitive to small changes in the zeolite structure.[97]

By comparing the isotherms determined at 323 K for the two films shown in Figures 17 (a) and (b), it is evident that the isotherm for the silicalite-1 film prepared by seeded growth does not reach a distinct saturation value, whereas the isotherm for the film grown in-situ, saturation is reached at a pressure of about 300 Pa. This difference is likely caused by fewer grain boundaries as a consequence of the larger crystals in the in-situ film, which will decrease the extent of capillary condensation.

Henry's constants determined from the isotherms in Figure 17 (a) are presented in Table 3 together with literature data.

Table 3. Henry's constants for p-xylene obtained in the present work including literature data.

Temp. (K)	Henry's constant (mmol/(g*Pa))			
	This work	Li and Talu[63]	Talu et al.[57]	Richards and Rees[56]
323	0.39	0.53	0.022	1.06
343	0.072	0.11	0.0054	0.18
368	0.020	0.019	0.0012	0.027
393	0.0038	0.0043	$3.0*10^{-4}$	0.0049
423	$5.5*10^{-4}$	$8.9*10^{-4}$	$7.5*10^{-5}$	$8.5*10^{-4}$

The literature constants were obtained by Monte Carlo simulations[63] and gravimetry.[56, 57] The results obtained in this work agrees well with previous reported data although as for n-hexane, the literature data scatter considerably.
The adsorption enthalpy was determined from the Henry's constants in the same manner as for n-hexane to -73 kJ/mol. This value is in good agreement with previous reported data ranging between -40 and -80 kJ/mol, as compiled by Li and Talu,[63] although most reports are closer to the latter value as the result in the present work.

Dichroism and orientation of adsorbed species [V,VI]

Several of the absorption bands originating from p-xylene adsorbed in the b-oriented ZSM-5 film showed a large dichroism (**Paper V**). Bands having transition moments in the direction of the longest axis in p-xylene showed considerably higher absorbances for p-polarized radiation, implying that the molecules mainly were oriented with the long axis close to the surface normal. Dichroic ratios were determined from the 1518 cm^{-1} band and corresponding tilt angles were determined using equation 19, the results are presented in Figure 18.

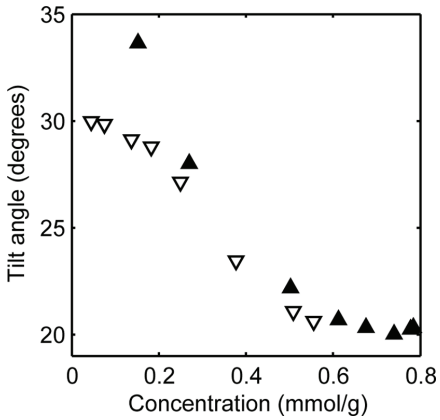

Figure 18. Tilt angle as a function of concentration of p-xylene in the film recorded at 323 K (▲) and at 373 K (∇).

The general trend at both temperatures, is that the tilt angle decreases with increasing p-xylene concentration in the film. The tilt angle at high

concentrations is 20° at both temperatures. This value agrees well with the value of 18° reported by Schüth[62], as determined by FTIR microscopy on large crystals at ca 310 K. However, these values are larger than the values reported by van Koningsveld et al.[41] viz. 7.5° and by Fyfe et al.[36] of 0°. van Koningsveld et al. determined the tilt angle using XRD at room temperature, whereas Fyfe et al. employed $^{1}H/^{29}Si$ CP MAS NMR spectroscopy. The authors stated that, completely reliable data could only be obtained below 213 K, and data recoded above room temperature could not be used for determining the orientation due to extensive molecular motions. From the previous reports on tilt angles, there is a trend that the tilt angle decreases with decreasing temperatures. This is probably related to the increased mobility of the molecules with increasing temperatures as was also observed by Fyfe at al. The present work was conducted at higher temperatures than the previous reports, hence, high mobility of the adsorbate may account for the higher values obtained in the present study. Other possible explanations might be the slightly misaligned crystals as observed in the pole figure (Figure 12), and competitive adsorption on silanol groups as indicated in Figure 15.

At medium concentrations (ca 0.25-0.5 mmol/g) the average tilt angle increases as the concentration decreases and the rate of increase is approximately the same at both temperatures. At low concentrations, the result for the two temperatures differ, the tilt angle determined at 373 K seem to reach a limit of 30°, whereas the tilt angles determined at 323 K reaches 34°. The increase of tilt angles with decreasing adsorbate concentrations might at least partly be due to competitive adsorption on silanol groups.

An experiment was conducted aimed at detecting any redistribution of n-hexane with loading, as was discussed in the literature study. For this purpose the absorption band at 2934 cm^{-1} assigned to the CH_2 asymmetric stretching vibration was used. Figure 19 show the dichroic ratio as a function of n-hexane concentration in the film at 303 K.

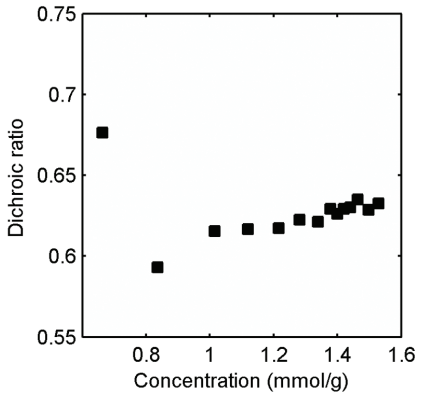

Figure 19. Dichroic ratio of the 2934 cm^{-1} absorbance band as a function of the concentration of n-hexane in ZSM-5 at 303 K.

At higher concentrations (ca 1.0-1.5 mmol/g) the dichroic ratio is fairly constant, only shifting from 0.62 to 0.63 as the concentration increases. In contrast, at concentrations below 0.7 mmol/g in the dichroic ratio is about 0.68, which may indicate a redistribution of the adsorbed n-hexane. Further, the position of the CH_2 asymmetric stretching band was constant over the concentration range studied, indicating that the observed change in dichroism is not a result of a change in average conformation of n-hexane. The result obtained, supports the findings reported by Vlugt et al.,[49] Maginn et al.,[46] Smit and Maesen[48] and Mentzen.[39]

To determine a tilt angle for n-hexane it has to be assumed that the molecules are fully extended i.e. are in all-trans conformation, however it has been shown that this is not the case for n-hexane adsorbed in MFI,[44, 46, 98] therefore no tilt angle was reported in the present work.

Adsorption on silanol groups [IV-VI]

As was illustrated in Figures 14 and 15, both n-hexane and p-xylene adsorb on silanol groups which may affect both concentration measurements as well as the determination of dichroic ratios. An isotherm of p-xylene adsorbed on silanol groups was determined at 323 K, see **Paper V**. The isotherm shows resemblance to a type 1 isotherm however without a distinct saturation point. Adsorption on

silanol groups may at least partially be responsible for the observed change in tilt angle, see Figure 18. If the Henry's constants for adsorption on silanol groups and for adsorption in zeolites are different, this may result in a slope in the plot of tilt angle versus concentration since the two sites are saturated at different rates in that case. When the silanol sites are saturated, the molecules on these sites will give a constant error in the determined tilt angles, resulting in slightly higher tilt angles than what would be the case on a sample without silanol groups.

Conclusions

Silicalite-1 and ZSM-5 films were successfully grown on ATR waveguides of various materials. Films grown by seeded growth were dense and continuous, the films consisted of small (<200 nm) crystals yielding a high concentration of grain boundaries. Films grown in-situ were b-oriented and consisted of large (~1 μm), well intergrown crystals, however these films were discontinuous. Due to the larger crystals, these films had a lower concentration of grain boundaries than the films prepared by seeded growth.

ATR elements coated with zeolite films were applied in FTIR/ATR spectroscopy for the first time. The coated elements were very sensitive to hydrocarbons. The sensitivity was also compared with a standard 10 cm gas cell. It was also shown that the response time of the sensor was relatively fast.

The coated elements were further used for studying adsorption of n-hexane and p-xylene in MFI films. The coated elements were successfully used for determining both isotherms and average molecular orientation. Isotherms for n-hexane were typical for adsorption in a microporous adsorbent, whereas isotherms for p-xylene did not show a second step in the isotherm at lower temperatures as reported for powders. This was attributed to the zeolite framework being less flexible when attached to a surface or to strain in the crystals, as reported by several groups. From the isotherms, Henry's constants and adsorption enthalpies were determined, the results were in agreement with previous findings reported for powders. For films prepared by seeded growth, the isotherms indicated capillary condensation at higher pressures.

Polarized radiation was employed for determining the average orientation of p-xylene and n-hexane adsorbed in a ZSM-5 film. It was found that p-xylene was oriented mainly with the long axis going in the crystallographic b-direction in concert with previous findings. Measurements of n-hexane adsorbed in ZSM-5 indicated that a redistribution of the molecules occurs as reported by other groups.

Competitive adsorption on silanol groups was found to occur in all measurements and is a potential source of error.

The present work has shown that zeolite coated ATR elements in combination with FTIR spectroscopy can be used both as a sensitive sensors for detecting infrared active molecules and as a tool for studying adsorption in zeolite films.

Future work

Since this is a pioneering work on zeolite-coated waveguides, most of the work probably remains. Examples of possible future work are presented below.

- Coat ATR elements with films of other zeolites than MFI.
- Coat optical fibers with zeolite films for use in sensor applications.
- Study reactions catalyzed by the zeolite and possibly identify reaction intermediates.
- Compute defect distribution in the film by comparing isotherms from small (n-hexane) and bulky molecules (triisopropylbenzene).
- Study multi component sorption.
- Measure diffusion of molecules in zeolite films, perhaps even anisotropic diffusion.
- Detection of very small amounts of organic compounds in water.
- Apply zeolite film coated ATR elements to TIR-Raman to be able to detect/study adsorption of molecules that are not infrared active.

References

1. Ohrman, O.; Hedlund, J.; Msimang, V.; Moller, K. *Microporous Mesoporous Mater.* **2005,** 78, (2-3), 199.
2. Ruthven, D. M., *Principles of Adsorption and Adsorption Processes*. 1st ed.; John Wiley & Sons: New York, 1984.
3. Mintova, S.; Bein, T. *Microporous Mesoporous Mater.* **2001,** 50, (2-3), 159.
4. Breck, D., *Zeolite Molecular Sieves*. ed.; Krieger Publishing Company: Malabar, 1984.
5. The International Zeolite Association, S. C., Atlas of Zeolite Framework Types. URL: http://topaz.ethz.ch/IZA-SC/StdAtlas.htm
6. Weitkamp, J. *Solid State Ionics* **2000,** 131, (1-2), 175.
7. Weitkamp, J.; Puppe, L., *Catalysis and Zeolites*. ed.; Springer-Verlag: Berlin, 1999.
8. Szostak, R., *Molecular Sieves*. 2nd ed.; Blackie Academic & Professional: London, 1998.
9. Sing, K.; Everett, D.; Haul, R.; Moscou, L.; Pierotti, R.; Rouquerol, J.; Siemieniewska, T. *Pure Appl. Chem.* **1985,** 57, 603.
10. Do, D. D., *Adsorption analysis: Equilibria and kinetics*. ed.; Imperial College Press: London, 1998.
11. Yan, Y.; Wang, H., Nanostructured Zeolite Films. In *Encyclopedia of Nanoscience and Nanotechnology*, ed.; Nalwa, H. S., 2004, 763.
12. Gump, C. J.; Tuan, V. A.; Noble, R. D.; Falconer, J. L. *Ind. Eng. Chem. Res.* **2001,** 40, (2), 565.
13. Hedlund, J.; Sterte, J.; Anthonis, M.; Bons, A. J.; Carstensen, B.; Corcoran, N.; Cox, D.; Deckman, H.; De Gijnst, W.; de Moor, P. P.; Lai, F.; McHenry, J.; Mortier, W.; Reinoso, J. *Microporous Mesoporous Mater.* **2002,** 52, (3), 179.
14. Gump, C. J.; Lin, X.; Falconer, J. L.; Noble, R. D. *J. Membr. Sci.* **2000,** 173, (1), 35.
15. Hedlund, J.; Jareman, F.; Andersson, C., Factors affecting the performance of MFI membranes. In *Recent Advances In The Science And Technology Of Zeolites And Related Materials,* Pts A - C, ed. ;van Steen, E.; Callanan, L.; Claeys, M., (Eds.), Stud. Surf. Sci. Catal., 154, Elsevier Science, Amsterdam, 2004, p 640.
16. Hedlund, J.; Jareman, F.; Bons, A. J.; Anthonis, M. *J. Membr. Sci.* **2003,** 222, (1-2), 163.
17. Davis, S. P.; Borgstedt, E. V. R.; Suib, S. L. *Chem. Mater.* **1990,** 2, (6), 712.
18. Jansen, J. C.; van Rosmalen, G. M. *J. Cryst. Growth* **1993,** 128, 1150.
19. Yan, Y.; Chaudhuri, S. R.; Sarkar, A. *Chem. Mater.* **1996,** 8, (2), 473.
20. Lovallo, M. C.; Tsapatsis, M. *AIChE J.* **1996,** 42, (11), 3020.
21. Hedlund, J.; Schoeman, B. J.; Sterte, J., Synthesis of ultra thin films of molecular sieves by the seed film method. In *Progress In Zeolite And Microporous Materials,* Pts A-C, ed.; Chon, H.; Ihm, S.-K.; Uh; Y.S.,(Eds.), Stud. Surf. Sci. Catal., 105, Elsevier Science, Amsterdam, 1997, p 2203.
22. Geus, E. R.; Vanbekkum, H. *Zeolites* **1995,** 15, (4), 333.
23. denExter, M. J.; vanBekkum, H.; Rijn, C. J. M.; Kapteijn, F.; Moulijn, J. A.; Schellevis, H.; Beenakker, C. I. N. *Zeolites* **1997,** 19, (1), 13.
24. Dong, J.; Lin, Y. S.; Hu, M. Z. C.; Peascoe, R. A.; Payzant, E. A. *Microporous Mesoporous Mater.* **2000,** 34, (3), 241.
25. Stach, H.; Lohse, U.; Thamm, H.; Schirmer, W. *Zeolites* **1986,** 6, (2), 74.
26. Deckman, H. W.; Cox, D. M.; Bons, A. J.; Carstensen, B.; Chance, R. R.; Corcoran, E. W.; De Gijnst, W.; McHenry, J.; Reinoso, J.; Saunders, R. B.; Tindall, P. J. In *IWZMM2001* Book of abstracts, 2001, p 9.
27. Jareman, F.; Hedlund, J.; Creaser, D.; Sterte, J. *J. Membr. Sci.* **2004,** 236, (1), 81.

28. Gualtieri, M. L.; Gualtieri, A. F.; Hedlund, J.; Jareman, F.; Sterte, J.; Dapiaggi, M., Accurate measurement of the thermal expansion of MFI zeolite membranes by in situ HTXRPD. In *Recent Advances In The Science And Technology Of Zeolites And Related Materials,* Pts A - C, ed.;van Steen, E.; Callanan, L.; Claeys, M., (Eds.), Stud. Surf. Sci. Catal., 154, Elsevier Science, Amsterdam, 2004, p 703.
29. Jeong, H. K.; Lai, Z. P.; Tsapatsis, M.; Hanson, J. C. *Microporous Mesoporous Mater.* **2005,** 84, (1-3), 332.
30. Lassinantti-Gualtieri, M.; Gualtieri, A. F.; Andersson, C.; Hedlund, J.; Jareman, F.; Leoni, M.; Meneghini. *Submitted* **2006**.
31. Shaw, D. J., *Introduction to Colloid and Surface Chemistry*. Fourth edition ed.; Butterworth Heineman, Oxford, 1991.
32. Richards, R. E.; Rees, L. V. C. *Langmuir* **1987,** 3, 335.
33. Sun, M. S.; Talu, O.; Shah, D. B. *J. Phys. Chem. B* **1996,** 100, 17276.
34. Gelin, P.; Dutel, J. F.; Mentzen, B. F. *Microporous Mater.* **1995,** 4, (4), 283.
35. Thamm, H. *J. Phys. Chem.* **1987,** 91, 8.
36. Fyfe, C. A.; Diaz, A. C.; Grondey, H.; Lewis, A. R.; Forster, H. *J. Am. Chem. Soc.* **2005,** 127, (20), 7543.
37. Morell, H.; Angermund, K.; Lewis, A. R.; Brouwer, D. H.; Fyfe, C. A.; Gies, H. *Chem. Mater.* **2002,** 14, (5), 21928.
38. Reicshman, T. P.; Schmitt, K. D.; Olson, D. H. *J. Phys. Chem.* **1988,** 92, 5165.
39. Mentzen, B. F. *Mater. Res. Bull.* **1995,** 30, (11), 1333.
40. Mentzen, B. F.; Gelin, P. *Mater. Res. Bull.* **1995,** 30, (3), 373.
41. van Koningsveld, H.; Tuinstra, F.; van Bekkum, H.; Jansen, J. C. *Acta Cryst.* **1989,** B45, 423.
42. Ashtekar, S.; Hastings, J. J.; Gladden, L. F. *J. Chem. Soc., Faraday Trans.* **1998,** 94, (8), 1157.
43. Huang, Y. *J. Am. Chem. Soc.* **1996,** 118, (30), 7233.
44. Huang, Y.; Wang, H. *Langmuir* **2003,** 19, (23), 9706.
45. Bjorklund, R. B.; Hedlund, J.; Sterte, J.; Arwin, H. *J. Phys. Chem. B* **1998,** 102, (12), 2245.
46. Maginn, E. J.; Bell, A. T.; Theodorou, D. N. *J. Phys. Chem.* **1995,** 99, 2057.
47. Schenk, M.; Vidal, S. L.; Vlugt, T. J. H.; Smit, B.; Krishna, R. *Langmuir* **2001,** 17, (5), 1558.
48. Smit, B.; Maesen, T. L. M. *Nature* **1995,** 374, (6517), 42.
49. Vlugt, T. J. H.; Krishna, R.; Smit, B. *J. Phys. Chem. B* **1999,** 103, (7), 1102.
50. Arik, I. C.; Denayer, J. F.; Baron, G. V. *Microporous Mesoporous Mater.***2003,** 60, 111.
51. Lee, C. K.; Chiang, A. S. T. *J. Chem. Soc., Faraday Trans.* **1996,** 92, 3445.
52. Yang, Y. W.; Rees, L. V. C. *Microporous Mater.* **1997,** 12, (1-3), 117.
53. Song, L.; Rees, L. V. C. *Microporous Mesoporous Mater.* **2000,** 35-36, 301.
54. Mohanty, S.; Davis, H. T.; McCormick, A. V. *Chem. Eng. Sci.* **2000,** 55, (15), 2779.
55. Pope, C. G. *J. Phys. Chem.* **1986,** 90, 835.
56. Richards, R. E.; Rees, L. V. C. *Zeolites* **1988,** 8, (1), 35.
57. Talu, O.; Guo, C.-J.; Hayhurst, D. *J. Phys. Chem.* **1989,** 93, 7294.
58. Xomeritakis, G.; Nair, S.; Tsapatsis, M. *Microporous Mesoporous Mater.* **2000,** 38, (1), 61.
59. Mentzen, B. F.; Gelin, P. *Mater. Res. Bull.* **1998,** 33, (1), 109.
60. Takaishi, T.; Tsutsumi, K.; Chubachi, K.; Matsumoto, A. *J. Chem. Soc., Faraday Trans.* **1998,** 94, (4), 601.
61. Mentzen, B. F. *Mater. Res. Bull.* **1992,** 27, (8), 953.
62. Schüth, F. *J. Phys. Chem.* **1992,** 96, 7493.

63. Li, J.; Talu, O. *J. Chem. Soc., Faraday Trans.* **1993,** 89, 1683.
64. van Koningsveld, H.; Jansen, J. C.; van Bekkum, H. *Zeolites*, **1994,** 10, (4), 235.
65. Janata, J., *Principles of chemical sensors*. ed.; Plenum: New York, 1989.
66. Zhang, J.; Dong, J. H.; Luo, M.; Xiao, H.; Murad, S.; Normann, R. A. *Langmuir* **2005,** 21, (19), 8609.
67. Bein, T.; Brown, K.; Frye, G. C.; Brinker, C. J. *J. Am. Chem. Soc.***1989,** 111, (19), 7640.
68. Klap, G. J.; Wubbenhorst, M.; vanTurnhout, J.; Jansen, J. C.; vanBekkum, H., Modification of a pyroelectric detector by controlled electrocrystallization of thin zeolite layers. In *Progress In Zeolite And Microporous Materials,* Pts A-C, ed.; Chon, H.; Ihm, S.-K.; Uh; Y.S.,(Eds.), Stud. Surf. Sci. Catal., 105, Elsevier Science, Amsterdam, 1997,p 2093.
69. Vilaseca, M.; Coronas, J.; Cirera, A.; Cornet, A.; Morante, J. R.; Santamaria, J. *Catal. Today* **2003,** 82, (1-4), 179.
70. Colthup, N. B.; Daly, L. H.; Wiberley, S. E., *Introduction to Infrared and Raman Spectroscopy*. Third edition ed.; Academic Press: London, 1990.
71. Harrick, N. J., *Internal Reflection Spectroscopy*. ed.; John Wiley & Sons, Inc.: New York, 1967.
72. Mirabella, F. M., *Internal Reflection Spectroscopy: theory and applications*. ed.; Marcel Dekker, Inc.: New York, 1993.
73. Fredriksson, A.; Larsson, M. L.; Holmgren, A. *J. Colloid Interface Sci.* **2005,** 286, (1), 1.
74. Persson, P.; Zivkovic, K.; Sjoberg, S. *Langmuir* **2006,** 22, (5), 2096.
75. Giacinti-Baschetti, M.; Piccinini, E.; Barbari, T. A.; Sarti, G. C. *Macromolecules* **2003,** 36, (25), 9574.
76. Frey, S.; Tamm, L. K. *Biophys. J.* **1991,** 60, (4), 922.
77. Ras, R. H. A.; Németh, J.; Johnston, C. T.; Dékány, I.; Schoonheydt, R. A. *Phys. Chem. Chem. Phys.* **2004**, (6), 5347.
78. Hamminga, G. M.; Mul, G.; Moulijn, J. A. *Catal. Lett.* **2006,** 109, (3-4), 199.
79. Bruker Optics, *Guide for Infrared Spectroscopy*.
80. Harrick Scientific Materials
URL: http://www.harricksci.com/infoserver/optical%20materials.cfm
81. Kern, W.; Puotinen, D. A. *RCA Rev.* **1970,** 31, 187.
82. Prabhakaran, K.; Ogino, T. *Surf. Sci.* **1995,** 325, (3), 263.
83. Tompkins, H. G. *Appl. Spectrosc.* **1974,** 28, 335.
84. Ohta, K.; Iwamoto, R. *Appl. Spectrosc.* **1985,** 39, 418.
85. Sperline, R. P.; Muralidharan, S.; Freiser, H. *Langmuir* **1987,** 3, (2), 198.
86. Nair, S.; Tsapatsis, M. *Microporous Mesoporous Mater.* **2003,** 58, (2), 81.
87. Ahn, D. J.; Franses, E. I. *J. Phys. Chem.* **1992,** 96, (24), 9952.
88. Neivandt, D. J.; Gee, M. L.; Hair, M. L.; Tripp, C. P. *J. Phys. Chem. B* **1998,** 102, (26), 5107.
89. Kaye &Laby, *National Physical Laboratory, UK*
URL:*http://www.kayelaby.npl.co.uk/general_physics/2_5/2_5_7.html*.
90. Engstrom, V.; Mihailova, B.; Hedlund, J.; Holmgren, A.; Sterte, J. *Microporous Mesoporous Mater.* **2000,** 38, (1), 51.
91. Jentys, A.; Tanaka, H.; Lercher, J. A. *J. Phys. Chem. B* **2005,** 109, (6), 2254.
92. Green, J. H. S. *Spectrochim. Acta* **1970,** 26A, 1503.
93. Lin, Y. S.; Yamamoto, N.; Choi, Y.; Yamaguchi, T.; Okubo, T.; Nakao, S. I. *Microporous Mesoporous Mater.* **2000,** 38, (2-3), 207.
94. Jacobs, P. A.; Beyer, H. K.; Valyon, J. *Zeolites* **1981,** 1, (3), 161.
95. Fox, J. P.; Rooy, V.; Bates, S. P. *Microporous Mesoporous Mater.* **2004,** 69, (1-2), 9.

96. Clark, T. E.; Deckman, H. W.; Cox, D. M.; Chance, R. R. *J. Membr. Sci.* **2004,** 230, (1-2), 91.
97. Clark, L. A.; Snurr, R. Q. *Chem. Phys. Lett.* **1999,** 308, (1-2), 155.
98. Smit, B.; Siepman, I. J. *J. Phys. Chem.* **1994,** 98, 8442.

Paper I

Zeolite coated ATR crystals for new applications in FTIR ATR spectroscopy

Zheng Wang, Margareta L. Larsson, Mattias Grahn, Allan Holmgren and Jonas Hedlund

Chemical Communications 24 (2004) 2888

COMMUNICATION

ChemComm
www.rsc.org/chemcomm

Zeolite coated ATR crystals for new applications in FTIR-ATR spectroscopy

Zheng Wang[a], Margareta L.Larsson[b], Mattias Grahn[a], Allan Holmgren[b*] and Jonas Hedlund[a*],
[a] *Division of Chemical Technology, Luleå University of Technology, S-971 87 Luleå, Sweden. Fax: + 46 920 491199; Tel: + 46 920 492105; E-mail: jonas.hedlund@km.luth.se*
[b] *Division of Chemistry, Luleå University of Technology, S-971 87 Luleå, Sweden. Fax: + 46 920 491199; Tel: + 46 920 492140; E-mail: Allan.Holmgren@km.luth.se*

***This submission was created using the RSC ChemComm Template* (*DO NOT DELETE THIS TEXT*)**

(*LINE INCLUDED FOR SPACING ONLY - DO NOT DELETE THIS TEXT*)

Thin silicalite-1 films were grown on ATR crystals and used for detection of low amounts of organic molecules in a gas flow.

Molecular sieves have a number of unique properties that make them interesting in various application areas [1-2]. They are inorganic, microporous materials with large surface areas and well-defined channel systems due to the fact that they are crystalline [3]. Molecular sieves are currently used in large quantities as shape-selective catalysts, adsorbents and ion-exchangers. Selective and strong adsorption render molecular sieves interesting in sensors for detection of low concentrations of molecules in gas or liquid phase. A limitation in novel as well as in several of the established applications of molecular sieves is the lack of knowledge of the adsorption and transport phenomena determining the performance of the materials. Despite the fact that the number of studies devoted to the adsorption of various molecules in zeolites are numerous, few investigations exist where competitive adsorption from mixtures have been studied. Moreover, the reports focusing on kinetic aspects of adsorption, particularly competitive adsorption, are few. This is obviously related to the fact that such studies require well-defined materials, but also to a lack of simple analytical techniques making such studies possible.

In the last decade total internal reflection (TIR) spectroscopy using optical fibers and ATR (Attenuated Total Reflection) elements has become one of the fastest growing sensor applications within modern analytical chemistry [4-6]. In the ATR technique, the IR beam is totally reflected inside a waveguide. At each reflection an evanescent field is created at the surface of the waveguide. This field is used in ATR spectroscopy to probe the nearest vicinity of the waveguide. The ATR-technique is useful for investigation of interfacial phenomena in situ. Coated internal reflection elements (IRE) are especially interesting and have been used in various applications [7-8]. A number of studies report the use of polymer coated IREs for detection of organic pollutants and in particular chlorinated hydrocarbons in water [9-11]. It has been demonstrated that the thin film serves as an extractor phase enriching the analyte in close vicinity to the sensor surface. Such studies also suggest that the use of a solid film with high surface area, with maximum adsorbent/IRE contact, is vital. However, applications for various film/IRE combinations are really limited by the ability of depositing a thin, uniform, self-supporting film upon the IRE.

A method employing seeding has been developed in our laboratory for the synthesis of ultrathin as well as thick zeolite films [12]. The method is very flexible, not very surface sensitive, and allows for reproducible preparation of films of desired thickness and crystal orientation using a number of zeolite-substrate combinations [13-15]. The objective of the work described in the present communication is to synthesize and characterize thin silicalite-1 films on ATR-crystals and to demonstrate the use of the film for detection of organic compounds in a gas flow. To the best of our knowledge, well defined molecular sieve films supported by ATR-crystals for FTIR spectroscopy have not been reported in the literature before.

A schematic of the flow cell (volume ~ 3 ml) containing the silicalite-1 coated ATR crystal is shown in Fig. 1. The size of the Si IRE is 50 x 20 x 1 mm^3 with a trapezoidal form (45°). Only one side of the ATR element is coated with a silicalite-1 film. The flow cell is constructed of stainless steel and is sealed with a viton o-ring. The IRE in the cell was placed in the beam path in the spectrometer and a gas flow was fed to the cell via tubing through the lid of the spectrometer. The gas flows used in the experiment were produced by a gas delivery system consisting of three mass flow controllers and two saturators containing hydrocarbons.

The Si ATR crystal was first modified by the following procedure: The cutting edges and the back side were coated with an epoxy polymer (Araldite 2014, Vantico AG, Basel, Switzerland) and then moved into a preheated oven at 50 °C for 24h in order to complete the curing of the polymer. The polymer protects the edges and back side of the IRE from zeolite crystallization. The polymer protected Si IRE was rinsed for 10 minutes in acetone in an ultrasonic bath and then boiled for 5 minutes in a mixture having the volume composition of $5H_2O$: $1H_2O_2$: $1NH_3$ (30 wt % H_2O_2 and 25 wt % NH_3). The crystal was rinsed with distilled water and boiled for 5 minutes in another mixture with a volume composition of $6H_2O$: $1H_2O_2$: 1HCl (30 wt % H_2O_2 and 37 wt % HCl). Finally, the substrate was rinsed thoroughly with distilled water.

A short description of the synthesis of zeolite films follows; details can be found elsewhere [15]. The silica source used was tetraetoxysilane (TEOS, > 98 %, Merck). Tetrepropylammonium hydroxide (TPAOH, 40 % aqueous solution, Sigma) was used as the structure directing agent and the alkali source. Distilled water was used in all cases. The method used for film preparation in the present study basically consists of three main steps: i) Preparation of 60 nm colloidal molecular sieve seeds. The seeds are grown from a synthesis mixture with a molar composition of 9TPAOH: $25SiO_2$: $360H_2O$: 100EtOH. ii) Deposition of seeds onto cationic polymer (Redifloc 4150, Eka Chemicals) coated substrate by electrostatic adsorption. iii) Growth of the seed crystals into a continuous, polycrystalline film at 100 °C for 24 h in a synthesis solution with the molar composition 3TPAOH: $25SiO_2$: $1450H_2O$: 100EtOH. After completed film crystallization, the samples are rinsed overnight with a 0.1 M ammonia solution and dried at room temperature. Finally, in order to remove the TPA template molecules blocking the zeolite channels and to remove the polymer protecting the cutting edges and back side, all films were heated in air at 500 °C for 4 h using a heating and cooling rate of 0.8 °C/ minute.

A Philips XL 30 Scanning Electron Microscope (SEM) equipped with a LaB_6 emission source was used for studies of surface morphology and film thickness. A Siemens D5000 powder X-ray diffractometer (XRD) running in the Bragg-Brentano geometry was used to collect XRD data. The IR-spectrometer used was a Bruker IFS113V (pressure ~ 1mm Hg) equipped with a MCT-detector.

After 24 h crystallization at 100 °C, the adsorbed seed crystals had increased in size and formed a continuous and transparent film, see Fig. 2. A top view of the calcined silicalite-1 film on a Si crystal is shown in (a). The calcined film is dense and continuous. No cracks or other defects can be detected by SEM. Fig. 2 (b) shows a side view image of the film. The film thickness is constant and about 180 nm. XRD patterns were collected in the 2θ region from 5° to 27° where the most intense MFI reflections are located. The XRD data confirms that the films consist of pure MFI crystals.

In Fig. 3 the spectrum of a silicalite-1 film on a Si ATR element is shown (A). Silicalite-1 has some spectral features from 1600 – 2000 cm^{-1}; these are assigned to the overtones of silicalite-1 lattice vibrations. The spectrum also shows an IR band in the OH-stretching region at 3743cm^{-1} corresponding to terminal SiOH-groups. Before the spectrum of the film was recorded, the silicalite-1 coated Si IRE had been dried at 250 °C for more than 12 h in dry argon. Spectrum B was recorded 5 minutes after the cell had been connected to a flow of helium and n-hexane ($p/p_0 \approx 0.01$). For both spectrum A and B, a single beam spectrum of a dry uncoated Si IRE was used as background. In spectrum C, the background was the silicalite-1 coated IRE. The peak-height at 2960 cm^{-1} in spectrum C was about 0.1 absorbance units. This is a promising result since it should be possible to detect at least 100 times less than this amount and still achieve a good signal to noise ratio. It was not possible to detect n-hexane when the experiment was carried out with a Si IRE that was not coated with a silicalite-1 film.

In summary, this communication presents the synthesis and characterization of a thin silicalite-1 film on a Si IRE substrate. It was possible to detect low concentrations of organic molecules in a gas flow by this sensor. The sensor offers the possibility to study both the adsorbate and the adsorbent. Another intriguing possibility that should be mentioned is that of using ATR-FTIR for in situ studies of catalytic reactions taking place within the molecular sieve structure.

The Swedish Research Council (VR) is acknowledged for financial support of this work.

Notes and references

† Footnotes should appear here. These might include comments relevant to but not central to the matter under discussion, limited experimental and spectral data, and crystallographic data.

1 M.E. Davis, Nature 417 (2002) 813.
2. M. Tsapatsis, AICHE J. 48 (2002) 654.
3. D.W. Breck, Zeolite Molecular Sieves, Krieger Publ. Company, Malabar, (1984) p 5.
4. K.K. Chittur, Biomaterials, 19 (1998) 357.
5. D.R. Scheuing, ACS Symp. Ser. 447 (1991) 1.
6. J.J Workman, Appl. Spectrosc. Rev., 34 (1999) 1.
7. R.P. Sperline and Y. Song, Langmuir 13 (1997) 6985.
8. T. Snabe and S.B. Petersen, J. Biotechnol. 95 (2002) 145.
9. R. Krska, K. Taga and R. Kellner, Appl. Spectros. 47 (1993) 1484.
10. R. Göbel, R. Krska, R. Kellner, R.W. Seitz and S.A. Tomellini, Appl. Spectros. 48 (1994) 678.
11. R. Göbel, R.W. Seitz, S.A. Tomellini, R. Krska and R. Kellner, Vib. Spectrosc. 8 (1995) 141.
12. J. Sterte, J. Hedlund and B.J. Schoeman, " Procedure for preparing molecular sieve films" US Pat. 6,177,373, 2001.
13. J. Sterte, J. Hedlund, D. Creaser, O. Öhrman, Z. Wang, M. Lassinantti, Q. Li and F. Jareman, Catal. Today 69 (2001) 323.
14. Z. Wang, J. Hedlund and J. Sterte, Micropor. Mesopor. Mater. 52 (2002) 191.
15. J. Hedlund, S. Mintova and J. Sterte, Micropor. Mesopor. Mater. 28 (1999) 185.

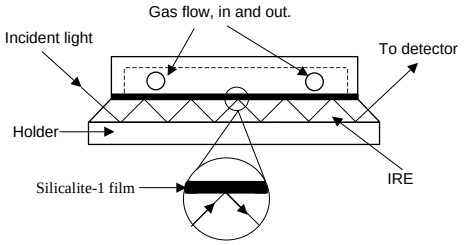

Fig.1 Schematic picture of the flow cell and IRE.

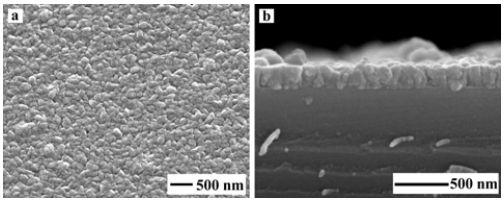

Fig. 2 Top (a) and side (b) view images of a silicalite-1 film on a Si IRE.

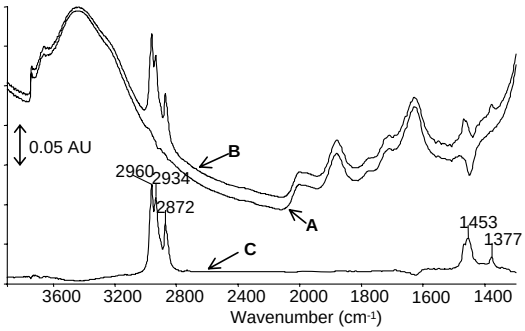

Fig. 3 (A) Spectrum of a silicalite-1 film on a silicon ATR-element, (B) spectrum of silicalite-1 film 5 minutes after the cell was filled with a dilute gas mixture of n-hexane in helium ($p/p_0 \approx 0.01$), (C) spectrum of the n-hexane adsorbed in the silicalite-1 film on the silicon ATR-element. For both spectrum (A) and (B), the single beam spectrum of a Si IRE was used as background. In spectrum (C), the silicalite-1 coated Si IRE was used as background.

Paper II

Zeolite coated ATR crystal probes
Zheng Wang, Mattias Grahn, Margareta L. Larsson, Allan Holmgren, Johan Sterte and Jonas Hedlund
Sensors and Actuators B: Chemical 115 (2006) 685

Available online at www.sciencedirect.com
SCIENCE DIRECT
Sensors and Actuators B 115 (2006) 685–690
SENSORS AND ACTUATORS B CHEMICAL
www.elsevier.com/locate/snb

Zeolite coated ATR crystal probes

Zheng Wang [a], Mattias Grahn [a], Margareta L. Larsson [b], Allan Holmgren [b], Johan Sterte [c], Jonas Hedlund [a,*]

[a] *Division of Chemical Technology, Luleå University of Technology, S-971 87 Luleå, Sweden*
[b] *Division of Chemistry, Luleå University of Technology, S-971 87 Luleå, Sweden*
[c] *Växjö University, SE-351 95 Växjö, Sweden*

Received 13 July 2005; accepted 28 October 2005
Available online 5 December 2005

Abstract

Thin and well-defined MFI type molecular sieve films were grown on a range of ATR crystals by employing a seeding method. The type of ATR crystal does not influence film morphology. FTIR spectroscopy was used to evaluate the coated ATR crystals as sensor probes. These novel sensor probes could be used to detect low concentrations of organic molecules in a gas flow.

Keywords: Zeolite film; Seeding method; ATR crystals; FTIR spectroscopy; Sensor

1. Introduction

In the last decade, total internal reflection (TIR) spectroscopy using optical fibers and attenuated total reflection (ATR) elements has become one of the fastest growing sensor applications within modern analytical chemistry. Attenuated total reflectance Fourier transform infrared spectroscopy (ATR-FTIR) is one of the most developed and increasingly used techniques, currently available to scientists for investigations of interfacial phenomena in situ. In ATR spectroscopy, the IR beam is totally reflected inside a waveguide brought in contact with the sample. At each reflection, a standing wave of the infrared radiation is formed, which is probing the vicinity of the waveguide and causing an attenuation of the totally reflected beam in the waveguide. The large amount of applications using ATR-FTIR spectroscopy is revealed by a number of comprehensive reviews [1–3]. The investigations using ATR-FTIR can roughly be summarized as studies of adsorption from fluid directly on the surface of the internal reflection element (IRE), on IRE coated with a thin film, or on a particulate solid with high surface area in contact with the IRE [4]. Coating of the IRE with a thin film is an extremely effective and interesting means of studying interfacial phenomena and has been successfully used in various applications. Lu et al. [5] detected low concentrations of benzene in water using a silicon IRE coated with a mesoporous silica film. Rivera and Harris [6] studied the kinetics of transport and binding of several probe molecules within thin silica sol–gel films using a Ge IRE. Sperline et al. [7,8] produced an alumina coated ZnSe IRE to quantitatively determine surface excess values and information of the orientation of adsorbed compounds. Snabe and Petersen [9] monitored enzymatic activity on lipase and starch films prepared directly on ZnSe ATR crystals. Chittur [2] demonstrated the feasibility of studying protein adsorption on bioceramic coatings deposited at germanium ATR crystals. Kellner and co-workers describe a number of reports of using polymer coated IREs for the detection of organic pollutants and in particular chlorinated hydrocarbons in water [10,11]. Recently, Roy and Mielczarski [12] claimed the simultaneous detection of six chlorinated hydrocarbons in their mixture with sensitivity as low as a few ppb using a polymer coated ZnSe crystal. The studies mentioned above demonstrated that the thin film serves as an extractor phase enriching the analyte in close vicinity to the sensor probe surface. Such studies also suggest that a maximum adsorbent/IRE contact could be reached by the use of a solid film with relatively high surface area. However, the application of various film/IRE combinations is limited by the lack of techniques for preparation of a thin, uniform and self-supporting film.

Traditionally, zeolites have been defined as natural or synthetic crystalline aluminosilicates with a microporous frame-

* Corresponding author. Tel.: +46 920 492105; fax: +46 920 491199.
E-mail address: Jonas.Hedlund@ltu.se (J. Hedlund).

0925-4005/$ – see front matter © 2005 Elsevier B.V. All rights reserved.
doi:10.1016/j.snb.2005.10.039

work, which is constructed by a network of AlO_4 and SiO_4 tetrahedra [13]. Zeolites are currently used in large quantities as shape-selective catalysts, adsorbents and ion-exchangers [14–17]. A great potential exists for further utilization in novel technologically sophisticated applications such as membranes for separation or as thin film catalysts and sensors [18]. Zeolite membranes can carry out separations based on differences in size, shape or adsorption strength of molecules in a mixture [19–21]. Significant adsorption at very low concentration and extremely large surface area further make molecular sieves interesting in sensor applications for detection of low concentrations of molecules in gas or liquid phase. The utilization of zeolite films in sensor probes has been reported previously. Examples are quartz crystal micro balances (QCM) [22] and surface acoustic wave (SAW) devices [23]. Thermal sensors in the form of pyroelectric devices utilizing zeolites [24] have also been reported. Bjorklund et al. reported an optical sensor probe using ellipsometry in combination with a molecular sieve film [25].

A number of methods for preparation of zeolite films have been developed. Generally, these methods can be separated in three groups: in situ crystallization, vapor-phase transport method (VPT) and seeding methods. Direct crystallization or in situ crystallization of molecular sieve films on the support is the simplest strategy for film preparation [26,27]. However, a considerable film thickness is often necessary to obtain a completely dense film. In the VPT method, the support is coated with an amorphous gel containing all the necessary nutrients and subsequently heated in a vapor containing structure-directing agents in order to transform the gel into a film [28]. A number of zeolite structures have been prepared by this method [29,30]. One disadvantage with this method seems to be crack formation in the amorphous gel layer. A method employing seeding has been developed in our laboratory for the synthesis of ultrathin (>100 nm), as well as thicker zeolite films [31,32]. In this technique, small seed crystals are first deposited on the substrate surface and subsequently grown into a continuous film under hydrothermal treatment. An advantage with this method is that the seeding increases the density of nuclei/seeds on the surface. Furthermore, nucleation/seeding and growth of the zeolite on the surface of the support is carried out in separate steps, which renders the method more flexible and less surface sensitive than the direct crystallization method. Various molecular sieves on a variety of supports have been synthesized with desired thickness and crystal orientation [33–38]. Furthermore, preparation of compositionally zoned MFI films, consisting of a ZSM-5 film with a silicalite-1 intergrowth, has been demonstrated [39,40]. In parallel, Tsapatsis and co-workers [41,42] have developed a similar method.

MFI type zeolite has a channel system of sinusoidal 10-ring (5.1 Å × 5.6 Å) and intersecting straight 10-ring (5.3 Å × 5.6 Å) channels [43]. The MFI type zeolites include two synthetic species with varying chemical composition: silcialite-1 and ZSM-5. According to the classical definition, silicalite-1 is a molecular sieve instead of a zeolite, since it is a pure silica analogue of ZSM-5. Silicalite-1 is more hydrophobic than ZSM-5 and has no ion-exchange capacity. It is an efficient adsorbent of organic molecules from water. ZSM-5 has a Si/Al ratio of 10 and upward, which results in acidity. The combination of catalytic activity and molecular sieve properties explain the use of ZSM-5 as a catalyst with unique shape selectivity in reactions such as toluene alkylation, alkyl-benzene disproportionation, dialkylbenzene isomerization and Fries rearrangement of aryl esters [44–48].

The objective of the present study is to grow and characterize thin, well-defined layers of MFI type molecular sieve on various ATR crystals and in combination with FTIR spectroscopy demonstrate the use of these composites as sensor probes.

2. Experimental

2.1. Materials and pretreatment

Deposition of zeolite films on a range of ATR crystals is demonstrated in the present work, properties of the selected IREs are given in Table 1. The IREs were purchased from Spectroscopy Central Ltd., UK. The size of most of the IREs was 50 mm × 20 mm × 2 mm with a trapezoidal form (45°), the Si IREs were 1 mm thick. The cutting edges of the ATR crystals were coated with an epoxy polymer (Araldite 2014, Vantico AG, Basel, Switzerland) in order to prevent zeolite growth. After application of the polymer, the IREs were placed in an oven preheated to 50 °C. After 1 h, the temperature of the oven was increased to 110 °C for 24 h in order to complete the curing of the polymer. After application of the polymer, the ATR substrates were cleaned. Method 1 was used for ZnS, ZnSe and ZrO_2 substrates. Crystals in this group were rinsed in acetone under ultrasound treatment for 10 min and then rinsed with distilled water. Method 2 was used for silicon substrates. In this case, the substrates were first treated according to method 1. The substrates were subsequently boiled for 5 min in a solution with a volume composition $5H_2O$:$1H_2O_2$:$1NH_3$ (volume parts

Table 1
Properties of IRE supports

IRE material	Refractive index at 1000 cm^{-1} (n)	Density, ρ (g/cm^3)	Melting point (°C)	Spectral range (cm^{-1})[b]	Pretreating method
ZnSe	2.4	5.27	1520	20000–650	1
ZnS	2.2	4.08	1830	17000–950	1
ZrO_2	2.4	5.9	2700	25000–1800	1
Si	3.4	2.33	1420	9500–1500 350–FIR	2
Ge	4.0	5.32	936	5500–870	3

of 30 wt% H_2O_2 and 25 wt% NH_3) and then boiled for 5 min in a solution with a volume composition $6H_2O$:$1H_2O_2$:1HCl (volume parts of 30 wt% H_2O_2 and 37 wt% HCl). Finally, the silicon substrates were washed with distilled water. Method 3 [49] was used to clean Ge ATR substrates. Following treatment according to method 1, the Ge crystals were dipped in a 38 wt% HF solution for 5–10 s and washed with distilled water. The Ge substrates were then dipped in a mixture of 27 wt% H_2O_2 for 10–15 s and rinsed with distilled water again. These two procedures were repeated four times to ensure the removal of several atom layers of Ge. Finally, the surface was oxidized by dipping the Ge crystal in a 27 wt% H_2O_2 solution for 10–15 s.

2.2. Growth of zeolite film on ATR crystals

The silica source for molecular sieve synthesis was tetraetoxysilane (TEOS, >98%, Merck) and the alumina source was aluminum isopropoxide (>98%, Sigma). Tetrepropylammonium hydroxide (TPAOH, 40% aqueous solution, Sigma) was used as the structure-directing agent and alkali source. The sodium source was NaOH beads (Eka Chemical, analysis grade). Distilled water was used in all cases.

The seeding method used for film preparation mainly consists of three steps. (i) Preparation of 60 nm colloidal molecular sieve seeds. The seeds were grown in a synthesis mixture with the molar composition of $9TPAOH:25SiO_2:360H_2O:100EtOH$. The synthesis mixture was allowed to hydrolyze at room temperature for 24 h and was then treated for 2 weeks in an oil bath at 60 °C under reflux at atmospheric pressure. The nano-sized crystals were purified by repeated centrifugation followed by redispersion in a 0.1-M ammonia solution four times. The seed sol obtained was finally adjusted to a dry content of 1.0% and a pH of 10.0 using 1 M ammonia solution. (ii) Deposition of seeds onto the substrate surface by electrostatic adsorption. A 0.4-wt% solution of cationic polymer in water was prepared by diluting a commercial polymer mixture (Redifloc 4150, Eka Chemicals, repeating unit $[CH_2CHOHCH_2N(CH_3)_2]_n^+$, average molecular weight 50.000 g/mol) with water. The pH was adjusted to 8.0 by addition of a dilute ammonia solution. The surface charge of the substrates was reversed by treatment in the cationic solution for 5 min. After charge reversal, the substrates were rinsed with 0.1 M ammonia solution three times to remove excess polymer and were immersed in the seed sol for 5 min to adsorb the 60 nm silicalite-1 seeds. (iii) Growth of the colloidal seed crystals into a continuous, polycrystalline film. Following seeding, the seeded substrates were mounted in Teflon holders and placed in the synthesis mixture for film crystallization in an oil bath at 100 °C under reflux and atmospheric pressure. The silicalite-1 films were grown for 24 h from a clear synthesis solution with molar composition $3TPAOH:25SiO_2:1450H_2O:100EtOH$. The ZSM-5 films were grown at 100 °C for 48 h using a synthesis solution with a molar composition of $3TPAOH:0.98Na_2O:0.25Al_2O_3:25SiO_2:1600H_2O:100EtOH$. After completed film crystallization, the samples were rinsed with a 0.1 M ammonia solution and then dried in an oven at 50 °C.

Finally, in order to remove the TPA molecules in the zeolite channels and remove the protective polymer from the edges of the ATR crystals, all samples were heated in air at 500 °C for 4 h using a heating and cooling rate of 0.8 °C/min.

2.3. Instrumentation

A Philips XL 30 Scanning Electron Microscope (SEM) equipped with a LaB_6 emission source was used for studies of surface morphology and film thickness. Prior to SEM characterization, the samples were coated with a thin layer of gold. A Siemens D5000 powder X-ray diffractometer (XRD) using Cu Kα radiation was used to determine the crystalline phase of films. The XRD patterns were collected in the 2θ region from 5° to 27° where the most intense MFI reflections are located. The IR-spectrometer was a Bruker IFS113V (chamber pressure ~1 mm Hg) equipped with a MCT-detector. The flow cell (volume ~3 ml) containing the IRE has been described in detail previously [50,51]. The cell is constructed of stainless steel and was sealed using a viton o-ring or graphite gaskets. The IRE in the cell was placed in the beam path in the spectrometer and a gas flow was fed to the cell via tubing through a lid in the spectrometer. A gas delivery system consisting of three mass flow controllers and two saturators containing hydrocarbons was used. Ethyl benzene, *n*-hexane and *p*-xylene used in adsorption measurements were supplied by Sigma–Aldrich (>99%) and the helium carrier gas was supplied by AGA (99.9999%). Prior to the measurements, background spectra were recorded by averaging 500 scans, the analyte was subsequently introduced and spectra were recorded by averaging 200 scans at equilibrium.

3. Results and discussion

3.1. Characterization by SEM and XRD

After growth of seed crystals, a continuous and transparent film was formed. The morphology was independent of the type of ATR substrate and no cracks or other defects could be observed in the films by SEM *before* calcination. Fig. 1 shows representative SEM top view images of (a) silicalite-1 and (c) ZSM-5 films on a ZnS substrate *after* calcination. Only a few cracks (not shown) were detected by SEM, and similar results were obtained on Si and ZrO_2. However, both silicalite-1 and ZSM-5 films on ZnSe were damaged and discontinuous, and some parts of the films even peeled off after calcination. This was most likely due to oxidation of the ZnSe surface during calcination and ZnO was detected by XRD. Similar results have been reported for steel, silicalite-1 and zeolite Y films were stable on stainless steel, but peeled off from carbon steel due to oxide formation during calcination [36,37].

Fig. 1 (b and d) show side view SEM images of silicalite-1 and ZSM-5 films on ZnS with a constant thickness of about 180 and 250 nm, respectively. The film thickness is independent of the type of ATR crystal, but dependent of the composition of the synthesis mixture. The results agree well with previous reports using Si wafers [34] and steel [36] substrates. These results fur-

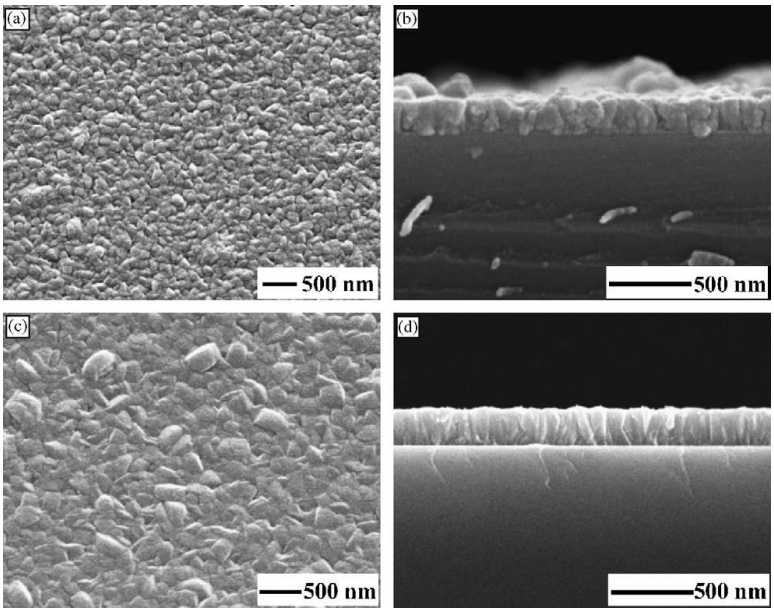

Fig. 1. SEM micrographs of calcined films on ZnS substrates. Top-and side-view images of a silicalite-1 film (a and b) and a ZSM-5 film (c and d).

ther confirm that the seeding method used here is flexible and not surface sensitive.

Fig. 2 shows X-ray diffraction patterns of: (a) a powder of calcined silicalite-1 crystals formed in the synthesis mixture during growth of a silicalite-1 film, (b) a calcined ZSM-5 film on ZnS and (c) a calcined silicalite-1 film on ZnS. The XRD pattern of the powder is typical for well-crystallized MFI material with random orientation. Patterns (b) and (c) show that the films consist of oriented MFI crystals, which is explained by dominant growth in the a-direction as reported previously [52]. Very similar XRD patterns were also obtained for films on silicon ATR elements. The reflection at about 14.5° in the patterns emanates from the ZnS substrate.

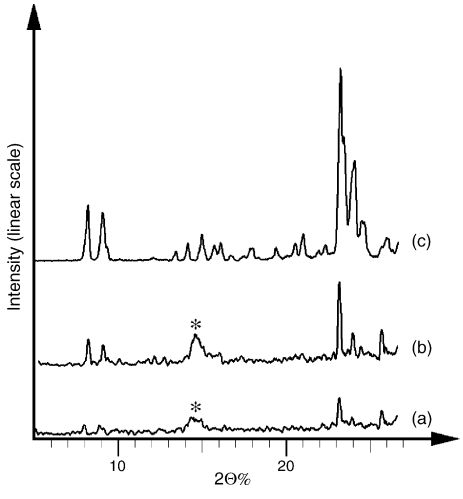

Fig. 2. X-ray diffraction patterns of: (a) a powder of calcined silicalite-1 crystals formed in the synthesis mixture during growth of a silicalite-1 film, (b) a calcined ZSM-5 film on a ZnS and (c) a calcined silicalite-1 film on a ZnS substrate. The peak labelled with a star emanates from the ZnS substrate.

3.2. Characterization of the probes by ATR-FTIR

Fig. 3 shows an infrared spectrum of ethyl benzene recorded using an uncoated Si element (a) and an element coated with silicalite-1 (b). In spectrum (a) no signal from ethyl benzene

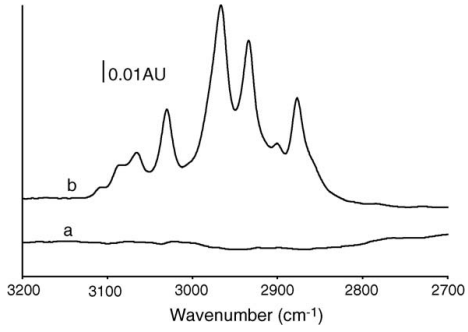

Fig. 3. Spectra of ethyl benzene recorded using: (a) an uncoated Si-ATR element and (b) a silicalite-1 coated Si-ATR element. The spectra were recorded at room temperature and the partial pressure of ethyl benzene in helium was 120 Pa.

Table 2
Absorbance measured as the peak height at 2960 cm^{-1} at various partial pressures of *n*-hexane in gas phase

Partial pressure (Pa)	Absorbance
1.3	0.164
2.7	0.195
7.7	0.238
16	0.252

could be detected whilst for spectrum (b) a strong signal from ethyl benzene was detected. The results show that the analyte is enriched in the silicalite-1 film. The experiments were performed at room temperature and the partial pressure of ethyl benzene in helium was 120 Pa. Prior to the experiments the crystals were dried over night at 250 °C in an argon environment and a flow of pure argon was used for protection during mounting the crystal into the cell. An infrared spectrum of a silicalite-1 film recorded using the ATR-technique has been reported elsewhere [51].

Table 2 shows the absorbance (peak height) of the band at 2960 cm^{-1} when a silicalite-1 film is in equilibrium with a mixture of *n*-hexane in helium. Results from an experiment where *n*-hexane was adsorbed in a silicalite-1 film from gas mixtures having different contents of *n*-hexane. The experiment was performed at room temperature using a ZnS ATR element. As the partial pressure is increased, the amount of *n*-hexane adsorbed in the film increases, resulting in higher absorbance. Consequently, the absorbance depends on the concentration of *n*-hexane in the gas, provided that the concentration is sufficiently low and the film is not saturated with *n*-hexane. Due to the relative strong absorbance (0.16 AU at 1.3 Pa), it should be possible to detect concentrations as low as 0.01 Pa, which corresponds to approximately 100 ppb at room temperature, i.e. zeolite coated ATR elements are very sensitive.

Fig. 4 shows a spectrum recorded by adsorbing a mixture of *n*-hexane and *p*-xylene in a silicalite-1 film (a), spectra (b) and (c) are reference spectra recorded by adsorbing pure *n*-hexane and *p*-xylene, respectively. A ZnS-ATR crystal was used and the sample was dried at 260 °C for 12 h under a flow of helium prior to the measurement using a heatable flow cell. Details of the heatable flow cell can be found elsewhere [52]. A mixture of *n*-hexane and *p*-xylene in helium was fed to the cell. The partial pressures of *n*-hexane and *p*-xylene was 611 Pa and helium was used to dilute the mixture to a total pressure of 1 atm. The composition of the gas mixture was calculated using the non random two liquid (NRTL) model. In spectrum (a) absorbance bands from both *n*-hexane and *p*-xylene can be detected at 1468 and 1518 cm^{-1}, respectively. Although there is an overlap of bands originating from *n*-hexane and *p*-xylene between 1470 and 1440 cm^{-1}, it should be possible to differentiate between the two species by deconvoluting the spectrum. This experiment shows that this technique can be used to quantify mixtures of hydrocarbons.

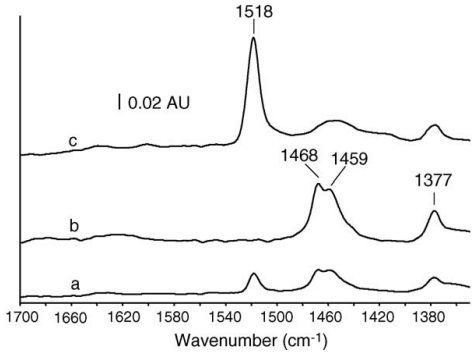

Fig. 4. Spectrum of *n*-hexane and *p*-xylene simultaneously adsorbed is a silicalite-1 film: (a) at room temperature. The partial pressure of both analytes was 611 Pa. Spectra (b) and (c) show reference spectra of *n*-hexane and *p*-xylene, respectively.

4. Conclusions

Thin MFI type zeolite films have been grown on a variety of ATR crystals using a seeding method. The thickness and morphology of the films and preferred orientation of the crystals are independent of the type of ATR crystal and agree well with previous results. It was demonstrated that these coated ATR crystals in combination with FTIR could be used as a novel sensor type with high sensitivity. The sensor can be used to detect low amounts of organic molecules in a gas flow and can be used to study competitive adsorption from mixtures. Additionally, the sensor may also be employed as a powerful characterization tool for molecular sieves.

Acknowledgement

The authors acknowledge the Swedish Research Council (VR) for financial support of this work.

References

[1] J.J. Workman, Review of process and non-invasive near-infrared and infrared spectroscopy: 1993–1999, Appl. Spectros. Rev. 34 (1999) 1–89.
[2] K.K. Chittur, FTIR/ATR for protein adsorption to biomaterial surfaces, Biomaterials 19 (1998) 357–369.
[3] C. Vigano, J.M. Ruysschaert, E. Goormaghtigh, Sensor applications of attenuated total reflection infrared spectroscopy, Talant 65 (2005) 1132–1142.
[4] A.R. Hind, S.k. Bhargava, A. McKinnon, At the solid/liquid interface: FTIR/ATR—the tool of choice, Adv. Colloid Interface Sci. 93 (2001) 91–114.
[5] Y. Lu, L. Han, J. Brinker, T.M. Niemczyk, G.P. Lopez, Chemical sensors based on hydrophobic porous sol–gel films and ATR-FTIR spectroscopy, Sens. Actuators B 35–36 (1996) 517–521.
[6] D. Rivera, J.M. Harris, In situ ATR-FT-IR kinetic studies of molecular transport and surface binding in thin sol–gel films: reactions of chlorosilane reagents in porous silica materials, Anal. Chem. 73 (2001) 411–423.
[7] R.P. Sperline, Y. Song, H. Freiser, Temperature dependent structure of adsorbed sodium dodecyl sulfate at the Al_2O_3/water interface, Langmuir 13 (1997) 3727–3732.
[8] R.P. Sperline, Y. Song, Temperature independent adsorbate structure of 4-octyle-, 4-decyl-, and 4-dodecylebenzenesulfonates at the Al_2O_3/water interface, Langmuir 13 (1997) 6985–6994.

[9] T. Snabe, S.B. Petersen, Application of infrared spectroscopy (attenuated total reflection) for monitoring enzymatic activity on substrate films, J. Biotechnol. 95 (2002) 145–155.
[10] R. Göbel, R. Krska, R. Kellner, R.W. Seitz, S.A. Tomellini, Investigation of different polymers as coating materials for IR/ATR spectroscopic trace analysis of chlorinated hydrocarbons in water, Appl. Spectros. 48 (1994) 678–683.
[11] R. Göbel, R.W. Seitz, S.A. Tomellini, R. Krska, R. Kellner, Infrared attenuated total reflection spectroscopic investigations of the diffusion behaviour of chlorinated hydrocarbons into polymer membranes, Vib. Spectrosc. 8 (1995) 141–149.
[12] G. Roy, J.A. Mielczarski, Infrared detection of chlorinated hydrocarbons in water at ppb levels of concentrations, Water Res. 36 (2002) 1902–1908.
[13] D.W. Breck, Zeolite Molecular Sieves, Krieger Publishing Company, Malabar, 1984, p. 5.
[14] M.E. Davis, R.F. Lobo, Zeolite and molecular sieve synthesis, Chem. Mater. 4 (1992) 756–768.
[15] T. Bein, Synthesis and applications of molecular sieve layers and membranes, Chem. Mater. 8 (1996) 1636–1653.
[16] A. Tavolaro, E. Drioli, Zeolite membranes, Adv. Mater. 11 (1999) 975–996.
[17] M.E. Davis, Ordered porous materials for emerging applications, Nature 417 (2002) 813–821.
[18] M. Tsapatsis, Molecular sieves in the nanotechnology era, AICHE J. 48 (2002) 654–660.
[19] J. Dong, Y.S. Lin, W. Liu, Multicomponent hydrogen/hydrocarbon separation by MFI-type zeolite membranes, AIChE J. 46 (2002) 1957–1966.
[20] J. Hedlund, J. Sterte, M. Anthonis, A.J. Bons, B. Carstensen, E.W. Corcoran, H.W. Deckman, W. de Gijnst, P.P. de Moor, F. Lai, J. McHenry, W. Mortier, J. Reinoso, High flux MFI membranes, Microporous Mesoporous Mater. 53 (2002) 179–189.
[21] F. Kapteijn, W.J.W. Bakke, J. van de Graaf, G. Zheng, J. Poppe, J.A. Moulijn, Permeation and separation behaviour of a silicalite-1 membrane, Catal. Today 25 (1995) 213–218.
[22] S. Mintova, T. Bein, Nanosized zeolite films for vapor-sensing applications, Microporous Mesoporous Mater. 50 (2001) 159–166.
[23] T. Bein, K.K. Brown, G.C. Frye, C.J. Brinker, Molecular sieve sensors for selective detection at the nanogram level, J. Am. Chem. Soc. 111 (1989) 7640–7641.
[24] G.J. Klap, M. Wubbenhorst, J. vanTurnhout, J.C. Jansen, H. vanBekkum, Modification of a pyroelectric defector by controlled electrocrystallization of thin zeolite layers, in: H. Chon, S.-K. Ihm, Y.S. Uh (Eds.), Progress in Zeolite and Microporous Materials, Studies in Surface Science and Catalysis, vol. 105, Elsevier, Amsterdam, 1997, pp. 2093–2100.
[25] R.B. Bjorklund, J. Hedlund, J. Sterte, H. Arwin, Vapor adsorption in thin silicalite-1 films studied by spectroscopic ellipsometry, J. Phys. Chem. B 102 (1998) 2245–2250.
[26] S.P. Davis, E.V.R. Borgstedt, S.L. Suib, Growth of zeolite crystallites and coatings on metal surfaces, Chem. Mater. 2 (1990) 712–719.
[27] P.M. Slangen, J.C. Jansen, H. van Bekkum, Induction heating: a novel tool for zeolite synthesis, Zeolites 18 (1997) 63–66.
[28] W.Y. Xu, J.X. Dong, J.P. Li, F. Wu, A novel method for the preparation of zeolite ZSM-5, J. Chem. Soc. Chem. Commun. 10 (1990) 755–756.
[29] J.X. Dong, T. Dou, X.G. Gao, L.H. Gao, Synthesis of the membranes of zeolites ZSM-5 and ZSM-35 by the vapor phase method, J. Chem. Soc. Chem. Commun. 15 (1992) 1056b–1058b.
[30] M. Matasukata, E. Kikuchi, Zeolitic membranes: synthesis properties and prospects, Bull. Chem. Soc. Jpn. 70 (1997) 2341–2356.
[31] J. Hedlund, B.J. Schoeman, J. Sterte, Synthesis of ultra thin films of molecular sieves by the seed film method, in: H. Chon, S.-K. Ihm, Y.S. Uh (Eds.), Progress in Zeolite and Microporous Materials, Studies in Surface Science and Catalysis, vol. 105, Elsevier, Amsterdam, 1997, pp. 2203–2210.
[32] J., Sterte, J. Hedlund, B.J. Schoeman, Procedure for preparing molecular sieve films, US Patent 6,177,373, 2001.
[33] V. Valtchev, B.J. Schoeman, J. Hedlund, S. Mintova, J. Sterte, Preparation and characterization of hollow fibers of silicalite-1, Zeolites 17 (1996) 408–415.
[34] J. Hedlund, S. Mintova, J. Sterte, Controlling the preferred orientation in silicalite-1 films synthesized by seeding, Microporous Mesoporous Mater. 28 (1999) 185–194.
[35] S. Mintova, J. Hedlund, B.J. Schoeman, V. Valtchev, J. Sterte, Continuous films of zeolite ZSM-5 on modified gold surfaces, Chem. Commun. (1997) 15–16.
[36] Z. Wang, J. Hedlund, J. Sterte, Synthesis of thin silicalite-1 films on steel supports using a seeding method, J. Microporous Mesoporous Mater. 52 (2002) 191–197.
[37] Z. Wang, J. Hedlund, J. Sterte, Synthesis of FAU type films on steel supports using a seeding method, in: A. Galarneau, F. DiRenzo, F. Fajula (Eds.), J. Zeolites and Mesoporous Materials at the Dawn of The 21st Century, Studies in Surface Science and Catalysis, vol. 135, Elsevier, CD-ROM, Paper 20-P-08.
[38] O. Öhrman, J. Hedlund, V. Msimang, K. Möller, Thin ZSM-5 film catalysts on quartz and alumina supports, Microporous Mesoporous Mater. 78 (2005) 199–208.
[39] Q. Li, J. Hedlund, D. Creaser, J. Sterte, Zoned MFI films by seeding, Chem. Commun. (2001) 527–528.
[40] Q. Li, Z. Wang, J. Hedlund, J. Sterte, Synthesis and characterization of colloidal zoned MFI crystals, Microporous Mesoporous Mater. 78 (2005) 1–10.
[41] M.C. Lovallo, M. Tsapatsis, T. Okubo, Preparation of an asymmetric zeolite L film, Chem. Mater. 8 (1996) 1579–1583.
[42] G. Xomeritakis, Z. Lai, M. Tsapatsis, Separation of xylene isomer vapors with oriented MFI membranes made by seeded growth, Ind. Eng. Chem. Res. 40 (2001) 544–552.
[43] R. Szostak, Handbook of Molecular Sieves, Van Nostrand Reinhold, New York, 1992.
[44] A.A. Cichowlas, P.T. Wierzchowski, L.W. Zatorski, H-ZSM-5 catalyzed transformation of toluene, in: H.K. Beyer, H.G. Karge, I. Kiricsi, J.B. Nagy (Eds.), Catalysis by Microporous Materials, Studies in surface science and catalysis, vol. 94, Elsevier, Amesterdam, 1995, pp. 552–559.
[45] A. Vogt, H.W. Kouwenhoven, R. Prins, Fries rearrangement over zeolitic catalysts, Appl. Catal. A 123 (1995) 37–49.
[46] L.Y. Fang, S.B. Liu, I. Wang, Enhanced para-selectivity by selective coking during toluene disproportionation over H–ZSM-5 zeolite, J. Catal. 185 (1999) 33–42.
[47] N. Arsenova-Härtel, H. Bludau, R. Schumacher, W.O. Haag, H.G. Karge, E. Brunner, U. Wild, Catalytic and sorption studies related to the para selectivity in the ethylbenzene disproportionation over H-ZSM-5 catalysts, J. Catal. 191 (2000) 326–331.
[48] W.H. Chen, T.C. Tsai, S.J. Jong, Q. Zhao, C.T. Tsai, I. Wang, H.K. Lee, S.B. Liu, Effects of surface modification on coking, deactivation and para-selectivity of H-ZSM-5 zeolites during ethylbenzene disproportionation, J. Mol. Catal. A: Chem. 181 (2002) 41–55.
[49] K. Prabhakaran, T. Ogino, R. Hull, J.C. Bean, L.J. Peticolas, An efficient method for cleaning Ge(100) surface, Surf. Sci. 316 (1994) L1031–L1033.
[50] Z. Wang, M.L. Larsson, M. Grahn, A. Holmgren, J. Hedlund, Zeolite coated ATR crystals for new applications in FTIR-ATR spectroscopy, Chem. Commun. (2004) 2888–2889.
[51] M. Grahn, Z. Wang, M.L. Larsson, A. Holmgren, J. Hedlund, J. Sterte, Silicalite-1 coated ATR elements as sensitive chemical sensor probes, Microporous Mesoporous Mater. 81 (2005) 357–363.
[52] V. Engström, B. Mihailova, J. Hedlund, A. Holmgren, J. Sterte, The effect of seed size on the growth of silicalite-1 films on gold surfaces, Microporous Mesoporous Mater. 38 (2000) 51–60.

Paper III

Silicalite-1 coated ATR elements as sensitive chemical sensor probes

Mattias Grahn, Zheng Wang, Margareta L. Larsson, Allan Holmgren, Jonas Hedlund and Johan Sterte

Microporous and Mesoporous Materials 81 (2005) 357

Available online at www.sciencedirect.com
SCIENCE DIRECT®
Microporous and Mesoporous Materials 81 (2005) 357–363
MICROPOROUS AND MESOPOROUS MATERIALS
www.elsevier.com/locate/micromeso

Silicalite-1 coated ATR elements as sensitive chemical sensor probes

Mattias Grahn [a,*], Zheng Wang [a], Margareta Lidström-Larsson [b], Allan Holmgren [b], Jonas Hedlund [a], Johan Sterte [a]

[a] Division of Chemical Technology, Luleå University of Technology, SE-971 87 LULEÅ, Sweden
[b] Division of Chemistry, Luleå University of Technology, SE-971 87 LULEÅ, Sweden

Received 23 September 2004; received in revised form 23 February 2005; accepted 26 February 2005
Available online 18 April 2005

Abstract

A novel sensitive chemical sensor probe has been fabricated. The sensor principle is based on silicalite-1 coated ATR (attenuated total reflection) elements and FTIR spectroscopy. The microporous silicalite-1 film enriches the analyte to the probe surface, thus increasing the sensitivity. At a relative pressure of *n*-hexane in helium of 6×10^{-5} the sensitivity of the probe is approximately 85 times higher for the silicalite-1 coated element compared to a 10 cm transmission gas cell and ca. 180 times higher compared to an uncoated element. The performance of the probe is illustrated by determination of an adsorption isotherm for *n*-hexane in silicalite-1.

Keywords: FTIR; ATR; Silicalite-1; Probe; Sensor; Gas phase

1. Introduction

FTIR/ATR spectroscopy utilizes a waveguide through which the IR radiation passes. The IR-radiation reflects inside the waveguide creating an evanescent wave, which is probing the nearest vicinity of the surface of the waveguide. This technique has proven to be a useful tool for studying phenomena at interfaces and in films, such as adsorption of proteins [1], diffusion of chlorinated hydrocarbons in thin polymer membranes [2], in situ reaction monitoring [3], adsorption of hydrocarbons from aqueous solutions [4–6]. The intensity of the evanescent wave decreases exponentially with the distance from the surface of the waveguide, leading to low sensitivity for analytes in the surrounding fluid. A common technique to increase the sensitivity is to use a suitable coating to enrich the analyte to the probe surface. Examples of coatings reported in scientific journals are silica films [5], polytetrafluorethylene [7] and alkylated polystyrene [8,9].

Molecular sieves are solid porous materials with the ability to separate molecules on a size basis [10]. A subgroup of molecular sieves is the zeolites. A zeolite is a microporous crystalline material built from an aluminosilicate framework consisting of $[SiO_4]^{4-}$ and $[AlO_4]^{5-}$ tetrahedra linked by shared oxygen atoms. Each aluminium atom in the framework must be balanced with one charge equivalent from a non-framework cation. The crystalline structure of the framework results in well-defined channels and voids of discrete size [11].

More than 100 different zeolite structures, both natural and synthetic, are known today [12].

Zeolites are used in a variety of applications such as adsorption, ion exchange and catalysis. Several groups have reported the use of zeolite films in sensor applications, where the term "chemical sensor" refers to a device providing insight in the chemical composition of a system [13]. Bjorklund et al. [14] used silicon wafers coated with thin films of silicalite-1 in combination with

* Corresponding author.

1387-1811/$ - see front matter © 2005 Elsevier Inc. All rights reserved.
doi:10.1016/j.micromeso.2005.02.019

spectroscopic ellipsometry for detecting organic vapors and water in gas phase. Klap et al. [15] reports the modification of a pyroelectric probe by coating the probe by a thin zeolite film. Mintova and Bein [16] prepared zeolite films on a quartz crystal microbalance and detected organic and water vapor. Vilaseca et al. [17] coated semiconductor gas sensors with zeolitic films in order to improve the selectivity. The films were tested for detection of methane, propane and ethanol at different humidity levels. Zhou et al. [18] reports a microelectromechanical system (MEMS) sensor where zeolite is used to enrich freon in order to improve sensitivity and selectivity. Rauch and Liu [19] have applied a zeolite film to selectively limit exposure of gas to a amperometric sensor surface. Moos et al. [20] reports thick-film interdigital capacitors (IDCs) coated with zeolite films for detecting ammonia in automotive exhaust gas. An advantage with zeolites is that the properties can be modified in several ways. For instance, the polarity can be varied by controlling the silica to alumina ratio in the material. Moreover, the cations can be exchanged and various metals or metal oxides can be introduced in the zeolite pores or in the framework. This can be achieved either during or after the synthesis of the zeolite and some examples of techniques exploring that possibility can be found in Refs. [21–23]. One commonly used zeolite in catalysis is the synthetic ZSM-5 with MFI-structure. The molecular sieve silicalite-1 is a pure silica analogue of ZSM-5 and is strictly speaking not a zeolite (since it contains no aluminium), although it has the MFI-structure with well-defined sinusoidal (5.1×5.5 Å) and straight (5.3×5.6 Å) channels [10]. The well-defined system of micropores in the relatively non-polar silicalite-1 results in condensation of linear hydrocarbons even at low partial pressures. At room temperature, a partial pressure of 100 Pa of *n*-hexane is almost sufficient to saturate the pores in silicalite-1 [24].

This work aims to develop a highly sensitive and selective probe by utilizing the unique adsorption properties of thin silicalite-1 films in combination with the FTIR/ATR technique. The performance of the probe is demonstrated by adsorption of hydrocarbons from gas phase.

2. Experimental

2.1. ATR spectroscopy

In ATR spectroscopy, the incident IR beam is totally reflected at the surface of the waveguide (denser medium), and at each reflection an infrared evanescent wave propagates from the surface and interacts with analytes in the vicinity (rarer medium) of the waveguide. The amplitude of the electric field attenuates exponentially from the surface of the waveguide. The penetration depth of the evanescent field is defined as the distance from the waveguide/film (or waveguide/fluid) interface where the intensity of the electric field has dropped to e^{-1} of the intensity at the interface. This distance is given by

$$d_p = \frac{\lambda_1}{2\pi\left(\sin^2\theta - \left(\frac{n_2}{n_1}\right)^2\right)^{1/2}} \quad (1)$$

where d_p is the penetration depth, $\lambda_1 = \lambda/n_1$ is the wavelength of the IR radiation in the denser medium, θ is the angle of incidence of the radiation, in this case 45°, and n_1 and n_2 are the refractive indices of the denser and rarer medium, respectively [25]. The penetration depths, in a silicalite-1 film saturated with *n*-hexane, at 3000 cm^{-1} are approximated to 690 nm for a ZnS ATR element and 270 nm for a silicon ATR element. Refractive indices of 2.2, 3.41 and 1.35 were used for ZnS, Si and silicalite-1 saturated with *n*-hexane, respectively.

2.2. Instrumentation and materials

The silicalite-1 films were prepared using a seeding method [26–31]. In the present work, the hydrothermal treatment was carried out for 34 h under reflux boiling in an oil bath at 100 °C. Details of the synthesis and characterization will be published elsewhere. The films were characterized by scanning electron microscopy (SEM), X-ray diffraction (XRD) and spectroscopy, see below.

Spectra were recorded using a Bruker IFS 113 V infrared spectrometer equipped with a mercury cadmium telluride (MCT) detector. The ATR experiments were performed using a vertical ATR accessory (Spectratech) and trapezoidal ATR elements with 45° cut edges.

The ATR element was mounted in a stainless steel flow cell (Fig. 1a). The size of the ZnS element was $50 \times 20 \times 2$ mm and the silicon element was $50 \times 20 \times 1$ mm.

A gas delivery system was used to control the composition of the feed to the cell (Fig. 1b). The system consisted of three mass flow controllers (MFCs) and two saturators connected in series. The first saturator was held at room temperature and the second was fitted with a cooling jacket connected to a flow of thermostated cooling water. The temperature of the cooling water was controlled within ±0.05 °C. One of the MFCs controlled the flow of carrier gas through the saturators and the other two could be used to dilute the flow from the saturators to the desired partial pressure of the hydrocarbon. The partial pressure of the analyte was calibrated indirectly by calibrating the mass flow

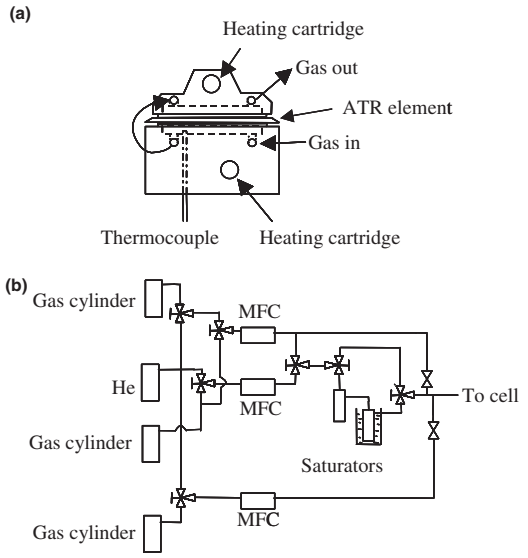

Fig. 1. Schematic figures of (a) the heatable cell and (b) the gas delivery system.

controllers using soap bubble flow meters and by assuming that the flow from the second saturator was saturated with the analyte. Helium was used as carrier gas (AGA, >99.99990%) and *n*-hexane (Sigma, >99%) was used as analyte.

Prior to the measurements, the film was dried in the cell for a minimum of 12 h under a flow of helium (100 ml/min) at 260 °C. When the uncoated element was used, it was cleaned in a plasma cleaner supplied from Harrick Scientific Corp. before mounting in the cell.

Before the adsorption measurements started, a background spectrum was recorded, averaged over 500 scans. During the scanning a continuous flow of pure helium (300 ml/min) was fed to the cell. The adsorption measurements were carried out by flowing gas mixtures through the cell at various partial pressures. Spectra were recorded by averaging 250 scans after reaching adsorption equilibrium and 10 scans were averaged for transient measurements.

When Henry's coefficient was estimated, a saturation concentration (C_{sat}) of 1.42 mol/kg [32] was used.

3. Results and discussion

3.1. Characterization of the films

The silicon ATR element was coated on one side with a silicalite-1 film whilst the ZnS element was coated on both sides. The SEM micrographs in Fig. 2 shows top (a) and side (b) view images of a silicalite-1 film supported on silicon. The film is about 200 nm thick. Very similar films were obtained on ZnS.

An XRD pattern of purified crystals formed in the bulk of the synthesis solution during growth of the silicalite-1 film is shown in Fig. 3(a). This XRD pattern is

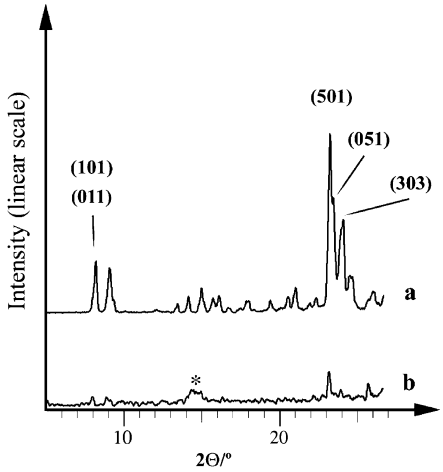

Fig. 3. X-ray diffraction patterns of (a) purified bulk product powder used as reference, (b) a silicalite-1 film synthesized on a ZnS element after 24 h hydrothermal treatment at 100 °C. The peak marked with a star originates from the ZnS substrate.

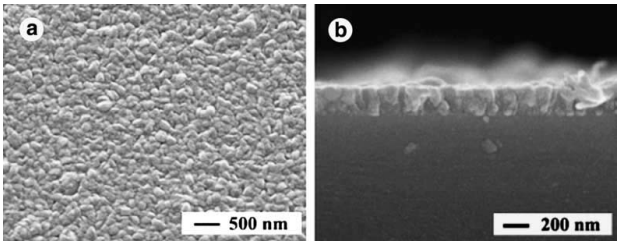

Fig. 2. SEM top (a) and side (b) view images of a silicalite-1 film synthesized on a silicon substrate after 24 h hydrothermal treatment at 100 °C.

typical for randomly oriented silicalite-1 crystals. Fig. 3(b) shows the XRD pattern of a silicalite-1 film on a ZnS substrate. The reflection labelled with a star originates from the ZnS substrate. The pattern shows that the film consists of MFI crystals. Further, the XRD pattern is dominated by the (501) reflection, which is in agreement with previous results for silicalite-1 films on silicon [33] and steel substrates [31] and explained by dominant growth in the *a*-direction. Very similar XRD patterns were also obtained for silicon-supported films.

3.2. Adsorption of n-hexane in a silicalite-1 film

Adsorption of *n*-hexane was detected at room temperature with a relative pressure of *n*-hexane in helium of 6×10^{-5}.

Fig. 4 presents spectra from an uncoated ZnS element (a) and a ZnS element coated with silicalite-1 films on both sides (b) during exposure to a gas flow of *n*-hexane in helium. For the coated ATR element, distinct absorption bands were detected in the spectral region between 2800 cm^{-1} and 3000 cm^{-1}. These bands originate from C–H stretching modes in *n*-hexane. An identical experiment using the uncoated element, showed very weak absorption bands from these C–H stretching modes, slightly above the noise level. Approximately 180 times stronger intensity was achieved with the coated element compared to the uncoated, measured as the peak height at the 2960 cm^{-1} absorption band.

3.3. Sensitivity of a silicalite-1 coated ATR-element compared with a gas cell

This experiment was carried out with the same settings as above, i.e. at room temperature and a relative pressure of *n*-hexane in helium of 6×10^{-5}. The gas mixture was fed to a 10 cm gas cell and a spectrum was recorded, see Fig. 5(a). A spectrum of the gas mixture was also recorded using a Si ATR element with a silicalite-1 coating on one side (Fig. 5(b)). The absorbance, measured as peak height at 2967 cm^{-1}, was approximately 85 times stronger for the silicalite-1 coated element than for the 10 cm gas cell.

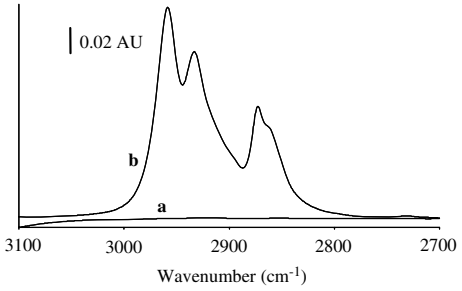

Fig. 4. FTIR-ATR spectra of *n*-hexane using (a) an uncoated ZnS element and (b) a ZnS element coated on both sides with a silicalite-1 film recorded at room temperature. The relative partial pressure of *n*-hexane was approximately 6×10^{-5}.

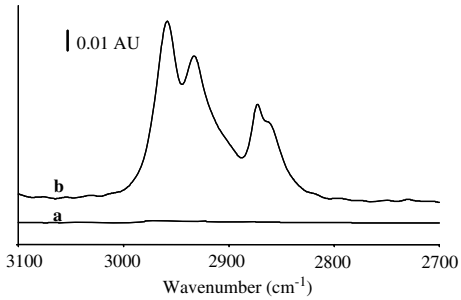

Fig. 5. Recorded IR spectra of *n*-hexane (a) using a 10 cm gas cell, (b) using a silicon element coated on one side with a silicalite-1 film. The experiment was carried out at room temperature and the *n*-hexane content in the gas mixture was 0.006% of saturation.

For the gas cell, the absorbance can be increased by using a cell with a longer path length e.g. 10 m, giving a sensitivity of the same order of magnitude as the coated element. On the other hand the intensity for IRS-methods (Internal Reflection Spectroscopy) can also be increased by coating both sides of the ATR-element, using a higher angle of incidence (gives more reflections inside the waveguide), increasing the film thickness (only effective to a certain limit depending on the penetration depth), and using a longer waveguide such as optical fibres. The possibility to prepare small ATR probes makes this technique especially valuable for application in confined spaces.

By comparing Figs. 4(b) and 5(b), it is obvious that almost identical spectra are obtained for ZnS and Si supported silicalite-1 films. If the films had been much thicker, i.e. thicker than the penetration depths, then the absorption would have been larger for ZnS supported films since the penetration depth is larger for ZnS. Since the films are thin (200 nm), the difference in intensity between spectra will be very small.

3.4. Adsorption isotherm and Langmuir plot

The adsorption of *n*-hexane in large (>4 μm) silicalite-1 crystals has been studied by several groups employing gravimetry [32,34–37] and Monte-Carlo simulations [38]. Dual site and other modified versions of the Langmuir model has been used to account for the heterogeneity of the adsorption sites in silicalite-1 in order to better fit the model to experimental data. Fig. 6 shows the adsorption isotherm at 35 °C of *n*-hexane for relative pressures ranging from 4.7×10^{-5} to 0.42 in a silicalite-1 film on a ZnS element. Each point in the isotherm was obtained by measuring the peak height

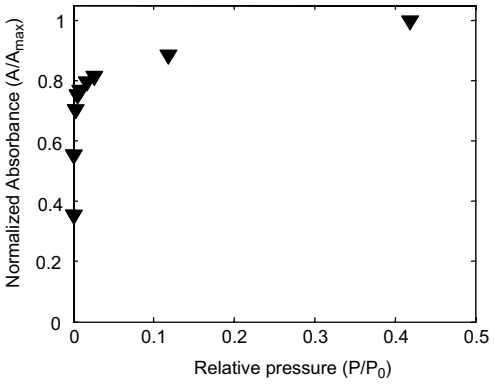

Fig. 6. Adsorption isotherm of *n*-hexane in silicalite-1 film measured at 35 °C using a coated ZnS element.

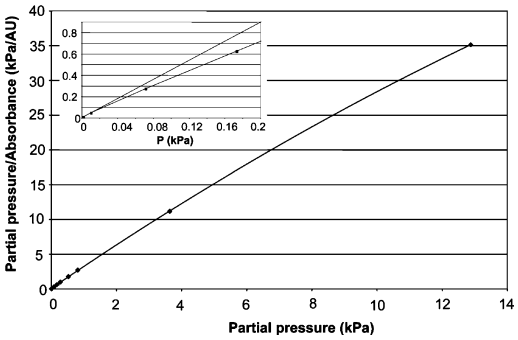

Fig. 7. A plot of partial pressure/absorbance versus partial pressure. A quadratic least squares fit of the data is shown in the figure. The insertion shows the slope from the first two points (upper line) compared to experimental data.

of the infrared absorption band at 2960 cm^{-1}. The single-site Langmuir equation (valid for monolayer adsorption) was used to evaluate the data.

The single-site Langmuir equation

$$\Theta = \frac{bp}{1+bp} \tag{2}$$

can be rearranged to

$$\frac{p}{A} = \frac{p}{A_\infty} + \frac{1}{bA_\infty} \tag{3}$$

where Θ is the fractional coverage. It was assumed that the absorbance (A) was proportional to the adsorbed amount of *n*-hexane, i.e. $\Theta = A/A_\infty$. The adsorption equilibrium constant is b, p is the partial pressure of the hydrocarbon in the bulk, A is the absorbance at equilibrium for a partial pressure p of the hydrocarbon, and A_∞ is the absorbance at complete surface coverage.

A plot of p/A as a function of p should yield a straight line where A_∞ and b can be determined from the intercept and the slope of the straight line. Henry's constant can subsequently be determined from:

$$K_H = bC_{sat} \tag{4}$$

K_H is Henry's constant and C_{sat} is the saturation capacity.

Fig. 7 shows a Langmuir plot of the data obtained from the adsorption isotherm in Fig. 6. A curvature is revealed upon careful inspection, see insert in Fig. 7. This is probably due to capillary condensation in pores larger than the zeolite pores (mesopores) in combination with adsorption on other sites in the zeolite. These larger pores may represent defects and open grain boundaries in the polycrystalline zeolite film. Silicalite-1 films are known to contain defects in the form of cracks and open grain boundaries [39,40]. The polycrystalline film is comprised of columnar crystals with a length of 200 nm (film thickness). The adsorption data from the film will thus resemble data from a powder with crystals with a diameter <200 nm. Such data will be influenced of capillary condensation in voids (pores) between the crystals. In order to circumvent any effects at higher pressures of multiple adsorption sites or capillary condensation, the adsorption equilibrium constant (b) was determined from low pressure data ($p < 10$ Pa) in the present work to 0.96 Pa^{-1}. This constant will correspond to b_1 in a dual site isotherm [35]. The Henry coefficient, K_H was determined using Eq. (4) to 1.37 mol/(kg Pa).

Extrapolated literature data are given in Table 1. The Henry constant obtained in the present work at 35 °C is close to literature data, especially data reported by Fox et al. [38], obtained by Monte-Carlo simulations.

3.5. Probe response time

The response time of the probe was investigated by exposing the probe to a step increase of *n*-hexane from $P/P_0 = 0$ to $P/P_0 = 0.01$ at 27 °C. A ZnS ATR element coated on both sides with a silicalite-1 film was used in the experiment. By following the progression of the 2960 cm^{-1} absorption band with time the response time of the probe was indicated, see Fig. 8. Equilibrium was achieved after approximately 250 s, but already at the

Table 1
Henry constants reported in literature and extrapolated to 35 °C

Reported Henry constants (mol/(kg Pa))	Temperature (°C)	Reference	Henry constants extrapolated to 35 °C (mol/(kg Pa))
2.35	30	[38]	1.49
0.032	100	[42]	3.42
0.13	30	[32]	0.08

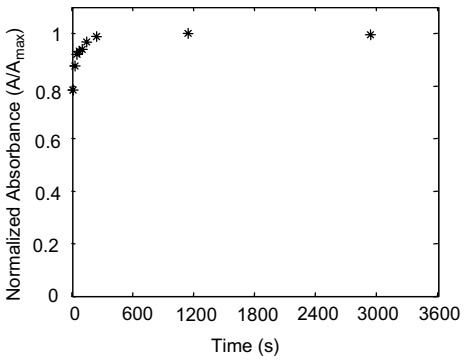

Fig. 8. Normalized absorbance (A/A_{max}) as a function of time for the system *n*-hexane adsorbed in a silicalite-1 film. The adsorption was performed at 27 °C and the absorbance was measured at 2960 cm^{-1}.

first measurement, average of data collected approximately between $t = 5$ s and $t = 15$ s, the absorbance was 79% of its equilibrium value. A spectrometer with rapid scan possibility would make it possible to record spectra at shorter time intervals and determine the transient response accurately. However, the data indicates that the probe may be relatively fast, especially at higher temperatures, where diffusion is faster. The film will be in equilibrium with the surrounding fluid. If the concentration is changed in the fluid, a corresponding change of the concentration in the film will thus occur. Furthermore, adsorbed molecules can be desorbed easily by increasing the temperature in the film [41].

4. Conclusions

A new chemical sensor probe, based on a silicalite-1 coated waveguide and FTIR/ATR spectroscopy, has been prepared and tested. The microporous silicalite-1 film adsorbs the analyte, thus facilitating an increased sensitivity. The shape of the isotherm, resulting in a strong signal that is directly proportional to the concentration at low pressures makes the probe suitable for detection of low bulk concentrations of the analyte. The response is also relatively fast.

It should be possible to optimize the properties of the probe for a certain application, by a careful selection of zeolite type, counter ions, etc. Furthermore, the molecular sieve used may be size and shape selective, which may result in a very selective probe.

Acknowledgement

The authors acknowledge the Swedish Research Council (VR) for financial support of this work.

References

[1] K. Chittur, Biomaterials 19 (1998) 357.
[2] R. Göbel, R.W. Seitz, S.A. Tomellini, R. Krska, R. Kellner, Vib. Spectrosc. 8 (1995) 141.
[3] U. Wolf, R. Leiberich, J. Seeba, Catal. Today 49 (1999) 411.
[4] B.J. Ninness, D.W. Bousfield, C.P. Tripp, Appl. Spectrosc. 55 (6) (2001) 655.
[5] Y. Lu, L. Han, C.J. Brinker, T.M. Niemczyk, G.P. Lopez, Sensor. Actuator. 35–36 (1996) 517.
[6] L. Han, T.M. Niemczyk, D.M. Haaland, G.P. Lopez, Appl. Spectrosc. 53 (4) (1999) 381.
[7] B. Murphy, P. McLoughlin, Int. J. Environ. Anal. Chem. 83 (7–8) (2003) 653.
[8] J. Yang, Y. Huang, Appl. Spectrosc. 54 (2) (2000) 202.
[9] R. Sperline, Y. Song, H. Freiser, Colloid. Surface. A 93 (1994) 111.
[10] D. Breck, Zeolite Molecular Sieves, Krieger Publishing Company, Malabar, 1984, pp. 2–4.
[11] R. Szostak, Molecular Sieves, Thomson Science, London, 1998, pp. 20–21.
[12] C. Baerlocher, W. Meier, D. Olson, Atlas of Zeolite Structure Types, fifth revised ed., Elsevier, Amsterdam, 2001, p. 185.
[13] J. Janata, Principles of Chemical Sensors, Plenum Press, New York, 1989, p. 1.
[14] R. Bjorklund, J. Hedlund, J. Sterte, H. Arwin, J. Phys. Chem. B 102 (1998) 2245.
[15] G. Klap, M. Wubbenhorst, J. van Turnhout, J. Jansen, H. van Bekkum, Progress in Zeolites and Microporous Materials, in: H. Chon, S.-K. Ihm, Y. Uh (Eds.), Stud. Surf. Sci. Catal., 105, Elsevier Science, B.V. Amsterdam, 1997, p. 2093.
[16] S. Mintova, T. Bein, Micropor. Mesopor. Mater. 50 (2001) 159.
[17] M. Vilaseca, J. Coronas, A. Cirera, A. Cornet, J. Morante, J. Santamaría, Catal. Today 82 (2003) 179.
[18] J. Zhou, S. Zhang, F. Zhou, Y. Huang, P. Yang, M. Bao, IEEE Int. Symp. Appl. Ferr. (2002) 471.
[19] W. Rauch, M. Liu, J. Mater. Sci. 38 (2003) 4307.
[20] R. Moos, R. Müller, C. Plog, A. Knezevic, H. Leye, E. Irion, T. Braun, K. Marquardt, K. Binder, Sensor. Actuat. B 83 (2002) 181.
[21] T. Selvam, M. Vinod, Appl. Catal. A 134 (2) (1996) L197.
[22] C. M'Kombe, M. Dry, C. O'Connor, Zeolites 19 (2–3) (1997) 175.
[23] L. Qian, Z. Yan, Colloid. Surface. A 180 (2001) 311.
[24] T. Vlugt, R. Krishna, B. Smit, J. Phys. Chem. B 103 (1999) 1102.
[25] N. Harrick, Internal Reflection Spectroscopy, John Wiley & Sons, Inc., 1967, pp. 30–31.
[26] J. Hedlund, B.J. Schoeman, J. Sterte, Progress in zeolites and microporous materials, in: H. Chon, S.-K. Ihm, Y.S. Uh (Eds.), Stud. Surf. Sci. Catal., 105, Elsevier Science, Amsterdam, 1997, p. 2203.
[27] J. Hedlund, B. Schoeman, J. Sterte, Int. Pat. Appl. WO 97/33684, 1997.
[28] M. Lassinantti, J. Hedlund, J. Sterte, Micropor. Mesopor. Mater. 38 (2000) 25.
[29] Q. Li, J. Hedlund, D. Creaser, J. Sterte, Chem. Commun. 7 (6) (2001) 527.
[30] O. Öhrman, U. Nordgren, J. Hedlund, D. Creaser, J. Sterte, in: A. Galarneau, F. Di Renzo, F. Fajula, J. Védrine (Eds.), Zeolites and mesoporous materials at the Dawn of the 21st century, Proceedings Thirteenth International Zeolite Conference, Montpellier, 2001. (2001) pp. 20-P-09.
[31] Z. Wang, J. Hedlund, J. Sterte, Micropor. Mesopor. Mater. 52 (2002) 191.
[32] M. Sun, O. Talu, D. Shah, J. Phys. Chem. 100 (1996) 17276.
[33] J. Hedlund, S. Mintova, J. Sterte, Micropor. Mesopor. Mater. 28 (1999) 185.
[34] R. Richards, L. Rees, Langmuir 3 (3) (1987) 335.

[35] A. Micke, M. Bülow, M. Kocirik, P. Struve, J. Phys. Chem. 98 (1994) 12337.
[36] L. Song, L. Rees, J. Chem. Soc., Faraday Trans. 93 (4) (1997) 649.
[37] F. Eder, J. Lercher, Zeolites 18 (1997) 75.
[38] J. Fox, V. Rooy, S. Bates, Micropor. Mesopor. Mater. 69 (2004) 9.
[39] F. Jareman, J. Hedlund, D. Creaser, J. Sterte, J. Membrane Sci. 236 (1–2) (2004) 81.
[40] J. Hedlund, J. Sterte, M. Anthonis, A.-J. Bons, B. Carstensen, N. Corcoran, D. Cox, H. Deckman, W. de Gijnst, P.-P. de Moor, F. Lai, J. McHenry, W. Mortier, J. Reinoso, J. Peters, Micropor. Mesopor. Mater. 52 (2002) 179.
[41] Y. Yang, L. Rees, Micropor. Mater. 12 (1997) 223.
[42] T. Clark, H. Deckman, D. Cox, R. Chance, J. Membrane Sci. 230 (2004) 91.

Paper IV

Adsorption of n-hexane and p-xylene in thin silicalite-1 films studied by FTIR/ATR spectroscopy
Mattias Grahn, Allan Holmgren and Jonas Hedlund
Submitted

Adsorption of n-hexane and p-xylene in thin silicalite-1 films studied by FTIR/ATR spectroscopy

Mattias Grahn[a*], *Allan Holmgren*[b] *and Jonas Hedlund*[a]

a) Div. of Chemical Technology, Luleå University of Technology, SE-971 87, LULEÅ, Sweden

b) Div. of Chemistry, Luleå University of Technology, SE-971 87, LULEÅ, Sweden

* To whom correspondence should be addressed: Mattias.Grahn@ltu.se; Fax: +46 920 491 199; Tel: +46 920 491 928

RECEIVED DATE

ABSTRACT

Adsorption isotherms for p-xylene and n-hexane in silicalite-1 films with a thickness of 200 nm were determined at 323, 343, 368, 393 and 423 K using FTIR/ATR spectroscopy. For both adsorbates, the low-pressure data agreed well with literature data for MFI powder and the estimated Henry's constant and adsorption enthalpy were close to previously reported results. The upper region of the n-hexane isotherm (p>2 kPa at 323 K) was likely influenced by micropores in open grain boundaries, as expected for a polycrystalline film of small (<200 nm) crystals. As for n-hexane, the first part ($0 \leq p \leq 65$ Pa at 323 K) of the p-xylene isotherm agreed well with data for powder. However, the saturation capacity was only about half of that previously reported for powders, which indicates that p-xylene molecules do not adsorb in the sinusoidal channels in the film. We speculate that strain in the crystals of the supported film, and/or that the crystals in the film are more rigid than in a powder, and cannot undergo the

necessary structural changes to accommodate p-xylene in the sinusoidal channels, may be mechanisms responsible for this effect.

KEYWORDS Silicalite-1, thin film, adsorption, n-hexane, p-xylene, FTIR, ATR.

INTRODUCTION

Molecular sieves are porous materials that can separate molecules based on their size or shape.[1] Thin films of molecular sieves are of great interest in various applications such as catalysis, chemical sensors and membranes.[2-7] In sensor applications, the film should be selective and thin to give a short response time. One subset of molecular sieves is the zeolites. These are crystalline, microporous aluminosilicates with well-defined pore structures. The molecular sieve silicalite-1 is a pure silica analogue of the zeolite ZSM-5 with a pore system consisting of straight (5.3x5.6Å) and sinusoidal (5.1x5.5 Å) channels.[1] Both silicalite-1 and ZSM-5 belongs to the MFI type framework. The separation properties of silicalite-1 membranes have been studied and reported in numerous papers.[8-13] The separation mechanism for these membranes is based on molecular sieving, varying diffusivity and/or preferential adsorption. Defects such as cracks and open grain boundaries are known to form in supported films and can decrease the selectivity for zeolite membranes.[3] In all applications for molecular sieves and zeolites, it is of crucial importance to know the adsorption, diffusion and the reaction properties of the films. IR spectroscopy in combination with the attenuated total reflection (ATR) sampling technique is a powerful tool for studying processes at surfaces or in films, such as adsorption [14-17] and diffusion.[18-20] Since all components have a unique IR spectrum, also multi-component adsorption and diffusion can be studied. The technique has potential for use also at high temperature, which facilitates in-situ reaction studies. Our group has developed a method for the preparation of well-defined molecular sieve films with controlled thickness.[21-25] The films have been evaluated in membrane[3, 26, 27], catalysis [4, 6, 28] and sensor applications in a QCM device[29], by ellipsometry[30] and by FTIR/ATR spectroscopy.[31-33] Further, the

ability of the zeolite coated ATR elements as sensor probes was demonstrated.[31, 33]

Several groups have studied the adsorption of n-hexane and p-xylene in large silicalite-1 crystals experimentally by gravimetric methods[34-39] and Monte-Carlo simulations.[40-44] Both adsorbates show an adsorption behavior in silicalite-1 not in perfect agreement with a traditional single-site Langmuir isotherm, and consequently, various modified versions of the Langmuir model have been employed in order to account for heterogeneity of the adsorption sites.[34, 45, 46]

The present paper demonstrates measurements of single component adsorption isotherms for n-hexane and p-xylene in thin silicalite-1 films at various temperatures using a silicalite-1 coated ATR element and FTIR spectroscopy for the first time.

MATERIALS AND METHODS

MATERIALS

Silicalite-1 films were grown on both sides of trapezoidal ZnS ATR elements using a method employing seeds.[21, 32, 33] The size of the ZnS elements (SensIR Europe Ltd) was 50x20x2 mm and the angle of the cut edges was 45º. The synthesis was performed in three steps; 1) surface modification by adsorption of cationic polymer, 2) adsorption of silicalite-1 seed crystals on the surface, 3) film crystallization by hydrothermal treatment of the seeded substrate in a zeolite precursor solution. The samples were prepared as reported in detail previously[32] but in the present work, no polymer resin was used for protecting the edges of the ATR-element and prior to adsorption of cationic polymer, the element was treated in acetone, ethanol and distilled water in an ultrasonic bath for 10 minutes. The thickness of the films was determined to 200 nm using Scanning Electron Microscopy (SEM) and is in accordance with previous results.[32] A gas delivery system and a heatable stainless steel flow cell were used for the adsorption measurements, details have been reported previously.[31] Helium (AGA 99.99990%) was used as carrier gas and n-hexane (Sigma 99+%) and p-xylene (Aldrich 99+%) were

used as adsorbates. A fraction of the helium carrier gas was saturated with hydrocarbon at a given temperature and mixed with another stream of helium gas in order to arrive at the required partial pressure of hydrocarbon.

METHOD

In FTIR/ATR (Fourier Transform Infra Red / Attenuated Total Reflection) spectroscopy, an IR-beam is reflected within a waveguide, and at each reflection, an evanescent wave is created, probing the vicinity of the waveguide,[47] see Figure 1. The intensity of the electric field decays exponentially with distance from the waveguide surface, which makes ATR spectroscopy a useful tool for studying phenomena in thin films and at surfaces.

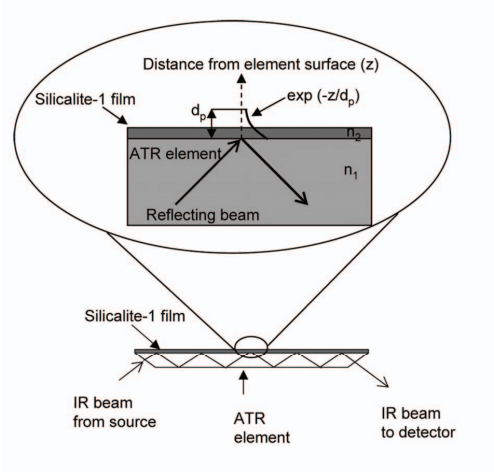

Figure 1. Principle of attenuated total reflection showing an element coated with a silicalite-1 film and the evanescent wave probing the film and the vicinity of the film.

The penetration depth d_p is defined as the distance from the surface where the intensity of the electric field has declined to e^{-1} of the intensity at the waveguide surface and is given by:[47]

$$d_p = \frac{\lambda_1}{2\pi\left(\sin^2\theta - n_{21}^2\right)^{1/2}} \qquad (1)$$

where the wavelength in the denser medium is λ_1 and n_{21} is the ratio of the refractive indices of the denser (waveguide) and rarer media. Further, θ is the angle of incidence and was equal to 45° during the experiments. All experiments were carried out at atmospheric pressure and isotherms were determined at 323, 343, 368, 393 and 423 K. The samples were dried in-situ in the flow cell at 573 K under a flow of helium prior to the measurements. Spectral data were collected using a Bruker IFS 66v/S spectrometer equipped with a liquid nitrogen cooled mercury cadmium telluride (MCT) detector. The integrated absorption intensity was taken as the area of selected absorption bands. In the case of n-hexane, the bands for the C-H stretching vibrations between 3100 – 2700 cm^{-1} were used and for p-xylene, the band at 1518 cm^{-1} was used. Background spectra of the dried silicalite-1 coated ATR-elements were recorded under a flow of helium (100 ml/min) prior to the measurements, by averaging 128 scans. After recording the background, adsorption was carried out by exposing the film to a certain partial pressure of the analyte in a helium flow at a total pressure of 101 kPa. At equilibrium, spectra were recorded by co-adding 64 scans. For n-hexane, the partial pressure was varied between 2 Pa and 14.8 kPa and for p-xylene, the partial pressure was varied between 0.2 Pa and 830 Pa.

MODELS

Concentrations of the adsorbate in the film was calculated as described by Tompkins[48] and Mirabella[49]. The absorption per reflection is given by:

$$A/N = \frac{n_{21}E_0^2\varepsilon}{\cos\theta}\int_0^{\infty} C(z)e^{-2z/d_p}\,dz \qquad (2)$$

where A is the integrated absorbance and N is the number of reflections (20) inside the gaskets sealing the cell. E_0 is the amplitude of the electric field at the film/element interface, ε is the molar absorptivity determined from liquid phase transmission measurements using CCl_4 as solvent and $C(z)$ is the concentration. $C(z)$ was assumed constant in the film and zero outside the film, i.e. the contribution from the gas bulk was considered to be negligible. Upon integration, the following expression is

obtained:

$$A/N = \frac{n_{21}E_0^2 d_p C}{2\cos\theta}\varepsilon\left(1-e^{-2d_a/d_p}\right)k \quad (3)$$

where d_a is the film thickness. By assuming that the MFI film has the same saturation capacity of n-hexane as MFI powder, and that the film was saturated at the same relative pressures as for powder, a correction factor k could be determined. This factor accounts for e.g., uncertainties in the effective film thickness since the model assumes a perfect, homogenous film without any grain boundaries, and for discrepancies in the molar absorptivities between the ones determined in this work in CCl_4 and the real ones in silicalite-1.

The "effective thickness" [47] of the electric field is estimated by:

$$d_e = \frac{n_{21}E_0^2 d_p}{2\cos\theta} \quad (4)$$

and is dependent on polarization direction which can be estimated as:[49]

$$d_e = \frac{I_{0II}}{I_{0II}+I_{0\perp}}d_{eII} + \frac{I_{0\perp}}{I_{0II}+I_{0\perp}}d_{e\perp} \quad (5)$$

where I_{0II} and $I_{0\perp}$ denote the intensity of the radiation without sample for parallel and perpendicular polarized radiation, respectively. Further, $d_{e\perp}$ is the effective thickness for perpendicular polarization and given by:

$$d_{e\perp} = (2n_{21}\, d_p \cos\theta)/(1-(n_{21})^2) \quad (6)$$

where $d_{e\,II}$ is the effective thickness for parallel polarization given by:

$$d_{eII} = \frac{2n_{21}d_p\cos\theta\left(2\sin^2\theta - n_{21}^2\right)}{\left(1-n_{21}^2\right)\left[\left(1+n_{21}^2\right)\sin^2\theta - n_{21}^2\right]} \quad (7)$$

the refractive index of the ZnS element was set to 2.27.[50] Nair and Tsapatsis[51] have measured the refractive index for a calcined empty MFI membrane as well as for a p-xylene loaded MFI membrane in the interval 1500 – 3000 cm^{-1} using IR reflectance. At 1500 cm^{-1}, the refractive index of the empty and p-xylene saturated membrane was ~1.22 and ~1.32, respectively. A linear dependency was applied in

our model for the film with the absorbance as the independent variable to compensate for the change of refractive index with p-xylene loading. The refractive index of the membrane at 2900 cm^{-1} was ~1.28[51] and again a linear dependency for the change in refractive index with adsorbate loading was applied for the film in the present work. The saturation capacity of n-hexane in MFI is about 0.18 cm^3/g[52] which corresponds to ~33% of the total zeolite volume. The refractive index for the saturated film was then calculated as a weighted volumetric average where the refractive index of n-hexane was set to 1.37.[53] This yielded a variation in the refractive index between 1.28 and 1.31 upon adsorption of hexane. The concentration in the film was finally calculated from equations 3-7.

Henry's constants were determined from the slope of the isotherm at low pressures, and to determine the heat of adsorption, the van't Hoff equation was used:

$$\frac{\partial \ln K_H}{\partial T} = \frac{\Delta H_{ads}}{RT^2} \tag{8}$$

where T is the temperature, R the gas constant, ΔH_{ads} is the adsorption enthalpy and K_H is the Henry's constant.

To correlate the pressure at which condensation occurs to the width of eventual open grain boundaries, a modified Horváth-Kawazoe equation was applied:[54, 55]

$$RT\, ln\left(\frac{P}{P_0}\right) = \frac{\Delta H_{ads}}{(d-d_0)}\left[\frac{\sigma^{10}}{9d_0^9} - \frac{\sigma^4}{3d_0^3} - \frac{\sigma^{10}}{9(2d-d_0)^9} + \frac{\sigma^4}{3(2d-d_0)^3}\right] \tag{9}$$

The equation relates the pore width to the pressure of condensable component in gas phase, assuming slit shaped pores. In this equation, d is the half width of the pore and σ is the distance where the interaction energy equals zero and is defined as:

$$\sigma = \left(\frac{2}{5}\right)^{1/6} \frac{d_A + d_S}{2} = \left(\frac{2}{5}\right)^{1/6} d_0 \tag{10}$$

where d_A is the critical diameter of the adsorbate. Critical diameters for p-xylene and n-hexane were taken as 0.585 nm[9] and 0.43 nm,[1] respectively. The diameter of the adsorbent, d_S, was set to 0.276 nm.[56] The defect width d_i is estimated with the relationship:

$d_i=2d-d_S$ (11)

for further details, see Jareman et al..[55]

RESULTS AND DISCUSSION

n-HEXANE

Figure 2 shows the prominent bands of a typical spectrum recorded at 323 K for 10 Pa n-hexane in helium balance.

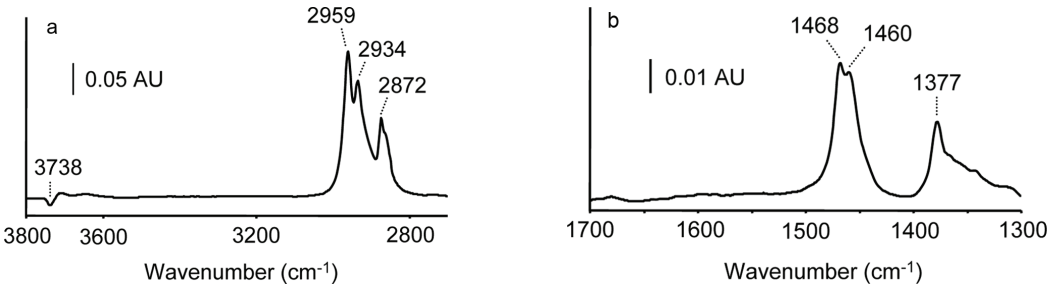

Figure 2. Infrared spectrum of n-hexane (10 Pa and 323 K) adsorbed in a silicalite-1 film. The prominent bands at higher- and lower wavenumbers are shown in (a) and (b), respectively.

Figure 2 a) shows the characteristic CH_3- and CH_2 stretching vibrations in the region 3000-2700 cm^{-1}, originating from n-hexane adsorbed in the pores of the silicalite crystals. A spectrum recorded at 373 K with an uncoated element and a n-hexane pressure of 14 kPa showed no signal from n-hexane, thus it was concluded that contribution from the gas phase could be ignored. Further, a negative band at 3738 cm^{-1}appears, this band has previously been assigned to silanol groups.[57] This negative band, in combination with the appearance of a new band at lower waveumbers, indicates that n-hexane adsorbs on the silanol groups. In figure 2 b) bands, also originating from n-hexane adsorbed in the pores, are shown with their positions indicated in the figure.[58] The bands are assigned to CH_3- and CH_2 deformation vibrations.[58]

By assuming that the saturation capacity of n-hexane in MFI powder and a silicalite-1 film are the same,

the correction factor k_{hexane} in equation 3 was determined to 0.76 at 2 kPa. Considering the possible sources of errors mentioned above, the observed correction factor is quite close to the ideal value of 1.

Adsorption isotherms for n-hexane in the temperature range between 323 and 423 K were determined by integrating the area of the C-H stretching vibration bands between 3100-2700 cm^{-1} and calculating the corresponding concentrations using equation 3, the isotherms are presented in Figure 3.

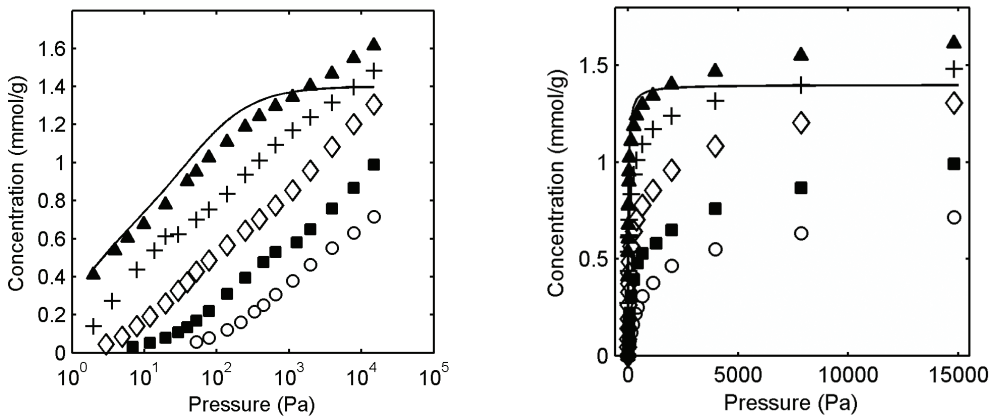

Figure 3. Adsorption isotherms for n-hexane in a silicalite-1 film determined experimentally at 323 (▲), 343 (+), 368 (◊), 393 (■), 423 K (○) in the present work. For comparison, calculated data (Monte-Carlo simulations) for perfect, infinitely large silicalite-1 crystals at 323 K reported by Schenk et al.[46] (solid line) is included. The isotherms are presented with both logarithmic (a), and linear (b) pressure scales.

The experimental isotherms are typical for microporous materials with some capillary condensation between the crystals as indicated with the good correlation with our and Schenks[46] data at low pressures ($p<2$ kPa) and that the experimental isotherms are not flat at higher pressures ($2\leq p\leq 15$kPa) as for the isotherm reported by Schenk[46]. Schenk's isotherm was determined by Monte Carlo simulations for a perfect silicalite-1 structure without any open grain boundaries. Our film is polycrystalline with an

average crystal size less than the film thickness (200nm) and capillary condensation in open grain boundaries can be expected, which explains the observed differences between our and Schenks data. Similar adsorption isotherms have been reported[59, 60] for MFI powder of small (<4 μm) crystals and also in this case, the non-flat parts at higher pressures were attributed to capillary condensation between the crystals. Our isotherm at 323 K deviates from Schenk's isotherm in the pressure range 2-14 kPa, which corresponds to pores with diameters between 1.2 and 2.3 nm according to equation 9. These pores may very well originate from open grain boundaries in the film. We have previously reported open grain boundaries with similar dimensions for MFI membranes.[55] Further, some n-hexane is probably adsorbed on silanol groups as indicated by the appearance of a negative IR band at 3738 cm^{-1} when n-hexane is introduced, see Figure 2 a).

Henry's constants from this work were determined from the slope of the isotherm at low pressures. The result is shown in Table 1 together with literature data.

Table 1. Henry's constants for n-hexane obtained in the present work and literature data.

	Henry's constant (mmol/(g Pa))			
Temp. (K)	This work	Fox et al.. [40]*	Sun et al. [39]**	Clark et al. [61] ***
323	0.21	0.41	0.023	0.98
343	0.076	0.088	0.005	0.22
368	0.018	0.016	$9.3*10^{-4}$	0.044
393	0.0040	0.004	$2.2*10^{-4}$	0.011
423	$8.6*10^{-4}$	$8.1*10^{-4}$	$4.7*10^{-5}$	0.0024

* Extrapolated from 303 K using $K_H = e^{\Delta S_{ads}/R} e^{-(\Delta H_{ads}/RT)}$ and ΔH_{ads} = -70800 J/mol.

** Extrapolated using ΔH_{ads} = -70500 J/mol and the relationship $K_H = 9.18 * 10^{-14} * e^{-(\Delta H_{ads}/RT)}$, as reported in that paper.

*** Extrapolated using $K_H = e^{\Delta S_{ads}/R} e^{-(\Delta H_{ads}/RT)}$ and ΔH_{ads} = -68400 J/mol and ΔS_{ads} = -119 J/(mol

K).

The literature data obtained, by Monte Carlo simulations[40], gravimetry[39] and by adsorption branch porosimetry[61], scatter significantly, and the Henry's constants estimated in the present work fall within this scatter of previously reported constants. It should be noticed that even with a correction k_{hexane} set to unity (no correction) the Henry's constants estimated in the present work decrease with about 20% and would still fall within the scatter of previously reported values. The adsorption enthalpy ΔH_{ads} was estimated to -63 kJ/mol from the Henry's constants, see Figure 4. This agrees reasonably well with previously reported values around -70 kJ/mol.[39, 40, 61]

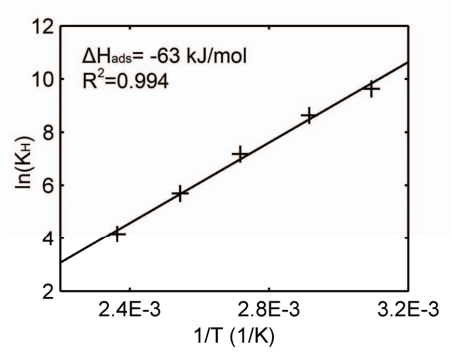

Figure 4. Plot of the logarithm of the Henry constant for n-hexane as a function of the reciprocal of the temperature.

p-XYLENE

Figure 5 a) and b) shows the prominent bands in a typical spectrum recorded at 323 K for 108 Pa p-xylene in helium balance.

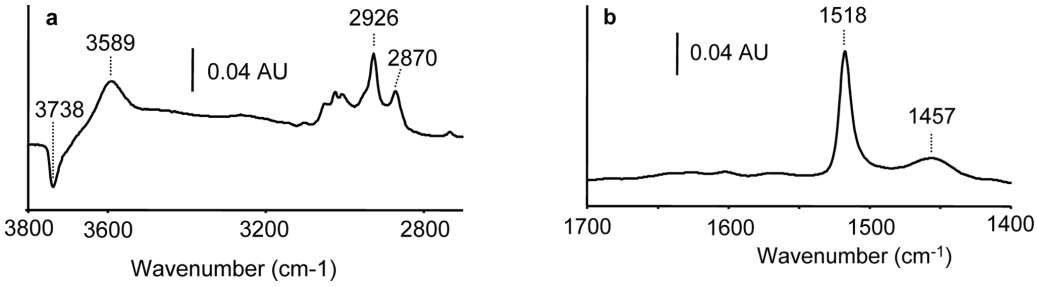

Figure 5. Infrared spectrum of p-xylene (108 Pa and 323 K) adsorbed in a silicalite-1 film. The prominent bands at higher- and lower wavenumbers are shown in (a) and (b), respectively.

In (a) the bands between 3100 and 2800 cm^{-1} emanates from p-xylene adsorbed in the silicalite pores, these have previously been assigned to C-H stretching vibrations in combination with overtones and combination bands.[62] In addition to the bands indicated in the Figure at 2926 and 2870 cm^{-1}, there are three quite strong bands at 3004, 3024 and 3050 cm^{-1}. The positions of all bands are in excellent agreement with the positions reported previously by Schüth for p-xylene in silicalite-1.[62] In accordance with the results for n-hexane, no p-xylene in gas phase could be detected and again it was concluded that contribution from the gas phase could be ignored. Again, a negative band appears at 3738 cm^{-1} accompanied by the appearance of a new band 3589 cm^{-1} indicative of adsorption on silanol groups. In Figure 5 b) two bands appear, one strong band at 1518 cm^{-1} assigned to a stretching vibration of the aromatic ring, and one broad, weaker band centered at 1457 cm^{-1} assigned to a C-H deformation vibration. Both of these bands also appear in the work by Schüth.[62]

The correction factor for p-xylene, k_{xylene}, was determined to 0.8 at a pressure of 40 Pa, which again must be considered as quite close to the ideal value.

Adsorption of p-xylene were recorded at the same temperatures as for n-hexane using the same silicalite-1 film and isotherms were determined by integrating the 1518 cm^{-1} band, the isotherms are shown in Figure 6.

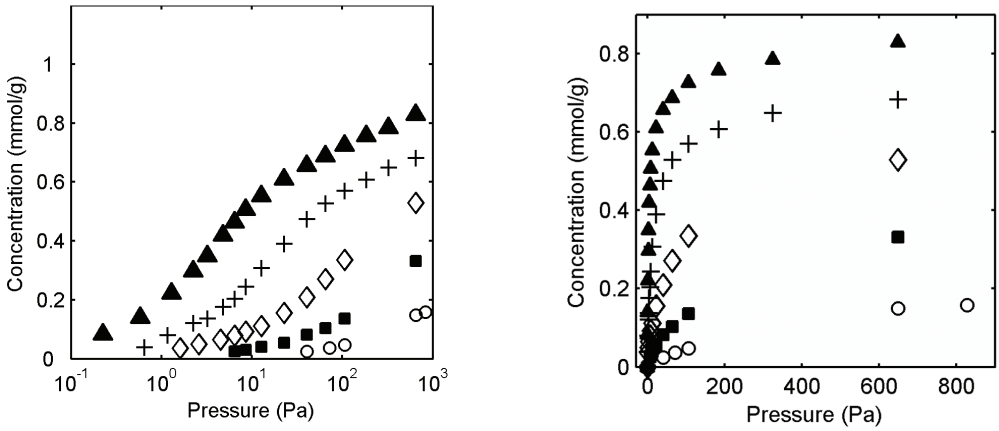

(a) (b)

Figure 6. Adsorption isotherms for p-xylene in a silicalite-1 film determined at 323 (▲), 343 (+), 368 (◊), 393 (■) and 423 K (○).The isotherms are presented with both logarithmic (a), and linear (b) pressure scales.

Again, the isotherms are typical for microporous materials with some open grain boundaries. At low pressures, the isotherms agree well with previously reported isotherms, for large crystals. As before, Henry's constants were determined from low pressure data and compared to literature data, see Table 2. Again the obtained results comply with previously reported data. The literature values were determined using Monte Carlo simulations[41] and gravimetry[63, 64] yet again there is considerable scattering of the reported values.

Table 2. Henry's constants for p-xylene obtained in the present work including literature data.

	Henry's constant (mmol/(g Pa))			
Temp. (K)	This work	Li and Talu[41] *	Talu et al.[64]**	Richards and Rees[63]***
323	0.39	0.53	0.022	1.06
343	0.072	0.11	0.0054	0.18
368	0.020	0.019	0.0012	0.027
393	0.0038	0.0043	$3.0*10^{-4}$	0.0049
423	$5.5*10^{-4}$	$8.9*10^{-4}$	$7.5*10^{-5}$	$8.5*10^{-4}$

* Extrapolated from 293 K using $K_H = e^{\Delta S_{ads}/R} e^{-(\Delta H_{ads}/RT)}$ and ΔH_{ads} = -72500 J/mol.

** Extrapolated from 293 K using $K_H = e^{\Delta S_{ads}/R} e^{-(\Delta H_{ads}/RT)}$ and ΔH_{ads} = -64400 J/mol.

*** Extrapolated from 293 K using $K_H = e^{\Delta S_{ads}/R} e^{-(\Delta H_{ads}/RT)}$ and ΔH_{ads} = -81000 J/mol and ΔS_{ads} = -157 J/(mol K) (both values extrapolated at low partial pressures).

The adsorption enthalpy was determined to -73 kJ/mol, see Figure 7, which agrees well with previous values as compiled by Li and Talu[41] viz. -41 to -80 kJ/mol, although most values reported in the literature are closer to the upper limit.

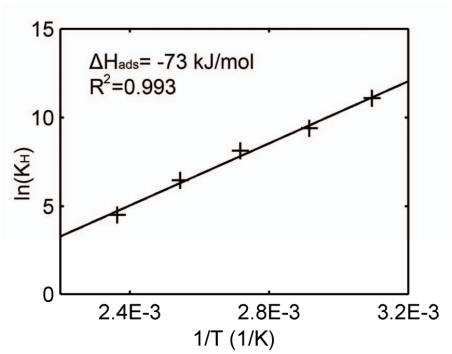

Figure 7. Plot of the logarithm of the Henry constant for p-xylene versus the reciprocal temperature.

Several groups, for instance Gélin et al.[35] have reported a distinct step in the p-xylene isotherm at a loading of about half the saturation capacity (~0.7 mmol/g) at temperatures below ca 353 K for MFI powder, see Figure 8. The step in the isotherm has been attributed to two different adsorption sites.

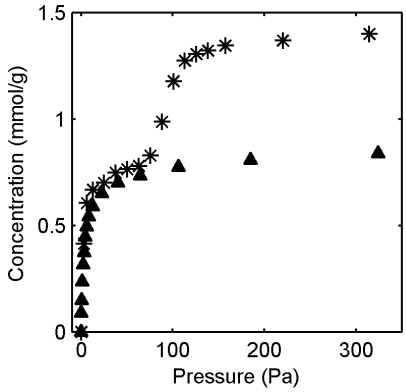

Figure 8. Adsorption isotherm for p-xylene in a silicalite-1 film determined at 323 K(▲) in the present work and isotherm measured gravimetrically on silicalite-1 powder at 323 K (∗), redrawn from Gélin et al.[35]

First the p-xylene molecules adsorb in the channel intersection and then at higher partial pressures the p-xylene is adsorbed also in the sinusoidal channels.[65, 66] During the adsorption of aromtic molecules, structural changes occurs in the MFI framework.[66, 67] At low temperatures (close to room temperature)

unloaded silicalite-1 has monoclinic symmetry. As p-xylene is adsorbed, the framework starts to change to orthorombic symmetry and at loadings < 2 molecules/unit cell, the two phases coexist. At loadings 2-4 molecules/unit cell, only orthorombic symmetry exists. At higher loadings (4-8 molecules/unit cell) another orthorombic symmetry appears. Upon adsorption of p-xylene, the framework deforms and the pores become more elliptical.[67] It has also been reported that at higher temperatures (~>353 K), the sinusoidal channels become unfavorable for adsorption.[64, 68]

As shown in Figures 6 and 8, these steps are absent in our isotherms at all temperatures. However, it has been reported[69-71] that the unit cell parameters differs between a supported MFI film and MFI powder, which was attributed to strain in the crystals of the supported film. The absence of a step in the p-xylene isotherms recorded in the present work may be related to strain in the film and/or that the MFI framework becomes less flexible when bonded to the substrate. This effect is currently under further investigation at our laboratories.

Conclusions

The adsorption of p-xylene and n-hexane in silicalite-1 was studied at various temperatures using FTIR spectroscopy in combination with ATR elements coated with polycrystalline 200 nm silicalite-1 films. The low pressure region of the isotherm agreed well with previously reported isotherms for large silicalite-1 crystals. The heat of adsorption and Henry's constants determined from low pressure data agreed well with literature values. At high pressures, adsorption on silanol groups and condensation in grain boundaries likely influenced the shape of the isotherms. For p-xylene, no step occurred in the isotherm as reported for powders and unsupported films. Instead only half the reported saturation loading was obtained in the present work. This may be related to strain in crystals in the supported film, and/or that the crystals become less flexible due to the bonding to the substrate.

ACKNOWLEDGMENT The Swedish Research Council (VR) is gratefully acknowledged for financial support of this work.

References

1. Breck, D., *Zeolite Molecular Sieves*. ed.; Krieger Poblishing Company: Malabar, 1984.
2. Caro, J.; Noack, M.; Kolsch, P.; Schafer, R. *Microporous Mesoporous Mater.* **2000,** 38, (1), 3.
3. Hedlund, J.; Jareman, F.; Bons, A. J.; Anthonis, M. *J. Membr. Sci.* **2003,** 222, (1-2), 163.
4. Hedlund, J.; Ohrman, O.; Msimang, V.; van Steen, E.; Bohringer, W.; Sibya, S.; Moller, K. *Chem. Eng. Sci.* **2004,** 59, (13), 2647.
5. Mintova, S.; Bein, T. *Microporous Mesoporous Mater.* **2001,** 50, (2-3), 159.
6. Ohrman, O.; Hedlund, J.; Sterte, J. *Applied Catalysis A-General* **2004,** 270, (1-2), 193-199.
7. Tavolaro, A.; Drioli, E. *Adv. Mater.* **1999,** 11, (12), 975.
8. Bernal, M. P.; Coronas, J.; Menendez, M.; Santamaria, J. *Microporous Mesoporous Mater.* **2003,** 60, (1-3), 99.
9. Gump, C. J.; Tuan, V. A.; Noble, R. D.; Falconer, J. L. *Ind. Eng. Chem. Res.* **2001,** 40, (2), 565.
10. Hedlund, J.; Sterte, J.; Anthonis, M.; Bons, A. J.; Carstensen, B.; Corcoran, N.; Cox, D.; Deckman, H.; De Gijnst, W.; de Moor, P. P.; Lai, F.; McHenry, J.; Mortier, W.; Reinoso, J. *Microporous Mesoporous Mater.* **2002,** 52, (3), 179.
11. Keizer, K.; Burggraaf, A. J.; Vroon, Z.; Verweij, H. *J. Membr. Sci.* **1998,** 147, (2), 159.
12. Lai, Z. P.; Tsapatsis, M. *Ind. Eng. Chem. Res.* **2004,** 43, (12), 3000.
13. Zhu, W.; Hrabanek, P.; Gora, L.; Kapteijn, F.; Moulijn, J. A. *Ind. Eng. Chem. Res.* **2006,** 45, (2), 767.
14. Dobson, K. D.; McQuillan, A. J. *Langmuir* **1997,** 13, (13), 3392.
15. Lu, Y. F.; Han, L.; Brinker, C. J.; Niemczyk, T. M.; Lopez, G. P. *Sens. Actuators, B* **1996,** 36, (1-3), 517.
16. Ninness, B. J.; Bousfield, D. W.; Tripp, C. P. *Appl. Spectrosc.* **2001,** 55, (6), 655.
17. Poston, P. E.; Rivera, D.; Uibel, R.; Harris, J. M. *Appl. Spectrosc.* **1998,** 52, (11), 1391.
18. GiacintiBaschetti, M.; Piccinini, E.; Barbari, T. A.; Sarti, G. C. *Macromolecules* **2003,** 36, (25), 9574.
19. Gobel, R.; Seitz, R. W.; Tomellini, S. A.; Krska, R.; Kellner, R. *Vib. Spectrosc.* **1995,** 8, (2), 141.
20. Hellstern, U.; Hoffmann, V. *J. Mol. Struct.* **1995,** 349, 329.
21. Hedlund, J.; Mintova, S.; Sterte, J. *Microporous Mesoporous Mater.* **1999,** 28, (1), 185.
22. Hedlund, J.; Schoeman, B.; Sterte, J. *Chem. Commun.* **1997**, (13), 1193.
23. Hedlund, J.; Schoeman, B.; Sterte, J. Int. Pat. WO 97/33684,1997.
24. Hedlund, J.; Schoeman, B. J.; Sterte, J., Synthesis of ultra thin films of molecular sieves by the seed film method. In *Progress In Zeolite And Microporous Materials, Pts A-C*, ed.; Chon, H.; Ihm, S.-K.; Uh; Y.S.,(Eds.), Stud. Surf. Sci. Catal., 105, Elsevier Science, Amsterdam, 1997, p 2203.
25. Hedlund, J.; Sterte, J. *Nanostruct. Mater.* **1999,** 12, (1-4), 413.
26. Hedlund, J.; Noack, M.; Kolsch, P.; Creaser, D.; Caro, J.; Sterte, J. *J. Membr. Sci.* **1999,** 159, (1-2), 263.
27. Lassinantti, M.; Jareman, F.; Hedlund, J.; Creaser, D.; Sterte, J. *Catal. Today* **2001,** 67, (1-3), 109.
28. Ohrman, O.; Hedlund, J.; Msimang, V.; Moller, K. *Microporous Mesoporous Mater.* **2005,** 78, (2-3), 199.
29. Mintova, S.; Schoeman, B.; Valtchev, V.; Sterte, J.; Mo, S. Y.; Bein, T. *Adv. Mater.* **1997,** 9, 585.
30. Bjorklund, R. B.; Hedlund, J.; Sterte, J.; Arwin, H. *J. Phys. Chem. B* **1998,** 102, (12), 2245.
31. Grahn, M.; Wang, Z.; Lidstrom-Larsson, M.; Holmgren, A.; Hedlund, J.; Sterte, J. *Microporous Mesoporous Mater.* **2005,** 81, (1-3), 357.

32. Wang, Z.; Grahn, M.; Larsson, M. L.; Holmgren, A.; Sterte, J.; Hedlund, J. *Sens. Actuator, B* **2006,** 115, (2), 685.
33. Wang, Z.; Larsson, M. L.; Grahn, M.; Holmgren, A.; Hedlund, J. *Chem. Commun.* **2004**, (24), 2888.
34. Eder, F.; Lercher, J. A. *Zeolites* **1997,** 18, 75.
35. Gelin, P.; Dutel, J. F.; Mentzen, B. F. *Microporous Mater.* **1995,** 4, 283.
36. Lee, C. K.; Chiang, A. S. T. *J. Chem. Soc., Faraday Trans.* **1996,** 92, 3445.
37. Song, L.; Rees, L. V. C. *Microporous Mesoporous Mater.* **2000,** 35-36, 301.
38. Song, L. J.; Rees, L. V. C. *J. Chem. Soc., Faraday Trans.* **1997,** 93, 649.
39. Sun, M. S.; Talu, O.; Shah, D. B. *J. Phys. Chem. B* **1996,** 100, 17276.
40. Fox, J. P.; Rooy, V.; Bates, S. P. *Microporous Mesoporous Mater.* **2004,** 69, (1-2), 9.
41. Li, J.; Talu, O. *J. Chem. Soc., Faraday Trans.* **1993,** 89, 1683.
42. Maginn, E. J.; Bell, A. T.; Theodorou, D. N. *J. Phys. Chem.* **1995,** 99, 2057.
43. Mohanty, S.; Davis, H. T.; McCormick, A. V. *Chem. Eng. Sci.* **2000,** 55, (15), 2779.
44. Vlugt, T. J. H.; Krishna, R.; Smit, B. *J. Phys. Chem. B* **1999,** 103, (7), 1102.
45. Micke, A.; Bülow, M.; Kocirik, M.; Struve, P. *J. Phys. Chem.* **1994,** 98, 12337.
46. Schenk, M.; Vidal, S. L.; Vlugt, T. J. H.; Smit, B.; Krishna, R. *Langmuir* **2001,** 17, (5), 1558.
47. Harrick, N. J., *Internal Reflection Spectroscopy*. ed.; John Wiley & Sons, Inc.: New York, 1967.
48. Tompkins, H. G. *Appl. Spectrosc.* **1974,** 28, 335.
49. Mirabella, F. M., *Internal Reflection Spectroscopy: theory and applications*. ed.; Marcel Dekker, Inc.: New York, 1993.
50. Harrick Scientific Materials
URL: http://www.harricksci.com/infoserver/optical%20materials.cfm
51. Nair, S.; Tsapatsis, M. *Microporous Mesoporous Mater.* **2003,** 58, (2), 81.
52. Wu, P.; Debebe, A.; Ma, Y. H. *Zeolites* **1983,** 3, (2), 118.
53. Ellis, H., *Book of Data*. ed.; Longman Group, Ltd.: Harlow, UK., 1989;.
54. Horvath, G.; Kawazoe, K. *J. Chem. Eng. Jpn.* **1983,** 16, 470.
55. Jareman, F.; Hedlund, J.; Creaser, D.; Sterte, J. *J. Membr. Sci.* **2004,** 236, (1), 81.
56. Rege, S. U.; Yang, R. T. *AIChE J.* **2000,** 46, 734.
57. Jentys, A.; Tanaka, H.; Lercher, J. A. *J. Phys. Chem. B* **2005,** 109, (6), 2254.
58. Colthup, N. B.; Daly, L. H.; Wiberley, S. E., *Introduction to Infrared and Raman Spectroscopy*. Third edition ed.; Academic Press: London, 1990.
59. Jacobs, P. A.; Beyer, H. K.; Valyon, J. *Zeolites* **1981,** 1, (3), 161.
60. Stach, H.; Lohse, U.; Thamm, H.; Schirmer, W. *Zeolites* **1986,** 6, (2), 74.
61. Clark, T. E.; Deckman, H. W.; Cox, D. M.; Chance, R. R. *J. Membr. Sci.* **2004,** 230, (1-2), 91.
62. Schüth, F. *J. Phys. Chem.* **1992,** 96, 7493.
63. Richards, R. E.; Rees, L. V. C. *Zeolites* **1988,** 8, (1), 35.
64. Talu, O.; Guo, C.-J.; Hayhurst, D. *J. Phys. Chem.* **1989,** 93, 7294.
65. Mentzen, B. F. *Mat. Res. Bull.* **1992,** 27, (8), 953.
66. van Koningsveld, H.; Tuinstra, F.; van Bekkum, H.; Jansen, J. C. *Acta Cryst.* **1989,** B45, 423.
67. Mentzen, B. F.; Gelin, P. *Mat. Res. Bull.* **1995,** 30, (3), 373.
68. Xomeritakis, G.; Nair, S.; Tsapatsis, M. *Microporous Mesoporous Mater.* **2000,** 38, (1), 61.
69. Dong, J.; Lin, Y. S.; Hu, M. Z. C.; Peascoe, R. A.; Payzant, E. A. *Microporous Mesoporous Mater.* **2000,** 34, (3), 241.
70. Gualtieri, M. L.; Gualtieri, A. F.; Hedlund, J.; Jareman, F.; Sterte, J.; Dapiaggi, M., Accurate measurement of the thermal expansion of MFI zeolite membranes by in situ HTXRPD. In *Recent Advances In The Science And Technology Of Zeolites And Related Materials,* Pts A - C, ed.;van Steen, E.; Callanan, L.; Claeys, M., (Eds.), Stud. Surf. Sci. Catal., 154, Elsevier Science, Amsterdam, 2004, p 703.
71. Jeong, H. K.; Lai, Z. P.; Tsapatsis, M.; Hanson, J. C. *Microporous Mesoporous Mater.* **2005,** 84, (1-3), 332.

Paper V

Orientation of p-xylene in zeolite ZSM-5 films studied by FTIR/ATR spectroscopy

Mattias Grahn, Antonina Lobanova, Allan Holmgren and Jonas Hedlund

Manuscript

Orientation of p-xylene in zeolite ZSM-5 films by FTIR/ATR spectroscopy

Mattias Grahn[a*], *Antonina Lobanova*[a], *Allan Holmgren*[b] *and Jonas Hedlund*[a]

a) Div. of Chemical Technology, Luleå University of Technology, SE-971 87, LULEÅ, Sweden

b) Div. of Chemistry, Luleå University of Technology, SE-971 87, LULEÅ, Sweden

* To whom correspondence should be addressed: Mattias.Grahn@ltu.se; Fax: +46 920 491 199; Tel: +46 920 491 928

RECEIVED DATE

TITLE RUNNING HEAD Orientation of p-xylene in zeolite MFI films

ABSTRACT

ZnS ATR elements were coated with well defined b-oriented ZSM-5 films by in-situ growth. Both adsorption isotherms, as well as molecular orientation of p-xylene adsorbed in the films were measured at 323 and 373 K by FTIR/ATR spectroscopy. The isotherms were very similar to previously reported isotherms of supported films, albeit those films showed another preferred orientation. The data showed that the molecules were mainly oriented with their long axis parallel to the b-direction of the MFI crystals in concert with previously reported results based on FTIR microscopy, Monte Carlo simulations, NMR-, and XRD data. At high concentrations, the tilt angle was in good agreement with the value reported for FTIR microscopy. However, these angles were higher than the values reported for

XRD and NMR. This may be due to that the latter investigations were conducted at lower temperatures where the adsorbate molecules are less mobile. Another plausible explanation may be competitive adsorption on silanol groups, as was also indicated in the spectra. The results indicate that the adsorption properties of zeolite films and powders may differ. Hence, care should be taken when extrapolating findings from zeolite powder to films, particularly in systems where the adsorbate and the pores of the zeolite are of the same size.

KEYWORDS FTIR, ATR, ZSM-5, p-xylene, polarized radiation, oriented film

Introduction

Zeolites are crystalline aluminosilicates having well defined pore structure with pore dimensions of the same magnitude as many of the molecules of interest for instance in the petrochemical industry. Their well defined pore system facilitates their use as molecular sieves for separating molecules based on their size or shape. In addition, their large surface area together with their adsorption properties enables the separation of different molecules by preferential adsorption.[1-3] Zeolite films have been targeted due to their large potential as selective membranes-,[4-10] catalysts-,[11-13] components in microelectronic devices[14] and sensors.[15-20] As a consequence, much effort has been devoted to studying zeolite films in these applications, particularly zeolite membranes for novel separation processes. Despite the large number of publications on zeolite membranes, studies of the adsorption properties of supported zeolite films are scarce, probably due to difficulties to accurately measure the adsorption in zeolite films with thicknesses typically ranging from 0.5[6, 7] to a few μm. Consequently, the adsorption parameters determined on zeolite powders have been assumed valid also for supported zeolite films. However, recent XRD studies of zeolite membranes[21-23] have shown that the unit cell parameters differ between zeolite powder and supported films. The observed differences were attributed to strain in the film[23] and it is reasonable to believe that these differences may influence the adsorption properties of the films, at least for molecules with diameters close to the diameter of zeolite channels. One such extensively

studied (membranes and adsorption) adsorbate/zeolite system is p-xylene/MFI. The kinetic diameter of p-xylene[5] is 5.85 Å. MFI crystals have straight channels (5.3x5.6Å) running in the crystallographic b-direction that are intersecting with sinusoidal channels (5.5x5.1Å)[24] running in the crystal a-direction, see Figure 1.

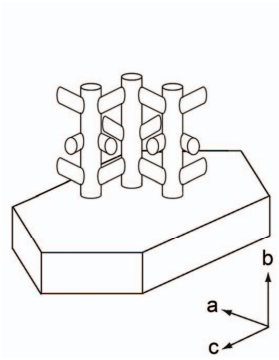

Figure 1. Schematic figure of MFI-crystal with channel system and crystallographic axes.

Several different techniques have been employed for studying the adsorption of p-xylene in MFI crystals, such as gravimetry,[25-27] calorimetry,[28] X-ray powder diffraction,[29-31] solid state NMR spectroscopy,[32-34] IR-spectroscopy,[35] FT-Raman spectroscopy[36, 37] and Monte Carlo simulations.[38-40] It has been found that p-xylene adsorb on two different sites in MFI powder and unsupported films.[29, 31, 41] At low partial pressures, p-xylene adsorb in the intersections of the two channels with the longest axis of the molecule oriented mainly in the b-direction of the crystal. At higher partial pressures, the molecules adsorb in the sinusoidal channels. At temperatures below ca 353 K, four molecules per unit cell adsorbs in the intersections and four molecules adsorbs in the sinusoidal channels, resulting in a type IV isotherm with a step at half of the saturation loading. At higher temperatures, the molecules adsorb only on the first site, resulting in a type I isotherm. Moreover, it has been shown that the structure of the MFI crystals change during adsorption of aromatic molecules.[30, 31] At room temperature, unloaded MFI has monoclinic symmetry. At low loadings (0-2 molecules /unit cell), the framework change gradually to orthorhombic symmetry and in this region the two phases coexists. In the intermediate loading region (2-4 molecules/ unit cell) only the orthorhombic phase exists and as the

loading is further increased (4-8 molecules/unit cell), the framework changes to a another orthorhombic phase. During this process, the framework is slightly distorted resulting in more elliptical pores.[31]

FTIR/ATR (Fourier Transform Infrared / Attenuated Total Reflection) spectroscopy is a technique especially well suited for studying thin films and surfaces.[42-46] We have recently published adsorption data for p-xylene and n-hexane in MFI films grown from seeds using this technique.[47] It was found that for n-hexane the results obtained agreed with findings reported for powder. However, as regarding p-xylene the results differed as compared to results reported for powder, in that only about half the saturation loading is reached at temperatures below 353 K, resulting in a type I isotherm. This indicates that the adsorption properties are different for zeolite powders and films as regarding tight-fit molecules. This phenomenon is further studied in the present work employing the same basic technique, i.e FTIR/ATR spectroscopy but with two very important differences. In the present work, b-oriented films were grown on the ATR waveguides and polarized light was employed. This combination will allow the determination of molecular orientation in zeolite films for the first time.

Experimental section

Materials – synthesis. b-Oriented ZSM-5 films were prepared on a trapezoidal ZnS element (50x20x2 mm, 45° cut edges , Spectroscopy Central Ltd., UK) using an in-situ method, details have been given elsewhere.[48] Prior to synthesis the elements were cleaned in acetone, ethanol and distilled water in an ultrasonic bath for ten minutes in each solvent. The element was then mounted in a Teflon holder that kept the element vertical during synthesis. The holder and element was subsequently placed in a Teflon lined stainless steel autoclave and a synthesis solution with a molar composition of 3TPAOH: 25SiO_2: 1600 H_2O: 100EtOH: 0.25 Al_2O_3: 1Na_2O was added. The autoclave was placed in a pre-heated oven at 150°C for 5.5h after which the autoclave was quenched with water. Thereafter, the sample was rinsed in a 0.1 M ammonia solution over night.

Characterization. Scanning electron microscopy (SEM) images were recorded of gold coated samples using a Philips XL 30 electron microscope equipped with a LaB_6 emission source. X-ray

diffraction (XRD) data was recorded using a Siemens D5000 x-ray diffractometer. Adsorption data of n-hexane (Sigma 99+%) and p-xylene (Aldrich 99+%) in helium carrier gas (AGA 99.99990%) was recorded by FTIR/ATR spectroscopy using a Bruker IFS 66v/S spectrometer equipped with a liquid nitrogen cooled mercury cadmium telluride (MCT) detector and a gas delivery system and in-situ cell as described elsewhere.[16] In the present work, an additional ZnSe wire grid polarizer was used. Before each adsorption experiment, the film was activated at 300°C (heating and cooling rate 1°C/min) for four hours under a flow of helium. After drying, the cell was mounted in the spectrometer and background spectra were recorded with and without polarizer by averaging 128 scans. Subsequently, the hydrocarbon was introduced and at equilibrium, spectra were recorded with and without polarizer by averaging 64 scans. Both the concentration and the dichroic ratio for p-xylene were determined from the integrated absorbance of the 1518 cm^{-1} band. The concentrations were subsequently determined using a procedure described elsewhere.[47] The isotherms for adsorption on silanol groups were determined from the integrated absorbance of the negative band at 3732 cm^{-1}.

Method. In FTIR/ATR spectroscopy, the IR beam is reflected inside an ATR element, see Figure 2. The electric field of the radiation penetrates a short distance outside the element enabling the detection of molecules close to the element surface.[49, 50]

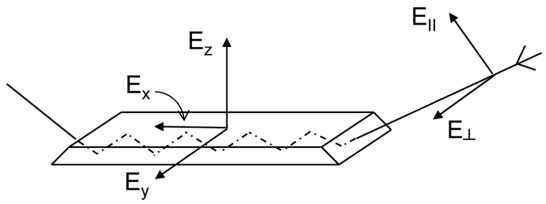

Figure 2. Direction and polarization of the IR beam in the ATR setup.

The intensity of the electric field decreases exponentially with distance (z) from the element surface. The penetration depth, d_p, of the electric field is usually between a couple of hundred nm to a few μm making the ATR method especially suited for studying thin films and surfaces and is defined as:

$$d_p = \frac{\lambda / n_1}{2\pi\left(\sin^2\theta - n_{21}^2\right)^{1/2}} \qquad (1)$$

where λ is the wavelength of the radiation in vacuum and n_1 is the refractive index of the element. Further, the angle of incidence, θ, was 45° during the experiments and $n_{21} = n_2/n_1$ where n_2 is the refractive index of the film. The refractive index of ZnS was taken as 2.25,[51] the refractive index of the gas was assumed to be 1.0 and since it has been found that the refractive index of the film changes with loading of the adsorbate,[52] a linear model was adopted where the refractive index varies between 1.22 and 1.32 as the p-xylene loading increases in the film.[52] Here it was assumed that the film had a p-xylene loading of 4 molecules per unit cell, as our previous findings suggests.[47] The Lambert-Beer law is not directly applicable in ATR spectroscopy but a method for estimating the concentration of adsorbed species has been developed.[49, 50]

One advantage of the ATR-technique is that when combined with polarized radiation it is possible to determine the direction of transition moments of normal vibrations and consequently, to obtain information of the orientation of molecules close to the element. The IR beam is propagating in the x-z plane (plane of incidence), see Figure 2. The surface of the element is in the x-y plane, orthogonal to the plane of incidence. Radiation polarized in the plane of incidence is referred to as parallel- or p-polarized radiation whereas radiation polarized in the plane of the surface is denoted perpendicular- or s-polarized radiation. The ratio of absorbance between s- and p-polarized radiation is denoted the dichroic ratio, $D = \frac{A_s}{A_p}$ and is given by:[53]

$$D = \frac{A_s}{A_p} = \frac{E_y^2\left(\sin^2\gamma\left(2 - 3\sin^2\Theta\right) + 2\sin^2\Theta\right)}{\left(E_x^2 + E_z^2\right)2\sin^2\Theta + \left(2 - 3\sin^2\Theta\right)\left(E_x^2\sin^2\gamma + 2E_z^2\cos^2\gamma\right)} \qquad (2)$$

where γ is the angle between the surface–normal and the main axis of the molecule, here defined as the axis going through the CH_3-groups. The angle between the direction of the transition moment and the main axis of the molecule is denoted Θ. For the breathing mode of the aromatic ring at 1518 cm^{-1} the transition moment is in the same direction as the main axis of the molecule[54] i.e. $\Theta = 0°$ yielding:

$$D = \frac{E_y^2 \sin^2 \gamma}{E_x^2 \sin^2 \gamma + 2E_z^2 \cos \gamma} \quad (3)$$

E_x, E_y and E_z are the electric field components in x-, y- and z-direction, respectively.

For a three-layer refractive index model (ATR element, film and gas) the components of the electric field are given by:[55]

$$E_x = \frac{2(\cos\theta)(\sin^2\theta - n_{31}^2)^{0.5}}{(1-n_{31}^2)^{0.5}[(1+n_{31}^2)\sin^2\theta - n_{31}^2]^{0.5}} \quad (4)$$

$$E_y = \frac{2\cos\theta}{(1-n_{31}^2)^{0.5}} \quad (5)$$

$$E_z = \frac{2n_{32}^2 \sin\theta\cos\theta}{(1-n_{31}^2)^{0.5}[(1+n_{31}^2)\sin^2\theta - n_{31}^2]^{0.5}} \quad (6)$$

where n_3 is the refractive index of the gas outside the film and $n_{31} = n_3/n_1$ and $n_{32} = n_3/n_2$.

For comparison, the dichroic ratio for an isotropic distribution is given by:

$$D = \frac{E_y^2}{E_x^2 + E_z^2} \quad (7)$$

By first determining the dichroic ratio experimentally, the average molecular tilt of the adsorbate from the z-axis can be estimated by solving equation 3 for γ. By comparing the experimental dichroic ratio with the isotropic value it is possible to estimate the anisotropy of the adsorbate. In the present work, a uniaxial distribution of the adsorbate was assumed.

Results and discussion

Characterization by SEM and XRD. The SEM images in Figure 3 are representative for the samples. The images show that the ZSM-5 film to a great extent consists of b-oriented crystals with tablet habit and that some parts of the element were not covered with film. Furthermore, most the crystals constitute a monolayer of intergrown crystals with a thickness of about 420 nm. A few crystals are deposited on top of this layer and a minor fraction of the crystals seems to be a-oriented.

Figure 3. ZSM-film on ZnS, (a) top- and (b) side-view.

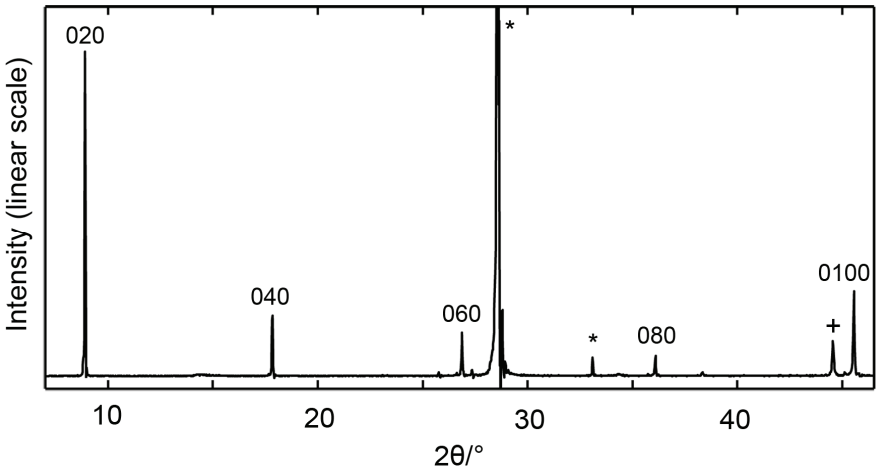

Figure 4. XRD pattern of the coated substrate. The indexed reflections emanates from the ZSM-5 film. The reflection labeled with * emanates from the ZnS element whereas the reflection labeled with + originates from the aluminum holder. The strong reflection at about 28.5° emanating from the ZnS element was ca. 14 times stronger than the 020 reflection.

The XRD pattern in Figure 4 shows that the film consists of merely b-oriented crystals since merely reflections from b-planes are observed. This supports the SEM observations that showed that most of the crystals were b-oriented and indicated that only a small fraction of the crystals were a-oriented. The XRD pattern is very similar to previously reported patterns for b-oriented MFI films.[56-58]

FTIR/ATR measurements. Adsorption measurement of n-hexane was carried out to determine the surface coverage of film on the ATR element using FTIR/ATR spectroscopy. It has previously been reported that the saturation loading of n-hexane in a silicalite-1 film grown from seeds is in good agreement with values reported for powders.[15] Thus, it was assumed that the saturation capacity of n-hexane was the same in the films used in the present work as in powders, yielding a surface coverage parameter of about 0.43. Though, this figure also contains any discrepancies between the molar absorptivity as was determined in CCl_4 and the real molar absorptivity in the zeolite.

To investigate if uncoated parts of the element or p-xylene in gas phase influenced the measurements, adsorption of p-xylene on an uncoated element was carried out. Figure 5 shows spectra recorded with an uncoated and a coated element recorded at 323 K and a p-xylene pressure of 648 Pa (maximum pressure in this study).

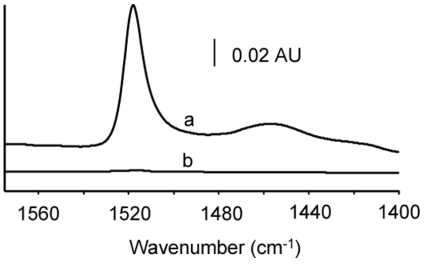

Figure 5. Part of spectra of p-xylene recorded at 323 K and 648 Pa. Spectrum (a) was recorded with a coated ATR element whilst spectrum (b) was recorded with an uncoated element.

The peak height of the 1518 cm^{-1} band is about 84 times larger for the coated element, thus it was concluded that p-xylene adsorbed on uncoated parts of the element and p-xylene in gas phase did not influence the measurements significantly and were therefore neglected.

The adsorption of p-xylene were measured without polarizer at 323 and 373 K. Figure 6 shows examples of spectra, recorded at 323 K without a polarizer and at p-xylene pressures of 0.8, 4.8 and 106 Pa.

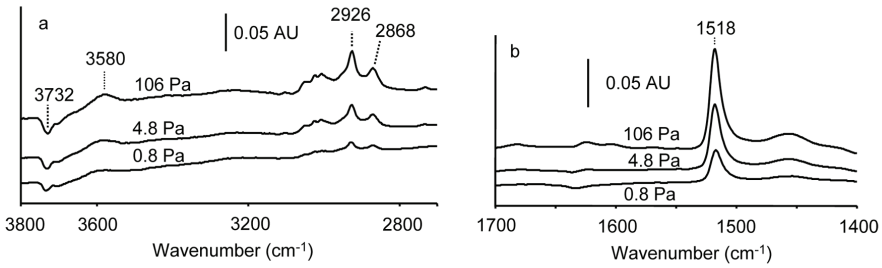

Figure 6. Spectra of p-xylene in the ZSM-5 film at different concentrations. The spectra were recorded without polarizer at 323 K.

The most prominent absorption bands are indicated in the figures and as expected the intensity of the absorption bands increases with increasing p-xylene pressure in the feed. In the C-H stretching spectral region (2700 and 3100 cm^{-1}), several overlapping bands appear, from which two prominent bands are observed at 2926 and 2868 cm^{-1}. These bands have previously been assigned to C-H stretching vibration and to a C-H deformation overtone, respectively.[35] The adsorption of xylene on silanol groups has been reported previously[59, 60] and is further indicated in Figure 5 (a) by the negative band at 3732 cm^{-1} accompanied with the appearance of a new band at 3580 cm^{-1}. In the region 1700 to 1400 cm^{-1}, a strong band appears at 1518 cm^{-1}assigned to stretching vibration of the aromatic ring.[35]

Isotherms extracted from the spectra are presented in Figure 7 (a). The isotherms are very similar to the isotherms we reported for supported films grown from seeds.[47] No step appears in the isotherm and only about half the saturation loading is reached indicating that p-xylene only adsorbs in the intersections and does not adsorb in the sinusoidal channels. This is in accordance with previous results on films grown from seeds,[47] but in contrast to isotherms determined on powder and non supported films.[26, 41, 61] We speculate that bonding of the film to the support leads to strain in the crystals or to the crystals becoming less flexible, which may prevent p-xylene to adsorb in the sinusoidal channels.

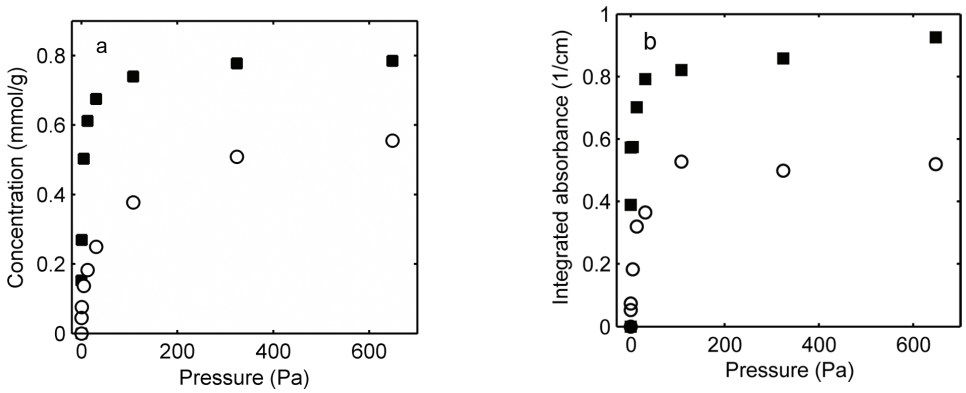

Figure 7. Adsorption isotherms of p-xylene in ZSM-5 (a) and on silanol groups (b) recorded at 323 K (■) and at 373 K (○).

Figure 7 (b) shows the adsorption isotherm of p-xylene on silanol groups at 323 and 373 K. Both plots resemble type I isotherms.

At each partial pressure, spectra were recorded with polarized radiation as well, an example is shown in Figure 8. Spectrum (1) is recorded with p-polarized radiation, spectrum (2) is recorded without polarizer and spectrum (3) is recorded with s-polarized radiation, all spectra were recorded at 323 K and 648 Pa.

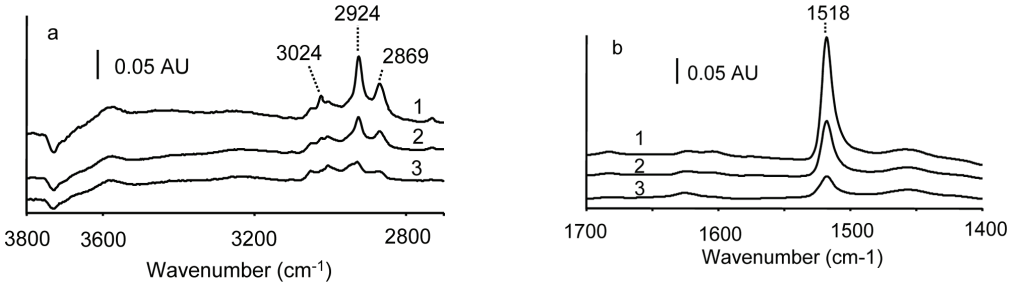

Figure 8. Parts of spectra of p-xylene recorded at T=323 K and P=648 Pa with p-polarized radiation (1), without polarizer (2) and with s-polarized radiation (3).

Our spectra show that there is strong polarization of several absorption bands, from which the most prominent are indicated in the figure. For all designated bands, much higher absorbance is obtained for the spectrum recorded with p-polarized radiation, indicating that there is a preferential orientation of the

adsorbed molecules. Moreover, the designated bands are all assigned to vibrations having transition moments in the same direction,[35, 54] hence the same trend is observed in both spectral regions shown in Figures 8 (a) and (b). Figure 9 shows the dichroic ratio as a function of concentration in the film at two temperatures.

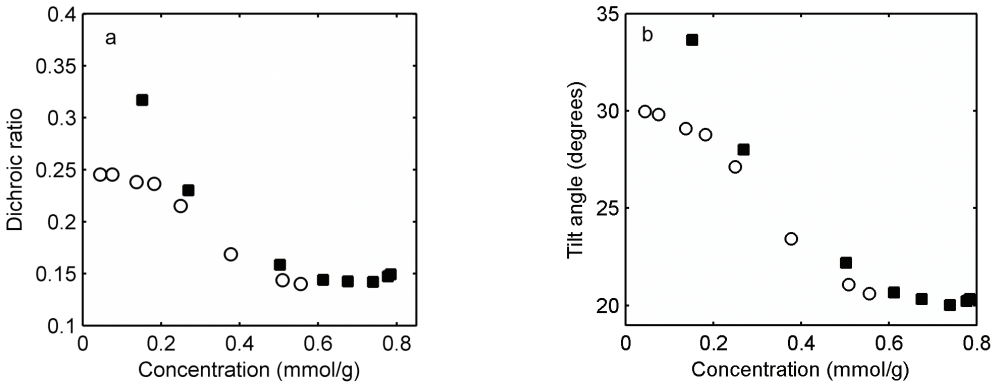

Figure 9. Dichroic ratio (a) and tilt angle (b) as a function of concentration of p-xylene in the film recorded at 323 K (■) and at 373 K (○).

At both temperatures, the dichroic ratio decreases with loading indicating that the average tilt angle also decreases. Moreover, it can be seen that the slope of the curves are approximately the same in the concentration interval 0.25 to 0.5 mmol/g and that the limiting value at high concentrations seems to be the similar at both temperatures. At lower concentrations the dichroic ratios at 373 K seem to reach a limiting maximum value of about 0.25 whereas at 323 K the dichroic ratio reaches higher values. The results implies either that the molecules are more mobile at lower loadings, and/or that adsorption on silanol groups affects the measurements more at lower loadings.

Further, the tilt angles determined in this work are substantially lower than that for an isotropic distribution of the adsorbates of 54.7° showing that the molecules are mainly oriented with the long axis in the b-direction of the zeolite crystals. This is consistent with previous reports for low loadings of p-xylene in MFI, as was discussed in the introduction. The tilt angles estimated in this work at high pressures agrees well with the tilt angle of 18° as reported by Schüth[35] for p-xylene adsorbed in the

intersections. The tilt angle was determined by IR microscopy on large crystals (380 x 70 μm) at ca 310 K. However, van Koningsveld et al.[31]reported a tilt angle of 7.5° for p-xylene in the intersections using XRD at room temperature and Fyfe et al.[32] reports a best fitted tilt angle of 0° using NMR. However, these measurements were performed at or below room temperature and in the case of the NMR measurements, the authors' concluded that completely reliable data could only be obtained at and below 213 K. Moreover, NMR data acquired above room temperature could not be used for structure determinations due to extensive molecular motions. Hence, mobile adsorbates may, at least partially, be responsible for the higher tilt angles obtained by the two FTIR methods since these were conducted at higher temperatures. Furthermore, competitive adsorption on silanol groups on the outer surface may also influence the determined tilt angles, especially in this work where the surface to volume ratio is quite large. The result from the present work, both the measurements conducted with polarized radiation and the isotherms support our previous findings, that at low temperatures, a type I isotherm appear with the p-xylene molecules mainly oriented in the b-direction of the zeolite crystals.[47] The lack of a second step in the isotherm was previously attributed to strain in the crystals or that the crystals are less flexible when attached to a support, preventing p-xylene to adsorb in the sinusoidal channels. The decrease in tilt angle with loading may originate from competitive adsorption of p-xylene on silanol groups at low pressures and that these sites are saturated faster than the zeolite, or by the adsorbates being more mobile at lower loadings. By comparing the results obtained in this work with the work by Schüth[35] on large crystals, our film, which consists of small crystals, has a larger surface to volume ratio and hence it is reasonable to assume that our sample has a larger density of external silanol groups leading to slightly larger tilt angles.

Conclusions

b-Oriented ZSM-5 films were successfully grown on ZnS ATR-elements. Adsorption isotherms for p-xylene were measured at 323 and 373 K by FTIR/ATR spectroscopy. The isotherms resemble type 1 isotherms in concert with previous findings for supported films but in contrary to what have been

reported for adsorption in MFI powder and unsupported films. Measurements with polarized radiation showed that the long axis of the p-xylene molecules where mainly oriented in the crystallographic b-direction. The tilt angle at higher loadings was in agreement with previously reported data determined by FTIR microscopy, however these angles were larger than angles obtained by NMR and XRD. The inconsistency between the FTIR data and XRD/NMR data may be due to a higher mobility of the adsorbates in the FTIR measurements since these were performed at higher temperatures. Competitive adsorption on external silanol groups may also affect the measurements, especially in the present work where the surface to volume ratio is large. This may also explain the slightly higher tilt angles obtained in this work compared to the tilt angle determined by FTIR microscopy on large crystals. The findings in this work shows that care should be taken when extrapolating properties for zeolite powder as valid also for zeolite films, especially for systems where the adsorbate and the pores are of the same size.

The result also shows that this novel technique can be used for determining both adsorption isotherms as well as average molecular orientation in zeolites. The technique could also become a useful tool for studying anisotropic diffusion and multicomponent adsorption in zeolites, two research fields of very high importance.

References

1. Gump, C. J.; Lin, X.; Falconer, J. L.; Noble, R. D. *J. Membr. Sci.* **2000,** 173, (1), 35.
2. Junhang Dong, Y. S. L. W. L. *AIChE J.* **2000,** 46, (10), 1957.
3. Yang, M.; Crittenden, B. D.; Perera, S. P.; Moueddeb, H.; Dalmon, J. A. *J. Membr. Sci.* **1999,** 156, (1), 1.
4. Bernal, M. P.; Coronas, J.; Menendez, M.; Santamaria, J. *Microporous Mesoporous Mater.* **2003,** 60, (1-3), 99.
5. Gump, C. J.; Tuan, V. A.; Noble, R. D.; Falconer, J. L. *Ind. Eng. Chem. Res.* **2001,** 40, (2), 565.
6. Hedlund, J.; Sterte, J.; Anthonis, M.; Bons, A. J.; Carstensen, B.; Corcoran, N.; Cox, D.; Deckman, H.; De Gijnst, W.; de Moor, P. P.; Lai, F.; McHenry, J.; Mortier, W.; Reinoso, J. *Microporous Mesoporous Mater.* **2002,** 52, (3), 179.
7. Lai, Z.; Bonilla, G.; Diaz, I.; Nery, J. G.; Sujaoti, K.; Amat, M. A.; Kokkoli, E.; Terasaki, O.; Thompson, R. W.; Tsapatsis, M.; Vlachos, D. G. *Science* **2003,** 300, 456.
8. Matsufuji, T.; Watanabe, K.; Nishiyama, N.; Egashira, Y.; Matsukata, M.; Ueyama, K. *Ind. Eng. Chem. Res.* **2000,** 39, (7), 2434.
9. Noack, M.; Mabande, G. T. P.; Caro, J.; Georgi, G.; Schwieger, W.; Kolsch, P.; Avhale, A. *Microporous Mesoporous Mater.* **2005,** 82, (1-2), 147.
10. Zhu, W.; Hrabanek, P.; Gora, L.; Kapteijn, F.; Moulijn, J. A. *Ind. Eng. Chem. Res.* **2006,** 45, (2), 767.

11. Hedlund, J.; Ohrman, O.; Msimang, V.; van Steen, E.; Bohringer, W.; Sibya, S.; Moller, K. *Chem. Eng. Sci.* **2004,** 59, (13), 2647.
12. Li, Y.; Huang, S.; Wu, S.; Yuan, X. *Catal. Letters* **2003,** 87, (1), 31.
13. Oudshoorn, O. L.; Janissen, M.; van Kooten, W. E. J.; Jansen, J. C.; van Bekkum, H.; van den Bleek, C. M.; Calis, H. P. A. *Chem. Eng. Sci.* **1999,** 54, (10), 1413.
14. Li, S. A.; Li, Z. J.; Yan, Y. S. *Adv. Mater.* **2003,** 15, (18), 1528.
15. Bjorklund, R. B.; Hedlund, J.; Sterte, J.; Arwin, H. *J. Phys. Chem. B* **1998,** 102, (12), 2245.
16. Grahn, M.; Wang, Z.; Lidstrom-Larsson, M.; Holmgren, A.; Hedlund, J.; Sterte, J. *Microporous Mesoporous Mater.* **2005,** 81, (1-3), 357.
17. Mintova, S.; Schoeman, B.; Valtchev, V.; Sterte, J.; Mo, S. Y.; Bein, T. *Adv. Mater.* **1997,** 9, (7), 585.
18. Plog, C.; Maunz, W.; Kurzweil, P.; Obermeier, E.; Scheibe, C. *Sens. Actuators, B* **1995,** 25, (1-3), 403.
19. Vilaseca, M.; Coronas, J.; Cirera, A.; Cornet, A.; Morante, J. R.; Santamaria, J. *Catal. Today* **2003,** 82, (1-4), 179.
20. Zhang, J.; Dong, J. H.; Luo, M.; Xiao, H.; Murad, S.; Normann, R. A. *Langmuir* **2005,** 21, (19), 8609.
21. Dong, J.; Lin, Y. S.; Hu, M. Z. C.; Peascoe, R. A.; Payzant, E. A. *Microporous Mesoporous Mater.* **2000,** 34, (3), 241.
22. Gualtieri, M. L.; Gualtieri, A. F.; Hedlund, J.; Jareman, F.; Sterte, J.; Dapiaggi, M., Accurate measurement of the thermal expansion of MFI zeolite membranes by in situ HTXRPD. In *Recent Advances In The Science And Technology Of Zeolites And Related Materials,* Pts A - C, ed.;van Steen, E.; Callanan, L.; Claeys, M., (Eds.), Stud. Surf. Sci. Catal., 154, Elsevier Science, Amsterdam, 2004, p 703.
23. Jeong, H. K.; Lai, Z. P.; Tsapatsis, M.; Hanson, J. C. *Microporous Mesoporous Mater.* **2005,** 84, (1-3), 332.
24. Breck, D., *Zeolite Molecular Sieves*. ed.; Krieger Poblishing Company: Malabar, 1984.
25. Lee, C. K.; Chiang, A. S. T. *J. Chem. Soc., Faraday Trans.* **1996,** 92, 3445.
26. Richards, R. E.; Rees, L. V. C. *Zeolites* **1988,** 8, (1), 35.
27. Song, L.; Rees, L. V. C. *Microporous Mesoporous Mater.* **2000,** 35-36, 301.
28. Thamm, H. *J. Phys. Chem.* **1987,** 91, 8.
29. Mentzen, B. F. *Mater. Res. Bull.* **1992,** 27, (8), 953.
30. Mentzen, B. F.; Gelin, P. *Mater. Res. Bull.* **1995,** 30, (3), 373.
31. van Koningsveld, H.; Tuinstra, F.; van Bekkum, H.; Jansen, J. C. *Acta Cryst.* **1989,** B45, 423.
32. Fyfe, C. A.; Diaz, A. C.; Grondey, H.; Lewis, A. R.; Forster, H. *J. Am. Chem. Soc.* **2005,** 127, (20), 7543.
33. Lefebvre, F.; Mentzen, B. F. *Mater. Res. Bull.* **1994,** 29, (10), 1049.
34. Reicshman, T. P.; Schmitt, K. D.; Olson, D. H. *J. Phys. Chem.* **1988,** 92, 5165.
35. Schüth, F. *J. Phys. Chem.* **1992,** 96, 7493.
36. Ashtekar, S.; Hastings, J. J.; Gladden, L. F. *J. Chem. Soc., Faraday Trans.* **1998,** 94, (8), 1157.
37. Huang, Y. *J. Am. Chem. Soc.* **1996,** 118, (30), 7233.
38. Li, J.; Talu, O. *J. Chem. Soc., Faraday Trans.* **1993,** 89, 1683.
39. Mohanty, S.; Davis, H. T.; McCormick, A. V. *Chem. Eng. Sci.* **2000,** 55, (15), 2779.
40. Snurr, R. Q.; Bell, A. T.; Theodorou, D. N. *J. Phys. Chem.* **1993,** 97, 13742.
41. Xomeritakis, G.; Nair, S.; Tsapatsis, M. *Microporous Mesoporous Mater.* **2000,** 38, (1), 61.
42. Ding, F. X.; Xie, H.; Arshava, B.; Becker, J. M.; Naider, F. *Biochemistry* **2001,** 40, (30), 8945.
43. Eun-Mi Shin; Koenig, J. L. *Appl. Spectrosc.* **2002,** 56, (10), 1251.
44. Fredriksson, A.; Larsson, M. L.; Holmgren, A. *J. Colloid Interface Sci.* **2005,** 286, (1), 1.
45. Keresszegi, C.; Ferri, D.; Mallat, T.; Baiker, A. *J. Phys. Chem. B* **2005,** 109, (2), 958.
46. Wang, Z.; Larsson, M. L.; Grahn, M.; Holmgren, A.; Hedlund, J. *Chem. Commun.* **2004**, (24), 2888.
47. Grahn, M.; Lobanova, A.; Holmgren, A.; Hedlund, J. *submitted* **2006**.

48. Wang, Z.; Hedlund, J.; Zhang, H.; Zou, X. D. *Microporous Mesoporous Materials* **2006,** 95, (1-3), 86.
49. Harrick, N. J., *Internal Reflection Spectroscopy*. ed.; John Wiley & Sons, Inc.: New York, 1967.
50. Mirabella, F. M., *Internal Reflection Spectroscopy: theory and applications*. ed.; Marcel Dekker, Inc.: New York, 1993.
51. Bruker Optics. *Guide for Infrared Spectroscopy*.
52. Nair, S.; Tsapatsis, M. *Microporous Mesoporous Mater.* **2003,** 58, (2), 81.
53. Ahn, D. J.; Franses, E. I. *Journal Of Physical Chemistry* **1992,** 96, (24), 9952.
54. Green, J. H. S. *Spectrochimica Acta* **1970,** 26A, 1503.
55. Neivandt, D. J.; Gee, M. L.; Hair, M. L.; Tripp, C. P. *J. Phys. Chem. B* **1998,** 102, (26), 5107.
56. Jansen, J. C.; van Rosmalen, G. M. *J. Crystal Growth* **1993,** 128, 1150.
57. Lai, Z. P.; Tsapatsis, M.; Nicolich, J. R. *Adv. Funct. Mater.* **2004,** 14, (7), 716.
58. Wang, Z. B.; Yan, Y. S. *Chem. Mater.* **2001,** 13, (3), 1101.
59. Jentys, A.; Tanaka, H.; Lercher, J. A. *J. Phys. Chem. B* **2005,** 109, (6), 2254.
60. Thibault-Starzyk, F.; Vimont, A.; Gilson, J.-P. *Catal. Today* **2001,** 70, (1-3), 227.
61. Gelin, P.; Dutel, J. F.; Mentzen, B. F. *Microporous Mater.* **1995,** 4, (4), 283.

Paper VI

A Novel Experimental Technique for Estimation of Molecular Orientation in Zeolite

Mattias Grahn, Antonina Lobanova, Allan Holmgren and Jonas Hedlund

Accepted for presentation and full length paper submitted for publication in the proceedings of the 15th International Zeolite Conference, Beijing, China

A Novel Experimental Technique for Estimation of Molecular Orientation in Zeolite

Mattias Grahn [a], Antonina Lobanova[a], Allan Holmgren[b] and Jonas Hedlund[a]
a) Division of Chemical Technology, Luleå University of Technology, SE-97187, Luleå, Sweden
b) Division of Chemistry, Luleå University of Technology, SE-97187, Luleå, Sweden
Tel. +46 920 491 928, Fax +46 920 491 199, E-mail: mattias.grahn@ltu.se

SUMMARY
FTIR spectroscopy in combination with polarized light and an ATR probe coated with a b-oriented ZSM-5 film was for the first time used to determine the orientation of adsorbed molecules in the ZSM-5 structure. Two adsorbates were studied, n-hexane and p-xylene and the results agreed with previously reported results obtained by other experimental techniques.

INTRODUCTION

Zeolites are extensively used in industry as ion exchangers, sorbents and catalysts and several novel applications such as membranes for separations and chemical sensors have been proposed. A detailed knowledge of the adsorption is fundamental in all these applications. In the present work, two systems that have been extensively studied previously, viz. n-hexane/MFI and p-xylene/MFI, were selected for investigation by a novel technique. An overview of the previously reported results for these systems is given below.
Several groups have studied the n-hexane/MFI system, and an inflection in the adsorption isotherm has been reported at a concentration of ca. 0.7 mmol/g, corresponding to about half the saturation loading [1,2]. The inflection was attributed to adsorption on different sites by Smit and Maesen [3], who studied the system using Monte Carlo simulations. They observed a redistribution of n-hexane as the concentration in the adsorbent increased. At low concentrations, the molecules are uniformly distributed in the intersections and in the channels. At higher concentrations, the molecules migrate into the sinusoidal channels leaving the intersections free, enabling a complete filling of the straight channels. Mentzen [4] employed powder x-ray diffraction (XRD) and observed a similar redistribution of n-hexane at room temperature. On the contrary, Morell et al. [5] could not observe any redistribution of the adsorbate at room temperature nor any preferred sites when investigating the n-hexane/silicalite-1 system with powder- and single crystal XRD as well as ^{29}Si MAS NMR and molecular modelling. However, clear ordering of n-hexane appeared when the temperature was lowered to 180 K, with molecules only adsorbed in the channels leaving the intersections unoccupied.
A type IV isotherm has been observed for p-xylene when adsorbed in MFI powder and unsupported films at temperatures around- and slightly above room temperature [6,7]. For the case of a type IV isotherm, the saturation capacity is 8 molecules/unit cell (or ~1.4 mmol/g). When the temperature is increased, a type I isotherm with a saturation capacity of only 4 molecules per unit cell is observed. The location and orientation of p-xylene molecules in MFI have been studied by means of XRD [8,9], FTIR microscopy, [10] Monte Carlo simulations [11] and NMR [12]. The first step in the type IV isotherm has been assigned to

adsorption of p-xylene in the intersections with the long axis (going through the CH_3- groups) mainly oriented in the b-direction of the crystals. Further, the second step in the type IV isotherm has been assigned to p-xylene adsorbed in the sinusoidal channels [9]. FTIR/ATR (Attenuated Total Reflection) has emerged as a powerful tool for studying surfaces and thin films of various systems, e.g. polymers [13], mineral flotation [14], membrane peptides [15], and catalysts [16]. An advantage with the technique is that, by applying polarized radiation, it is possible to gain information on orientation of adsorbed molecules [13-15].
This work aims at illustrating the utility of FTIR/ATR spectroscopy combined with polarized radiation and oriented MFI films for determining the arrangement of molecules in MFI crystals for the first time. In this context, an advantage with p-xylene as adsorbate is that the molecule is rigid, in that it can not take on different conformers. This makes it possible to determine an average tilt angle of the molecule relative the surface normal.

EXPERIMENTAL

General

Trapezoidal (50x20x2 mm, 45° cut edges) ZnS Attenuated Total Reflection (ATR) elements were coated with b-oriented ZSM-5 films using an in-situ method [17]. The films were subsequently characterized by Scanning Electron Microscopy (SEM) and XRD [17]. The infrared measurements were conducted using a Bruker IFS 66v/S spectrometer equipped with a liquid nitrogen cooled mercury cadmium telluride (MCT) detector. Polarized radiation was achieved by applying a rotatable ZnSe wire grid polarizer. A gas delivery system and an in-situ cell were used for exposing the film to a controlled environment, details of the equipment have been reported previously [18]. Helium (AGA 99.99990%) was used as carrier gas and n-hexane (Sigma 99+%) and p-xylene (Aldrich 99+%) were used as adsorbates. Prior to each measurement, the film was heated in-situ to 573 K for 4 hours at a heating/cooling rate of 1°/min. under a flow of pure helium to remove any molecules adsorbed in the zeolite. Subsequently, the cell was mounted in the spectrometer and background spectra without polarizer, and with 0° and 90° polarization were recorded by averaging 128 scans. Thereafter the hydrocarbon was introduced and spectra were recorded at equilibrium by averaging 64 scans. First one spectrum was recorded without polarizer, and then spectra with 0°, 90° and 0° polarization were recorded. Two spectra were recorded at 0° to ensure that the system was stable. In the evaluation, the mean value of the two measurements at 0° was used. IR spectra recorded without polarizer were used for determining the concentration of the adsorbate in the film, whereas spectra recorded with polarized radiation were used for determining the dichroic ratio. For n-hexane, the peak height of the methylene asymmetric stretching vibration band (2934 cm^{-1}) was used for determining the dichroic ratio, whereas for p-xylene, the integrated absorbance of a band assigned to a ring stretching vibration (1518 cm^{-1}) was used for determining the dichroic ratio.

The ATR-technique

In the ATR sampling technique, the infrared radiation is reflected inside a waveguide, also denoted an ATR element. At each reflection, a standing wave of the electromagnetic field is created. This field penetrates a short distance outside the element surface and interacts with molecules located close to the element surface. The intensity of the electromagnetic field decays exponentially with distance from the surface and a penetration depth, d_p, has been introduced to estimate the surface sensitivity of the technique [19]:

$$d_p = \frac{\lambda_1}{2\pi\left(\sin^2\theta - n_{21}^2\right)^{1/2}} \tag{1}$$

The wavelength of the radiation in the element is λ_1, θ is the angle of incidence (45° in this work), and $n_{21} = n_2/n_1$ is the ratio of the refractive indices in the film (n_2), and element (n_1), respectively. The penetration depth is usually in the range from a couple of hundred nm to a few μm, making the ATR technique especially well suited for studying thin films.

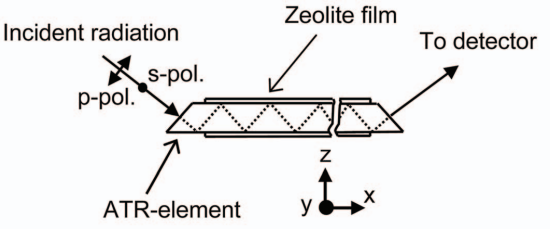

Figure 1. Geometry of the ATR set up.

As pointed out in the introduction, an advantage with the ATR-technique is that it is possible to determine average molecular orientation by applying polarized radiation. The key parameter when determining the orientation of molecules is the dichroic ratio, *D,* and by assuming an uniaxial distribution of the adsorbates, the dichroic ratio is given by [20]:

$$D = \frac{A_s}{A_p} = \frac{E_y^2\left(\sin^2\gamma\left(2-3\sin^2\Theta\right)+2\sin^2\Theta\right)}{\left(E_x^2+E_z^2\right)2\sin^2\Theta+\left(2-3\sin^2\Theta\right)\left(E_x^2\sin^2\gamma+2E_z^2\cos^2\gamma\right)} \tag{2}$$

The absorbance for a certain band determined with radiation polarized in the plane of the element surface is denoted A_s (s-polarized) and A_p is the absorbance for the same band recorded with radiation polarized in the plane normal to the element surface, see Figure 1. Moreover, Θ is the angle between the transition moment of the vibration of interest and the main axis of the molecule, for p-xylene, Θ = 0° for the ring stretching vibration observed at 1518 cm^{-1} [21]. Further, γ is the tilt angle of the main molecule axis from the surface normal.

The electric field amplitudes, E_x, E_y and E_z, in the x-,y- and z-directions are given for a three-layer system (ATR-element, film and gas) by equations, 3, 4 and 5, respectively [22].

$$E_x = \frac{2(\cos\theta)\left(\sin^2\theta - n_{31}^2\right)^{0.5}}{\left(1-n_{31}^2\right)^{0.5}\left[\left(1+n_{31}^2\right)\sin^2\theta - n_{31}^2\right]^{0.5}} \tag{3}$$

$$E_y = \frac{2\cos\theta}{\left(1-n_{31}^2\right)^{0.5}} \tag{4}$$

$$E_z = \frac{2n_{32}^2\sin\theta\cos\theta}{\left(1-n_{31}^2\right)^{0.5}\left[\left(1+n_{31}^2\right)\sin^2\theta - n_{31}^2\right]^{0.5}} \tag{5}$$

The refractive index of the gas is denoted n_3 and $n_{31}=n_3/n_1$ and $n_{32}=n_3/n_2$. By inserting $\Theta = 0°$ in eq. 2 a simplified version of the equation is obtained:

$$D = \frac{E_y^2 \sin^2 \gamma}{E_x^2 \sin^2 \gamma + 2E_z^2 \cos^2 \gamma} \quad (6)$$

From this expression, γ can be determined after measuring the dichroic ratio and calculating E_x, E_y and E_z from eq. 3-5.

RESULTS AND DISCUSSION

Figures 2 (a) and (b) show top- and side view images of a ZSM-5 film on a ZnS element. The images indicate that the film mostly consists of intergrown b-oriented crystals with tablet habit, and a minor fraction of a-oriented crystals. Further, a few b-oriented crystals are deposited on top of the film. The images also show that the film did not cover the element completely.

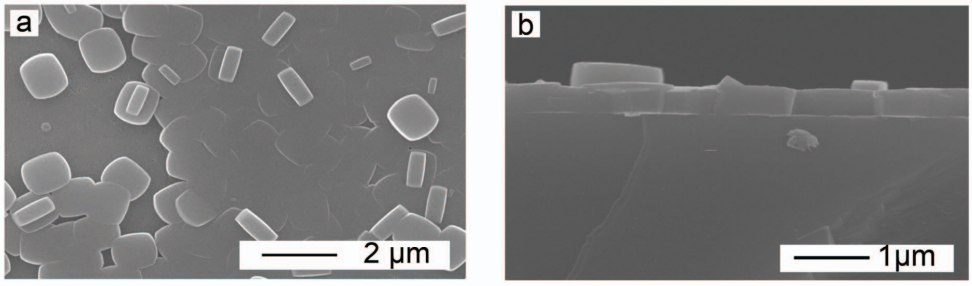

Figure 2. SEM images of the top (a) and side (b) of a MFI film on ZnS.

Bjorklund et al. [23] studied the adsorption of n-hexane in a silicalite-1 film grown from seeds and found that the saturation capacity was in good agreement with values reported for powders. By assuming that the result reported by Bjorklund et al. is valid also for the films used in this study, a parameter accounting for discrepancies both due to incomplete surface coverage and to any differences in molar absorptivity between the experimental value determined in CCl_4 and the real value in the zeolite can be defined, for details see [24]. The parameter, k_{hexane}, was determined to about 0.43. Spectra recorded without polarizer of n-hexane and p-xylene adsorbed in the film were very similar to previously reported spectra [24], examples are shown in Figure 3.

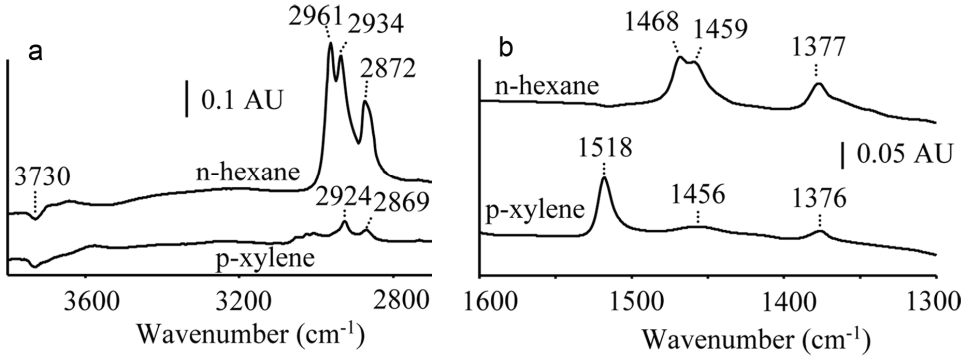

Figure 3. Spectra of n-hexane and p-xylene adsorbed in ZSM-5. The spectrum of n-hexane was recorded at 303 K and a n-hexane pressure of 12.9 kPa whereas the spectrum of p-xylene was recorded at 323 K and a p-xylene pressure of 650 Pa.

As expected, for n-hexane, bands appear in the CH stretching region between 3000-2700 cm^{-1} and in the CH deformation vibration region between 1500-1300 cm^{-1} [25]. In the p-xylene spectrum, several overlapping bands appear in the region 3200-2700 cm^{-1}, from which the most prominent are the bands at 2924 and 2869 cm^{-1}, assigned as symmetric methyl stretching vibration and asymmetric methyl deformation overtone [10]. At lower wavenumbers, bands appear at 1518, 1456 and 1376 cm^{-1}, these bands are assigned to benzene ring stretching vibration, asymmetric and symmetric methyl deformation vibrations, respectively. In addition, for both spectra, a negative band appears at 3730 cm^{-1} in combination with the appearance of a new band at lower wavenumbers. This band is assigned to silanol groups perturbed by adsorbate molecules resulting in a shift to lower wavenumbers [26].
The contribution from molecules adsorbed on uncoated parts of the element and the contribution from the gas phase was investigated by exposing an uncoated ZnS element to n-hexane at various partial pressures. A comparison of the spectra of n-hexane obtained with (a) and without (b) a film is presented in Figure 4.

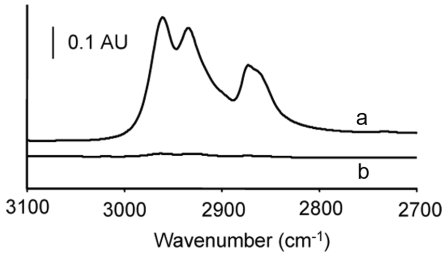

Figure 4. Part of infrared spectra of n-hexane using a ZSM-5 coated (a) and an uncoated (b) ATR element.

The integrated absorbance of the C-H stretching region for the uncoated element was only about 2.2 % of the value for the coated element. The corresponding value for p-xylene was about 1.2% determined from the peak height of the 1518 cm^{-1} absorption band. Therefore the contribution from gas phase and from molecules on uncoated parts of the element was considered negligible.

Spectra recorded with the polarized radiation showed significant polarization of several bands and examples are shown in Figure 5.

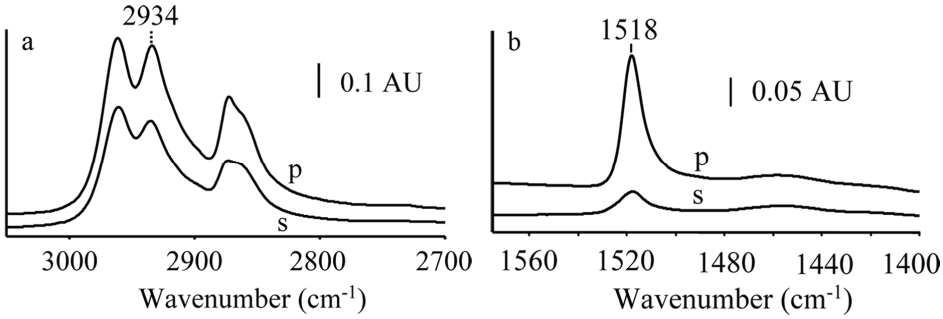

Figure 5. Parts of spectra recorded with polarized radiation of n-hexane (a) and p-xylene (b). The spectra of n-hexane were recorded at 303 K and an n-hexane pressure of 12.9 kPa, whilst the spectra of p-xylene were recorded at 323 K and a p-xylene pressure of 650 Pa. The direction of the polarized radiation is denoted by s (perpendicular) and p (parallel), respectively.

The bands indicated in the spectra were the ones used for determining the dichroic ratio, and in all cases, higher absorbance was observed with p-polarized radiation. The strong polarization, particularly observed in spectra of p-xylene, indicate a preferential orientation of the molecules. Dichroic ratios determined at different concentrations are presented in Table 1 together with calculated tilt angles for p-xylene. The dichroic ratio for n-hexane changes significantly when the concentration changes from 0.66 to 0.84 mmol/g, i.e. in the region where the inflection have been reported, while the ratio changes less in the concentration range 0.84 – 1.42 mmol/g.

Table 1. Dichroic ratio at different adsorbate concentrations in the film

n-hexane (303 K)		p-xylene (323 K)		
Concentration (mmol/g)	Dichroic ratio	Concentration (mmol/g)	Dichroic ratio	Tilt angle
0.66	0.68	0.15	0.32	34°
0.84	0.59	0.27	0.23	28°
1.10	0.62	0.5	0.16	22°
1.42	0.63	0.73	0.14	20°

The change in dichroic ratio in the concentration range 0.66 – 0.84 mmol/g indicates that some kind of molecular reorientation takes place. A change in the conformer distribution, i.e. the number of trans C-C bonds, could cause a change in the dichroic ratio for alkanes. However, the positions of the CH_2-stretching vibrations bands are known to be sensitive to the conformation of alkanes [27, 28]. Shifts to lower wavenumbers indicate that the number of trans bonds increases whereas a shift to higher wavenumbers is a sign of an increased number of gauche bonds. In the present study, the position of the asymmetric CH_2-stretching vibration band was fairly constant at 2934 cm^{-1} throughout the concentration range studied. Hence, the change in the dichroic ratio observed in the present work at about half the

saturation loading is attributed to a redistribution of n-hexane in concert with the findings of Smit and Maesen [3] and Mentzen [4].
Further, if all n-hexane molecules were in all-trans conformation it would have been possible to determine an average molecular orientation, however previous studies [29,30] have shown that this is not the case for n-hexane in MFI, hence no average tilt angles for n-hexane were determined in the present work.

For p-xylene, we observe a decrease in dichroic ratio and average tilt angle with increasing concentration. The tilt angle 20° obtained at a concentration of 0.73 mmol/g is very close to the one reported by Schüth (18°), as determined by FTIR microscopy on large single crystals at ca 310 K [10]. van Koningsveld et al. [9] investigated the p-xylene/MFI system at room temperature using XRD and found a tilt angle of 7.5 ° for p-xylene adsorbed in the channel intersections. Fyfe et al. [12] employed $^{1}H/^{29}Si$ CP MAS NMR spectroscopy to study the p-xylene/ZSM-5 system and found that the orientation of p-xylene in the intersection that best fitted experimental data is with the long axis parallel to the crystallographic b-direction. However, the authors states that completely reliable data was only obtained below 213 K, and data recorded above room temperature could not be used for distance and structure determinations due to extensive molecular motions averaging the interactions. The difference in tilt angle between the measurements in this report and the ones by van Koningsveld et al. and Fyfe et al. may, at least partially, be explained by molecules being more mobile at the higher temperatures used in the present study. Further, some contribution may also originate from p-xylene adsorbed on silanol groups, as indicated in Figure 3. Competitive adsorption on silanol groups may also explain the observed decrease in tilt angle with increasing concentration in the present work.

In addition to being a tool for studying molecular orientation, the FTIR/ATR technique has high sensitivity, making it suitable for studying the properties of very thin films. Furthermore, since FTIR spectroscopy is sensitive to the species adsorbed, it should be possible to determine the orientation of adsorbed molecules from a multicomponent mixture as long as the direction of the transition moments are known and the corresponding absorption bands are separated. Another interesting application would be to use the technique to study anisotropic diffusion in zeolites.

A challenge for quantitative measurements is the need of a molar extinction coefficient for the adsorbate in the zeolite film. Furthermore, the small size of the crystals constituting the film introduces some problems. Firstly, the large external surface area/volume ratio leads to relatively high concentration of external silanol groups, which may affect the quantitative measurements as well as the determination of adsorbate orientation. A second effect is that small crystals in a dense film results in more grain boundaries and some of these will always be open, enabling capillary condensation to occur which may also influence the data.

CONCLUSIONS

A novel technique for studying the orientation of adsorbates in zeolite at various concentrations of the adsorbate was developed. The technique utilizes ATR elements coated with oriented zeolite films in combination with FTIR spectroscopy and was demonstrated by studying the adsorption of n-hexane and p-xylene in a b-oriented ZSM-5 film. The obtained results agreed with previous findings.

REFERENCES

1. Richards, R. E.; Rees, L. V. C. Langmuir, 3, (1987), 335.
2. Sun, M. S.; Talu, O.; Shah, D. B. J. Phys. Chem. B, 100, (1996) 17276.
3. Smit, B.; Maesen, T. L. M. Nature, 100, (1995), 42.
4. Mentzen, B. F., Mater. Res. Bull., 30,(1995), 1333.
5. Morell, H.; Angermund, K.; Lewis, A. R.; Brouwer, D. H.; Fyfe, C. A.; Gies, H. Chem. Mater., 14, (2002), 2192.
6. Richards, R. E.; Rees, L. V. C. Zeolites, 8, (1988), 35.
7. Xomeritakis, G.; Nair, S.; Tsapatsis, M. Micropor. Mesopor. Mater., 38, (2000) 61.
8. Mentzen, B. F. Mater. Res. Bull., 27, (1992), 953.
9. van Koningsveld, H.; Tuinstra, F.; van Bekkum, H.; Jansen, J. C. Acta Cryst., B45, (1989), 423.
10. Schüth, F. J. Phys. Chem., 96, (1992) 7493.
11. Snurr, R. Q.; Bell, A. T.; Theodorou, D. N. J. Phys. Chem., 97, (1993) 13742.
12. Fyfe, C. A.; Diaz, A. C.; Grondey, H.; Lewis, A. R.; Forster, H. J. Am. Chem. Soc., 127, (2005), 7543.
13. Eun-Mi Shin, Koenig, J. L. Appl. Spectrosc., 56, (2002), 1251.
14. Fredriksson, A.; Larsson, M. L.; Holmgren, A. J. Colloid Interface Sci., 286, (2005), 1.
15. Ding, F. X.; Xie, H.; Arshava, B.; Becker, J. M.; Naider, F. Biochemistry, 40, (2001), 8945.
16. Keresszegi, C.; Ferri, D.; Mallat, T.; Baiker, A. J. Phys. Chem. B, 109, (2005), 958.
17. Wang, Z.; Hedlund, J.; Zhang, H.; Zou, X. D.; Micropor. Mesopor. Mater., 95, (2006), 86.
18. Grahn, M.; Wang, Z.; Lidstrom-Larsson, M.; Holmgren, A.; Hedlund, J.; Sterte, J. Micropor. Mesopor. Mater., 81, (2005), 357.
19. Harrick, N. J., Internal Reflection Spectroscopy. J. Wiley & Sons, Inc. New York, 1967.
20. Ahn, D. J.; Franses, E. I. J. Phys. Chem., 96, (1992), 9952.
21. Green, J. H. S. Spectrochim. Acta, (1970), 26A, 1503.
22. Mirabella, F. M., Internal Reflection Spectroscopy: theory and applications. ed.; Marcel Dekker, Inc., New York, 1993.
23. Bjorklund, R. B.; Hedlund, J.; Sterte, J.; Arwin, H. J. Phys. Chem. B, 102, (1998) 2245.
24. Grahn, M.; Holmgren, A.; Hedlund, J. Submitted to J. Phys. Chem. B.
25. Colthup, N. B.; Daly, L. H.; Wiberley, S. E., Introduction to Infrared and Raman Spectroscopy. Third edition ed.; Academic Press: London, 1990.
26. Jentys, A.; Tanaka, H.; Lercher, J. A. J. Phys. Chem. B,109, (2005), 2254.
27. Ihs, A.; Uvdal, K.; Liedberg, B. Langmuir, 9, (1993), 733.
28. Lu, Y.; Miller, J. D. J. Colloid Interface Sci., 256, (2002), 41.
29. Huang, Y.; Wang, H. Langmuir, 19, (2003), 9706.
30. Stepanov, A. G.; Shubin, A. A.; Luzgin, M. V.; Shegai, T. O.; Jobic, H. J. Phys. Chem. B, 107, (2003), 7095.